AD NUMBER: AD0868090

LIMITATION CHANGES

TO:

Approved for public release; distribution is unlimited.

FROM:

Distribution authorized to U.S. Gov't. agencies and their contractors; Export Controlled; Nov 1968. Other requests shall be
referred to Office of Naval Research, Arlington, VA 22203.

AUTHORITY

ONR notice dtd 27 Jul 1971

SPECTRONICS, INC.
122 GREEN AVENUE, WOODBURY, N. J. 08096

RADAR CLUTTER MODELING

W. Blau
J. Farber

November 1968

168

Technical Report 68/053

RADAR CLUTTER MODELING

by:

W. Blau

J. Farber

November 1968

Contractor:

SPECTRONICS, INC.
122 Green Avenue
Woodbury, New Jersey 08096

Sponsorship - This research was sponsored by the Office of Naval Research, Code 461, Department of the Navy, Washington, D.C. 20360 under ONR Contract No. N00014-68-C-0120.

CONTENTS

LIST OF ILLUSTRATIONS

ABSTRACT

A simulation method for the evaluation of radar performance in a clutter environment is explored. Three radar processors are tested on a common basis using measurement data in a theoretical model which displays both the spatial and frequency correlation properties of clutter. The effects of coherent, partially coherent, and specular scattering interacting with the radar processing are made evident.

BLANK PAGE

1.0 INTRODUCTION

1.1 OBJECTIVE*

1. To provide a simulation method for the evaluation of radar performance in a clutter environment

2. To provide a common basis of comparison among fleet radars, modifications to fleet radars, and new techniques when operating against a clutter background.

3. To provide a tool for the synthesis of radar processing techniques for the detection and discrimination of targets in clutter

Potential application of the radar-target-clutter simulator is widespread, including:**

a. Detection of overland/oversea "on the deck" low flying aircraft

b. Ship detection

c. Periscope detection

d. Anti-chaff and anti-decoy

e. Airborne early warning and control

f. Strategic, tactical, and interceptor fire control

g. Ground mapping

h. Accurate location, and positive identification of targets

i. Reconnaissance

j. Clutter measurement systems

---

* Figure 1-1

** Figure -12

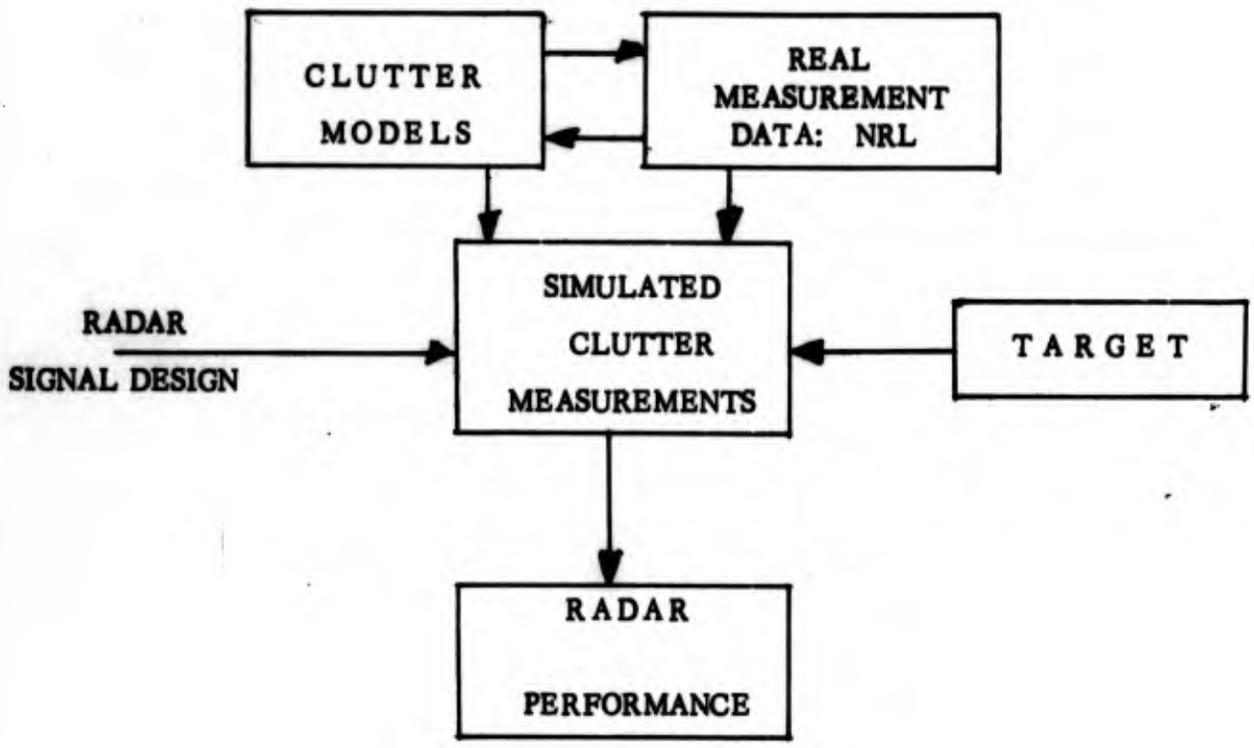

FIGURE 1-1 - SIMULATED CLUTTER MEASUREMENTS

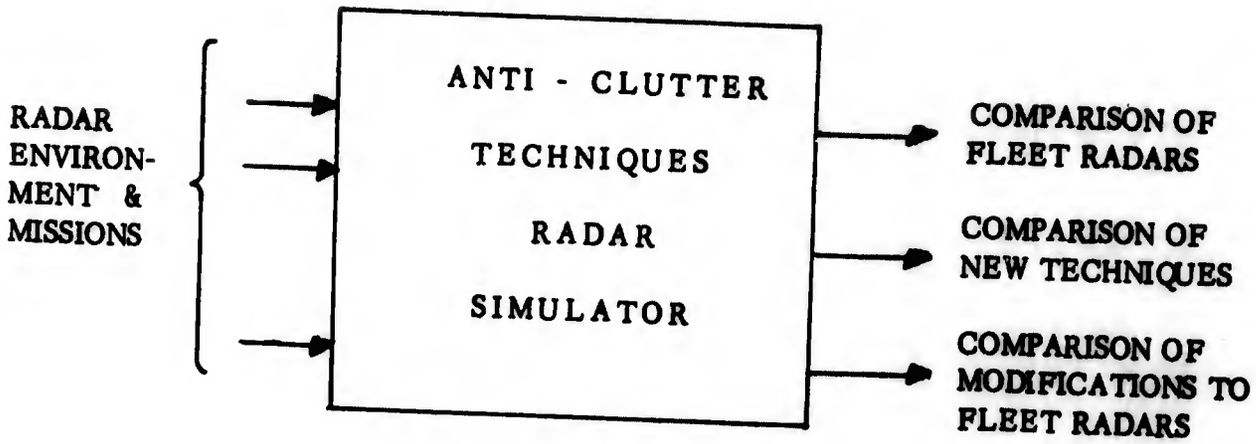

FIGURE 1-2 - RADAR SIMULATOR

1.2 STATE-OF-ART

In order to compare the performance of various radar types and/or to devise techniques for clutter reduction, a knowledge of the characteristics of clutter and its interaction with the radar must be determined. The current state of the art for determining clutter characteristics involves both theory and measurements. In either case, a mathematical model for the clutter and radar must be assumed.

The classical approaches to clutter treat it as a statistically stationary and uncorrelated random process*. The clutter model most often assumed for theoretical analysis is that of a large number of scatterers within the radar resolution cell. The phases of the echos from the individual scatterers are random, and the probability of receiving an echo from any particular scatterer is assumed to be independent of the echo signal from any other scatterer. The clutter amplitude at the radar output for a given range obeys a Rayleigh law from one sweep to the next. It does not describe the clutter amplitude along a single range sweep since the intensity of clutter varies radically and decreases with increasing range.

Radars for the discrimination of targets in clutter have been advanced which are theoretically correct based upon the assumed models for clutter as a statistically stationary process. However, many of these models are physically unrealizeable and do not sufficiently relate to real clutter observations. The greatest value of these models is for the comparison of various radar systems employing clutter reduction techniques based dominantly on the Doppler separation between the target and clutter. The stationary models for clutter provide a scale factor indicating the the relative merit of these systems <u>if</u> the clutter indeed had the appearance of random noise.

Recent work* on radar clutter models and radar signal processing has provided insights to the interaction between clutter scattering and radar coding. Specifically, a family of clutter models has been developed which can be related directly to the observations of the radar output, as, for example, the A-scope display.

---

* Refs. 1, 2

1.3 THE PROBLEM

The radar mission generally falls into one or more of the following categories: (1) detection, (2) estimation of position, velocity, acceleration, (3) resolution (4) identification. The ability of the radar to perform is corrupted by an unwanted background-clutter.

A similar situation exists even in a clutter-free environment due to noise appearing at the radar receiver input. The noise presents statistical fluctuations which produce false alarms depending upon the threshold setting at the radar output and the method of integrating. Because of the well-behaved statistics of the noise, signal-plus-noise, and assumed classes for target fluctuations, useful methods for ascribing probability of detection, probability of false alarms, false alarm time, etc. have evolved.

When clutter is the corrupting background, it is tempting to employ the same family of statistics which worked so well with receiver noise. This is generally recognized as an unsatisfactory and often erroneous procedure since both observation and theory are, in the main, in opposition. Receiver noise statistics are statistically stationary processes; clutter statistics are not necessarily stationary.

One can assume rather sophisticated models for the spatial, temporal, and/or frequency characteristics of various forms of clutter. However, care must be exercised in assuring their corroboration with the real world; otherwise, the assumed models have no real basis for their justification.

Recent investigations* on the nature of clutter and its translation to the radar output have been made which describe the variability of clutter in terms of its statistics, viewing aspect, and the effect of the radar signal processing. Of particular importance is the effect of speculars which are the dominant producers of clutter false alarms. If clutter is assumed to be random noise, the peak signal-to-mean clutter power output (S/C) increases in direct proportion to the transmitted bandwidth, i.e., a pulse radar will have its S/C increased ten times for a one-tenth reduction in its pulse length. When speculars are present, the effect of transmitted bandwidth is more pronounced since it has been shown** that a pure specular filling the resolution cell can be reduced by the square of the transmitted bandwidth, i.e., a pulse radar can have its S/C increased by as much as 100 times in specular scattering for a one-tenth reduction in its pulse length.

---

* Refs 1, 2, 3, 4, 5, 6,

** Refs 1, 2

Specular scattering (or partially coherent scattering which is a mixture of noise and specular scattering) alters the statistics in a manner which has been heretofore largely ignored. Assumptions for mathematical modeling are dependent upon the nature of specular, or partially coherent scattering.

1.4 CONTENT OF THE REPORT

Section 2 presents clutter models suitable for description of the interaction of the radar processor with the target-in-clutter environment. The models permit partially coherent scattering between the extremes of incoherent and coherent (specular) scattering. Of particular interest is the definition of the clutter ambiguity function which places in evidence the spatial and frequency correlation properties of spread targets and/or clutter and their interaction with the radar signal processing.

Emphasis has been placed upon models suitable for computer simulation purposes. In addition, specular reflections are treated because of their large response in the radar output, i.e., their effect in producing false target reports.

Section 3 outlines the clutter measurements obtained and the data reduction. Demonstration results of radar performance of a target-in-clutter are given in Section 4. The results are for three radar processing methods in both incoherent (noisy) and partially coherent (including speculars) clutter.

2.0 CLUTTER MODELS

2.1 CLUTTER DESCRIPTION

Detection of targets in clutter is based on the temporal, spatial, or frequency properties of both the target and clutter. The temporal, or time behavior, uses Doppler for discrimination; spatial clutter rejection is due to short pulse, or wideband transmission. The dissimilarity in the frequency properties of targets and clutter may also be used to detect targets in clutter.

The clutter model employed to describe these effects is summarized in Figures 2-1 through 2-16. Starting with Figure 2-1, we consider a simple radar. The transmitted pulse of width, T, scans the clutter. At any range-delay, τ_R, the radar output prior to detection is an instantaneous response specified in terms of both amplitude and phase.

Clutter is specified in terms of a complex reflection density, $\rho(\tau)$, having both amplitude and phase (Figure 2-2). At the specified range-delay, the radar pulse samples the clutter reflection density amplitude and phase (Figs. 2-3 and 2-4) i.e., all amplitude and phase components over the extent of the pulse length contribute to the radar output response. The sampled clutter amplitude (Fig. 2-3) is due to the product of the amplitudes of the clutter and radar pulse. The sampled phase response is due to the sum of the clutter and pulse range phase (Fig. 2-4). The instantaneous radar clutter response of Fig. 2-5 is expressed in terms of the clutter patch code-weighted reflection density $\rho_R(\tau)$. Fig. 2-6 emphasizes that the radar output is due to vectorial addition.

The largest radar output occurs for "phase-coherent clutter" (Fig. 2-7) which occurs when the phase slope of the clutter patch is the negative of the r-f carrier phase (Fig. 2-8); a uniform phase condition results in a linear summation of all the scatterers within the clutter patch.

The sampled clutter patch displays properties at the radar output which depend upon both the intrinsic clutter properties and the type of sampling employed. The same clutter patch will show different properties at the output of different radar processing methods. These properties are expressed in terms of phase and the partial correlation of clutter spatially, temporally and in frequency, (Fig. 2-9). The spatial correlation properties are affected by the r-f bandwidth of the radar transmission.

Recent work* has shown that clutter may be de-correlated based upon frequency. Fig. 2-11 describes the frequency de-correlation of rain clutter obtained from calculating the frequency correlation coefficient calculated from ensemble averages of measured data. Using this basis, clutter is uncorrelated when frequency diversity is employed, and the frequency shift exceeds the reciprocal of the pulse width. Similar results are obtained (Fig. 2-12) from measured data on the frequency de-correlation of sea return based upon a time-average frequency correlation coefficient.

These ensemble or time average frequency correlation coefficients are not measured directly by the radar. They are calculated from measured data to show the frequency de-correlation property of clutter.

The radar ambiguity function (Figs. 2-13, 2-14) defines the cross-correlation of a waveform (due to a point target) with itself Doppler and delay shifted. The Doppler shift is manifested as a reduced response when the frequency shift is greater than the reciprocal of the waveform time duration. For a simple rectangular pulse, the spatial resolution is the pulse width and in Doppler frequency is the reciprocal pulse width.

In this investigation, the clutter ambiguity function (Figs. 2-15, 2-16) is defined as the cross-correlation of the sampled clutter with itself frequency and delay shifted. This function has all the properties of ambiguity functions except that the waveform code is replaced by the sampled clutter patch reflection density, $\rho_R(\tau)$, i.e., it is apropos not only for a point target but also for spread targets, clutter. The clutter ambiguity function is useful for describing the clutter correlation properties observed at the radar output.

2.2 INSTANTANEOUS CLUTTER POWER OUTPUT

The instantaneous clutter power output is what the radar observes from clutter at a specified range. In this section, we assume the clutter has a narrow Doppler spread and is represented by an instantaneous complex reflection density, $\rho(\tau)$. Since our interest in this section is in the spatial and frequency correlation effects, we further specialize by specifying the clutter spread in range with zero Doppler shift. This specialization is apropos when coherent integration over many pulse repetition periods is absent, i.e., when the clutter Doppler spread (or Doppler shift) is much less than the reciprocal of the total coherent integration interval.

The matched filter output due to clutter prior to any(nonlinear) detection process is given by:

$$v(t) = e^{j\omega_o t} \int_{-\infty}^{\infty} \rho(\tau)\chi(t-\tau,0)e^{-j\omega_o \tau}\, d\tau . \qquad (2-1)$$

---

* Refs. 2, 4, 5, 6.

RADAR TRANSMITS PULSE

WHICH SCANS CLUTTER.

We observe

INSTANTANEOUS

AMPLITUDE and PHASE

RESPONSES AT

RANGE DELAY, τ_R

FIGURE 1-1 - INTRODUCTION

CLUTTER is described by

the COMPLEX REFLECTION DENSITY

$$\rho(\tau) = |\rho(\tau)|e^{j\beta(\tau)}$$

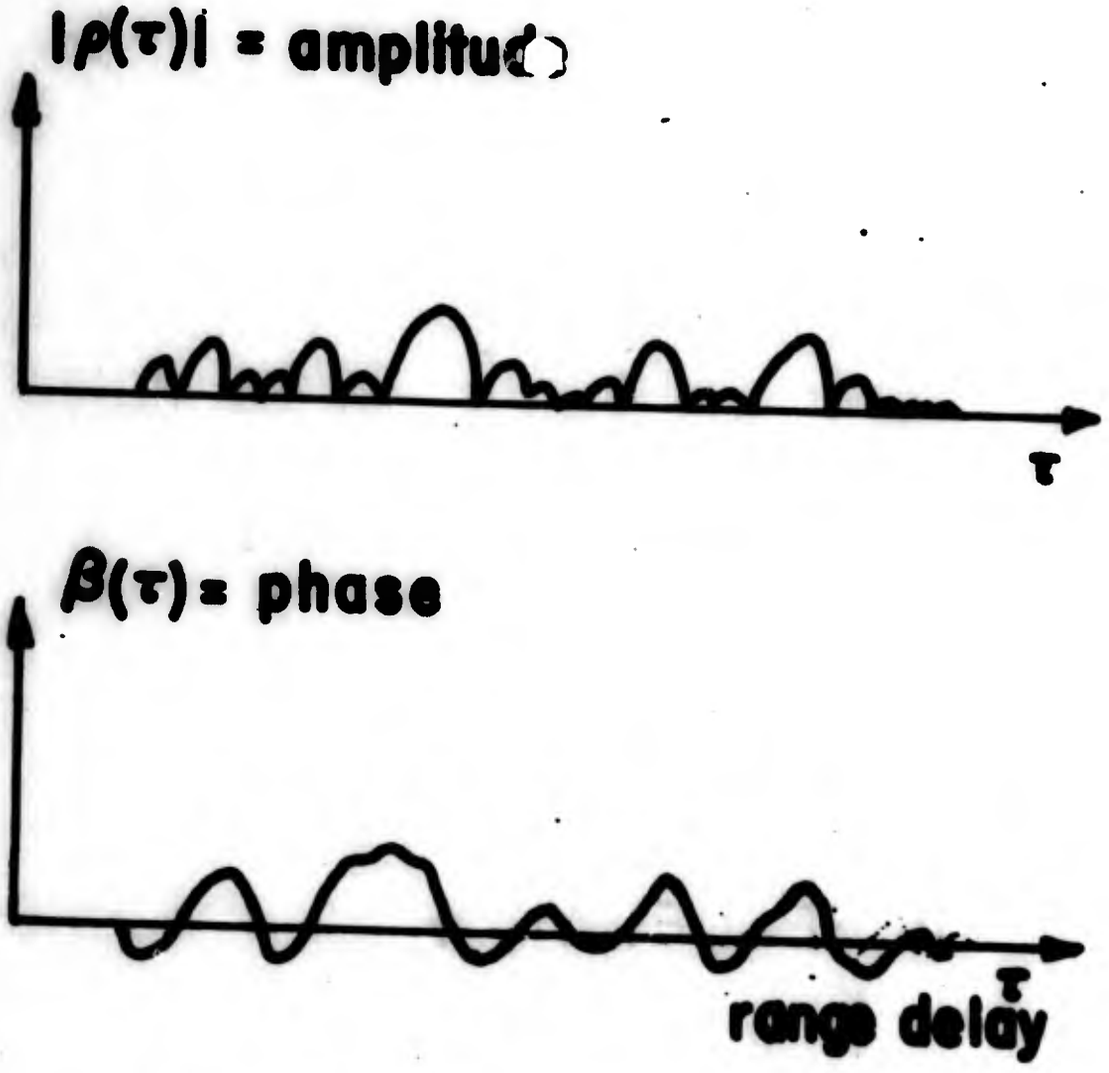

FIGURE 2-2 - CLUTTER COMPLEX REFLECTION DENSITY

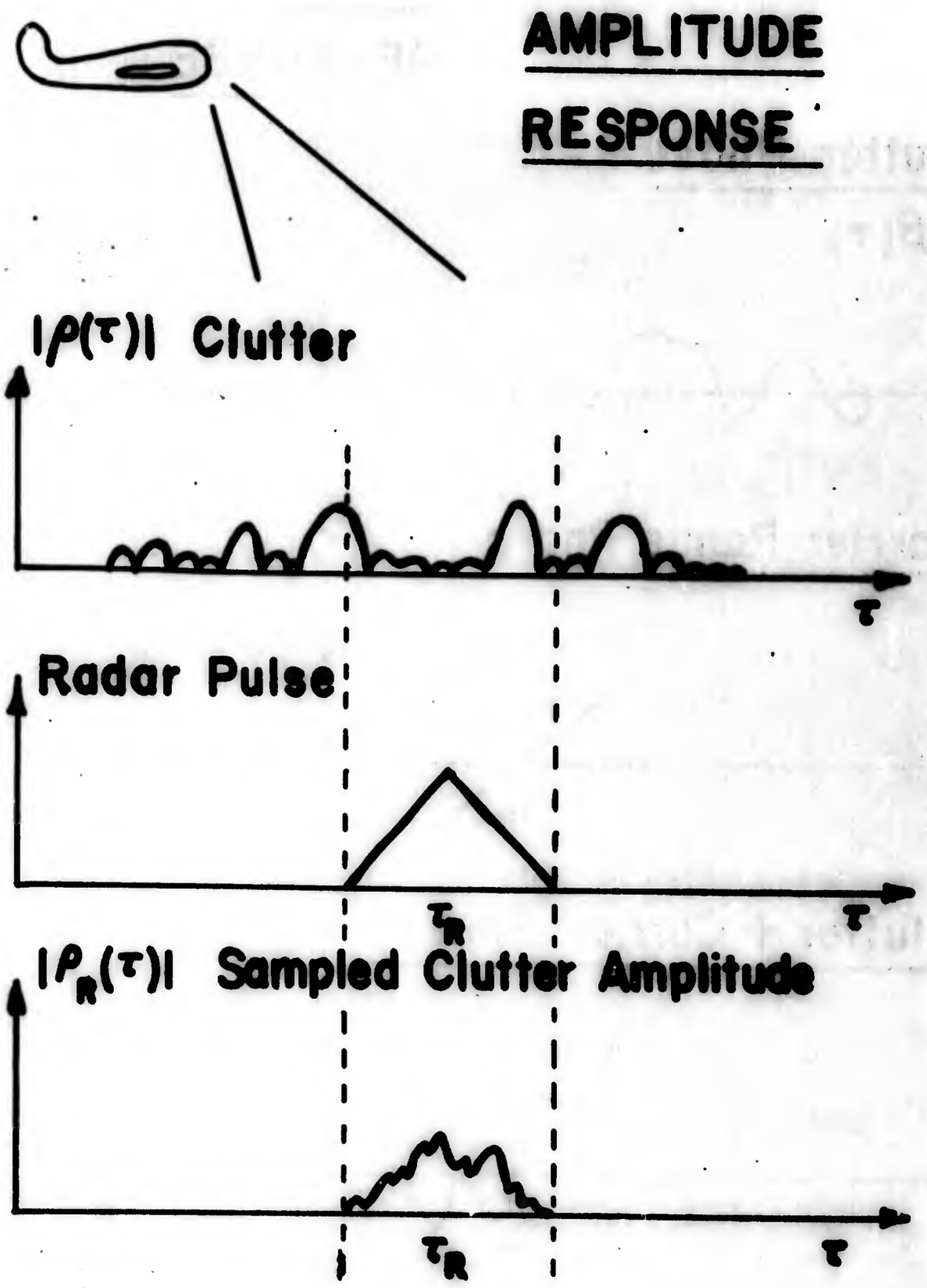

FIGURE 2-3 - CLUTTER PATCH AMPLITUDE RESPONSE

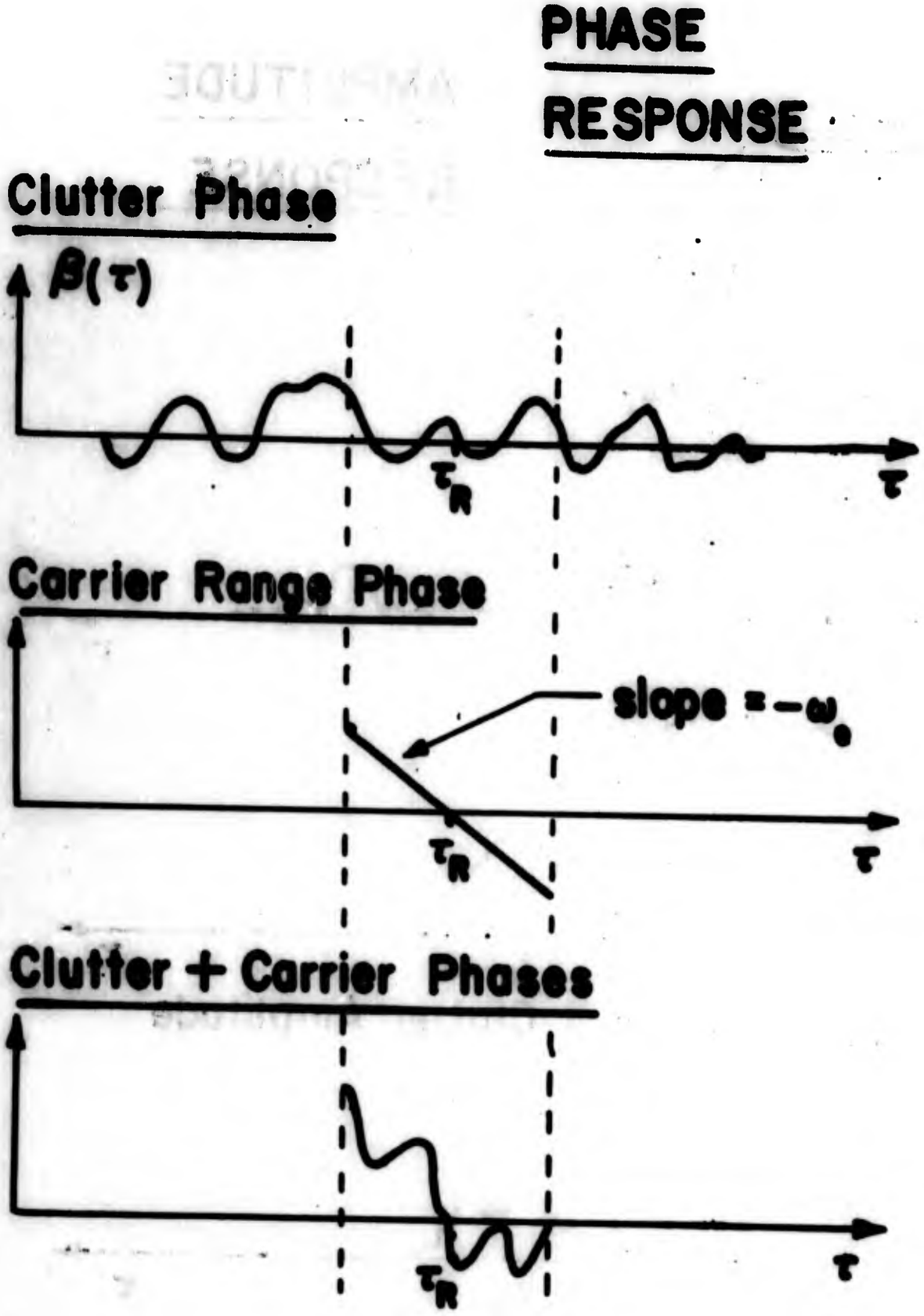

FIGURE 2-4 - CLUTTER PATCH PHASE RESPONSE

INSTANTANEOUS (pre detector) RADAR CLUTTER RESPONSE FROM RANGE DELAY, τ_R

$$v_R = e^{j\omega_o \tau_R} \underbrace{\int_{-\infty}^{\infty} \rho(\tau)\, \chi[-(\tau-\tau_R), 0]\, e^{-j\omega_o \tau}\, d\tau}_{\triangleq \rho_R(\tau)}$$

where

$$\rho(\tau) = |\rho(\tau)|\, e^{j\beta(\tau)}$$

= clutter reflection density

$$\chi(\tau,0) = |\chi(\tau,0)|\, e^{j\gamma(\tau)}$$

= pulse ambiguity function

$[\gamma(\tau) = 0$ for Rect. pulse$]$

FIGURE 2-5 - INSTANTANEOUS (Pre-Detector) RESPONSE

RADAR OUTPUT IS DUE TO VECTOR ADDITION

PHASE

$$V_R = \int_{-\infty}^{\infty} |\rho(\tau)| \, |X[(\tau - \tau_R), 0]| \, e^{j[\beta(\tau) - \omega_0(\tau - \tau_R)]} \, d\tau$$

AMPLITUDE

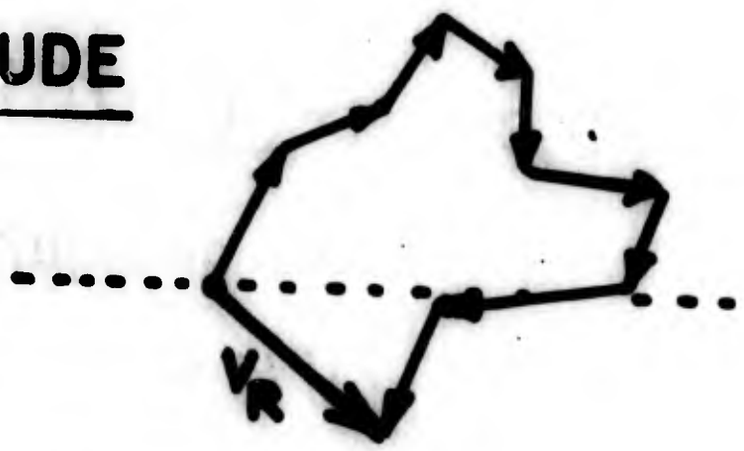

FIGURE 2-6 - VECTORIAL ADDITION OF SCATTERERS

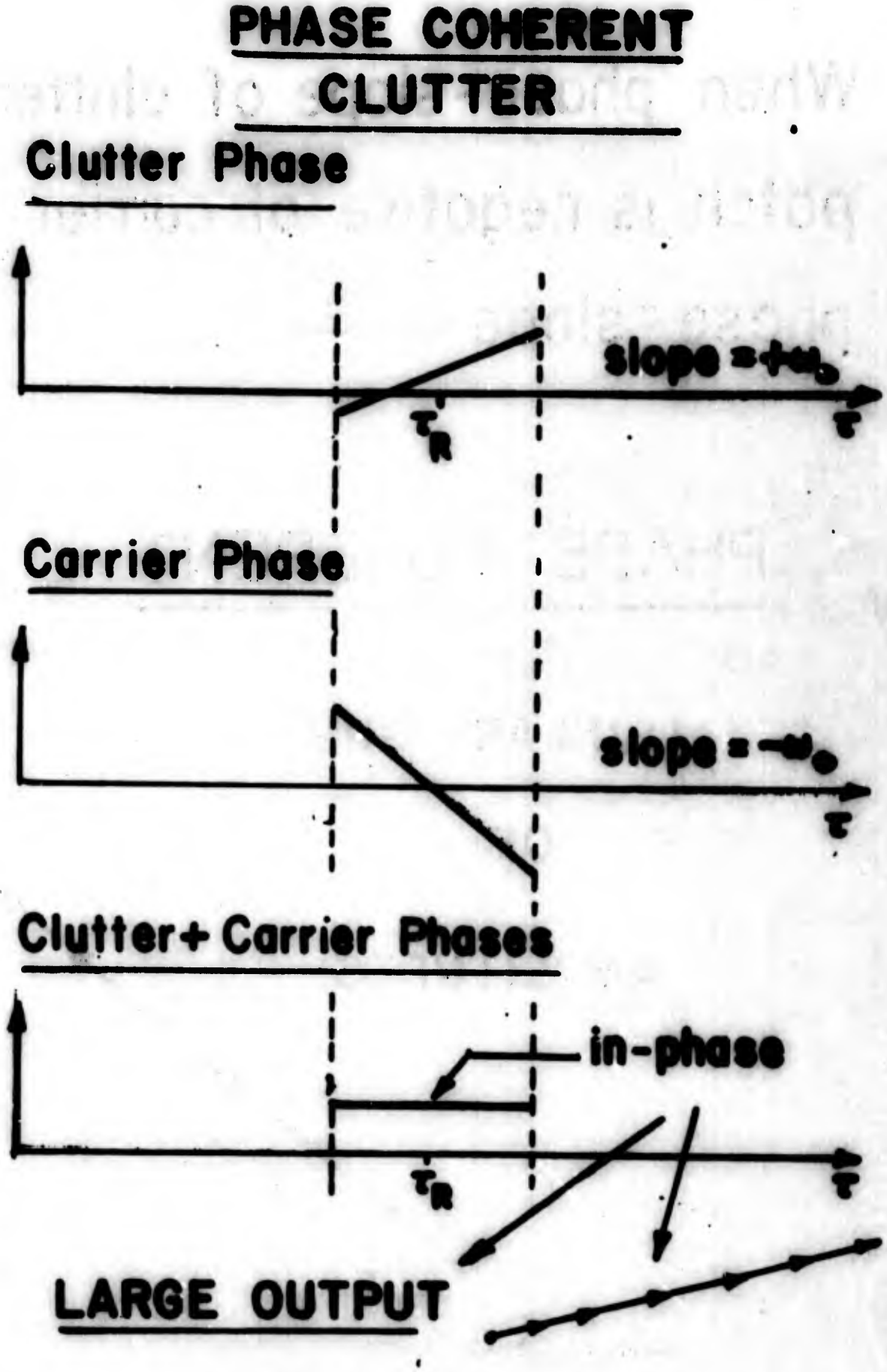

FIGURE 2-7 - PHASE-COHERENT CLUTTER

When phase-slope of clutter patch is negative of carrier phase-slope ——

PHASE COHERENT

(LINEAR SUM OF AMPLITUDES)

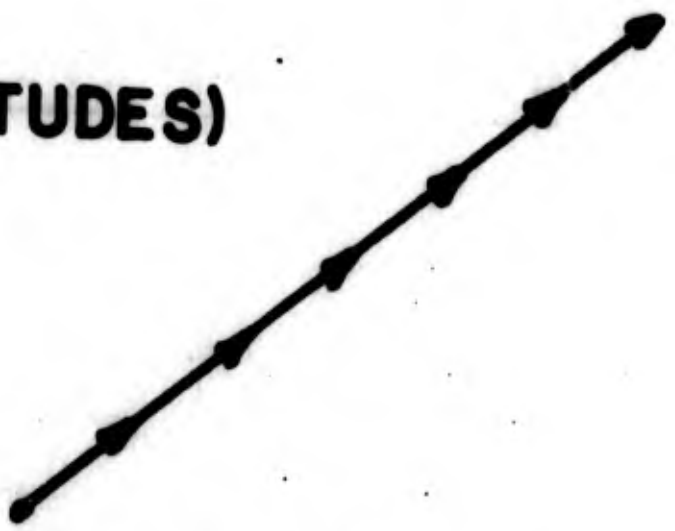

FIGURE 2-8 - PHASE-SLOPES

RADAR VIEWS CLUTTER WHICH CAN BE partially coherent, OR CORRELATED IN

- PHASE
- SPATIALLY (Bandwidth)
- FREQUENCY
- RADIAL VELOCITY (Doppler)

The same clutter patch will show different correlation properties at output of different radar techniques.

FIGURE 2-9 - PARTIALLY COHERENT CLUTTER FORMS

CLUTTER CORRELATION PROPERTIES MAY BE BASED UPON:

- ENSEMBLE AVERAGE (STATISTICS)
- TIME AVERAGE (STATISTICS)
- INSTANTANEOUS RESPONSE *

*Actual radar operation

FIGURE 2-10 - CLUTTER MODEL BASES

Example:*

"FREQUENCY" DE-CORRELATION OF RAIN CLUTTER

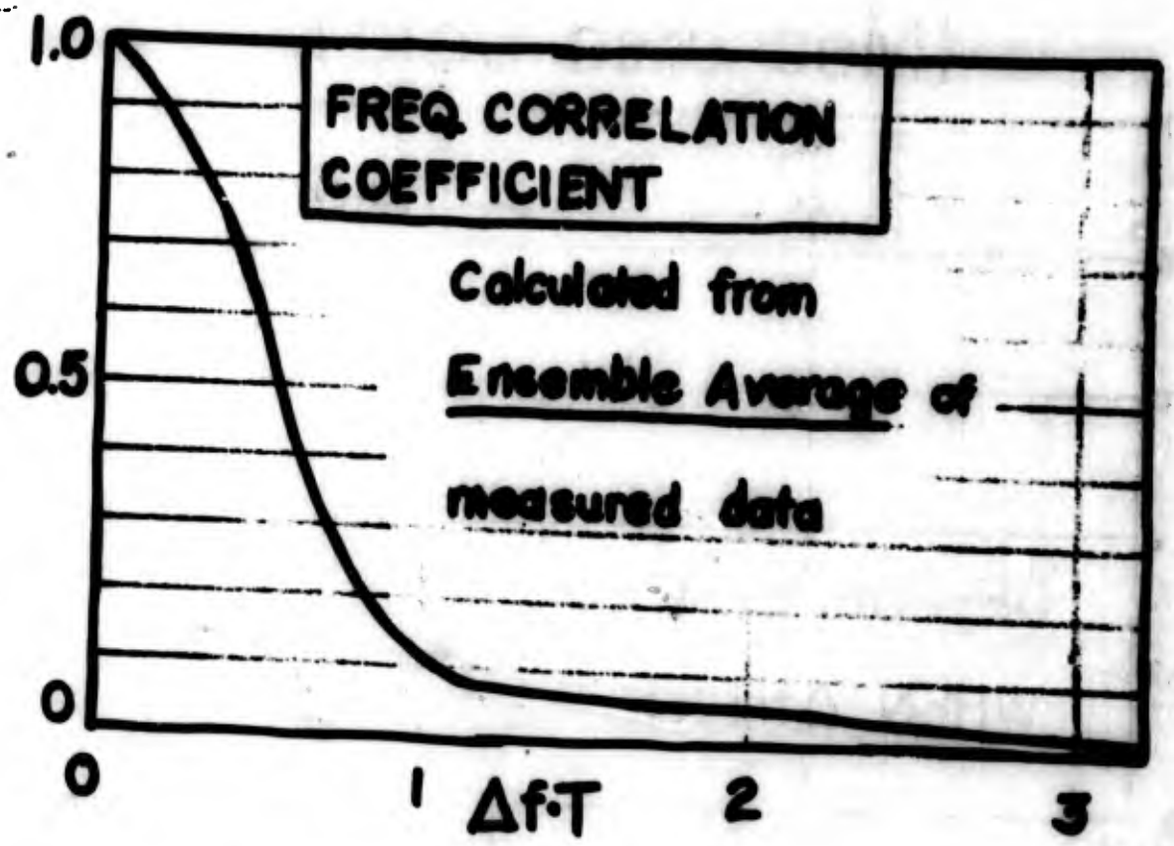

Δf = frequency separation

T = pulse width

RAIN CLUTTER IS DE-CORRELATED FOR

$$\Delta f \cdot T \geq 1$$

* Refs. 4, 5

FIGURE 2-11 FREQUENCY DE-CORRELATION OF RAIN CLUTTER

Example:*

"FREQUENCY" DE-CORRELATION OF SEA RETURN

(Measured Data)

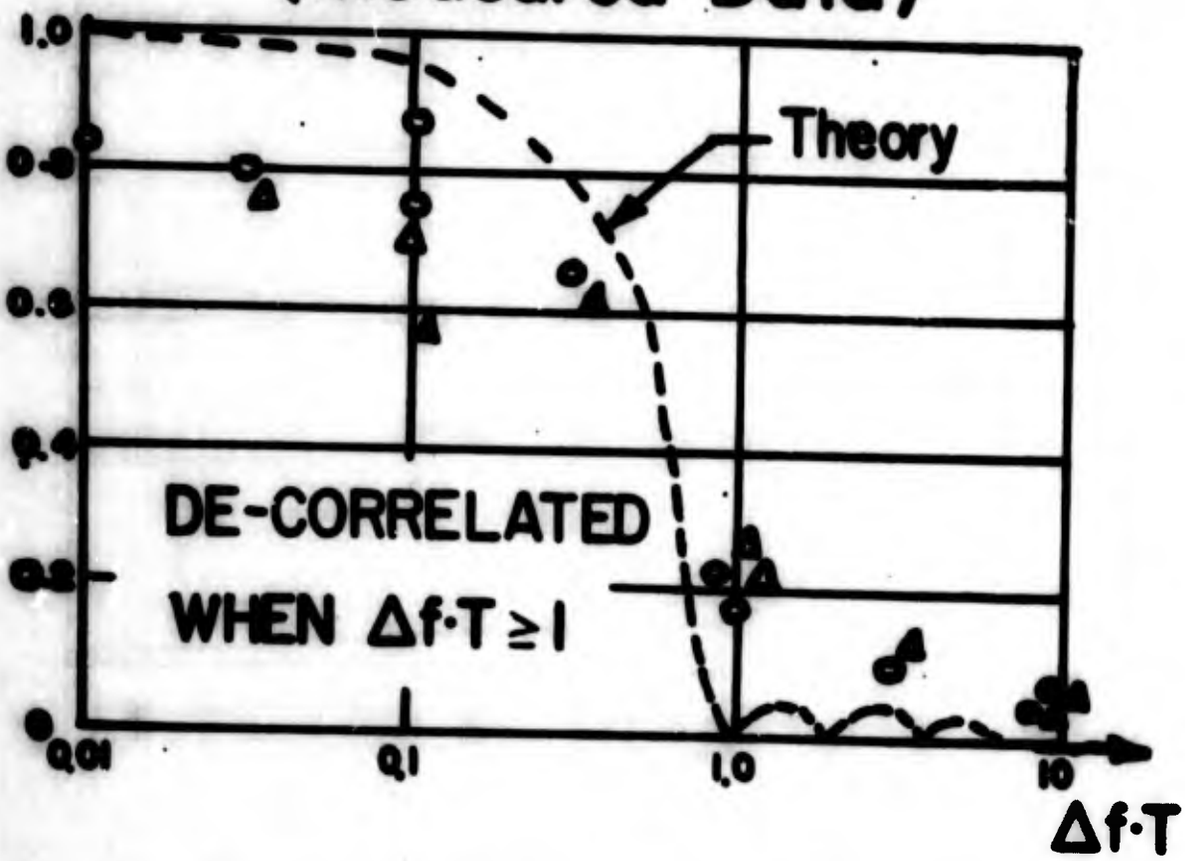

TIME AVERAGE CORRELATION COEFFICIENT - 2 FREQUENCIES SEPARATED BY Δf.

* Ref. 6

FIGURE 2-12 - FREQUENCY DE-CORRELATION OF SEA RETURN

RADAR AMBIGUITY FUNCTION

$$\chi(\tau,\phi) = \int_{-\infty}^{\infty} s^*(t)\, s(t+\tau)\, e^{j2\pi\phi t}\, dt$$

= CROSS-CORRELATION OF WAVEFORM, s(t), WITH ITSELF DOPPLER-SHIFTED, ϕ, AND DELAY-SHIFTED, τ.

Waveform, s(t):

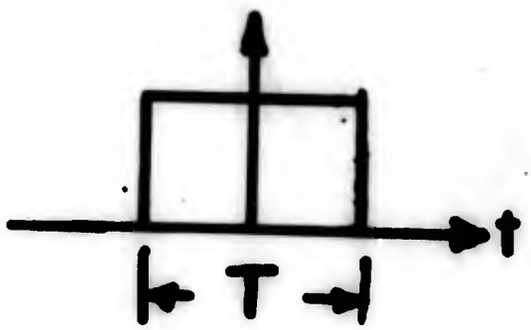

FIGURE 2-13 - RADAR AMBIGUITY FUNCTION

RADAR AMBIGUITY FUNCTION

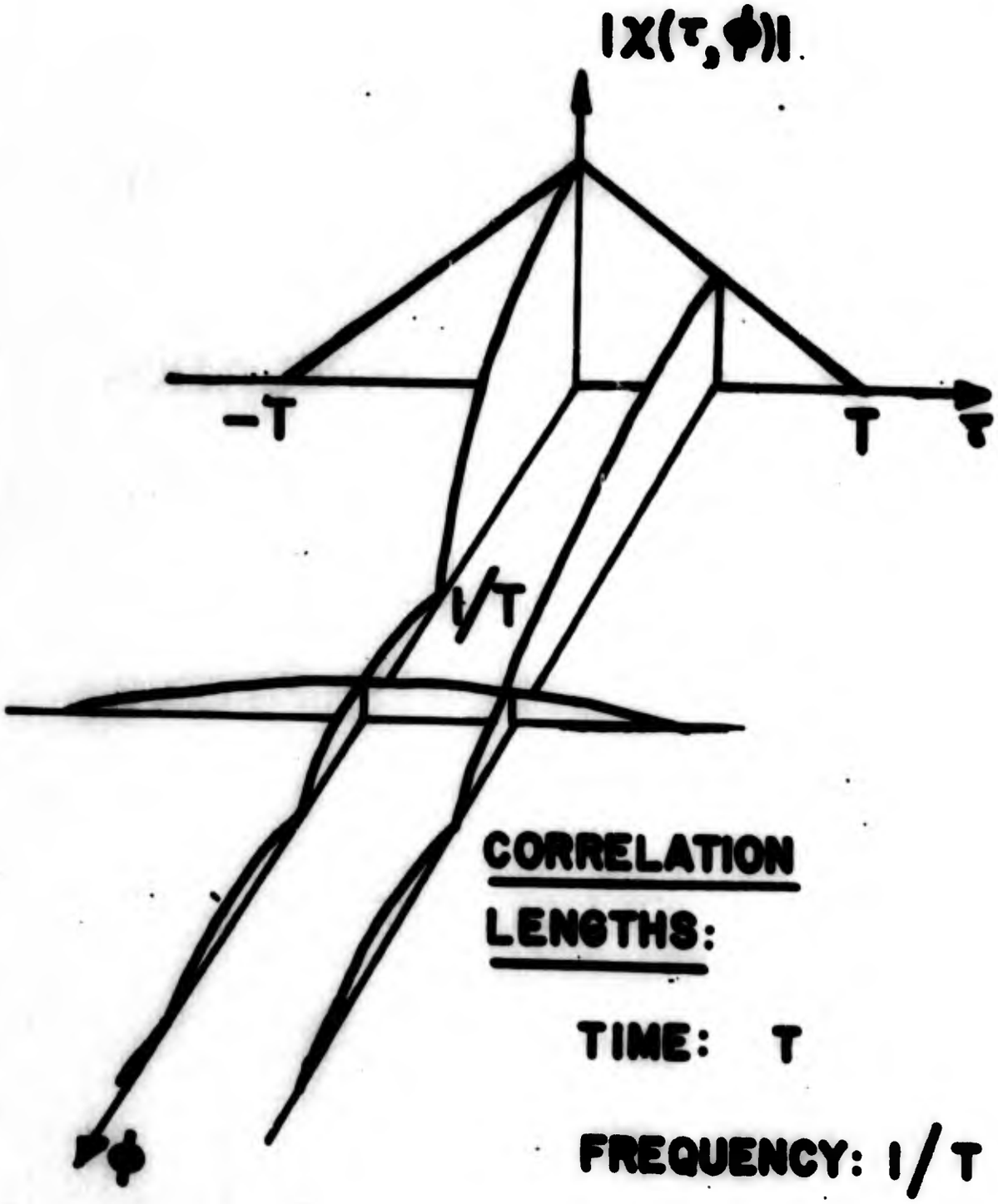

FIGURE 2-14 - RADAR AMBIGUITY FUNCTION CORRELATION LENGTHS

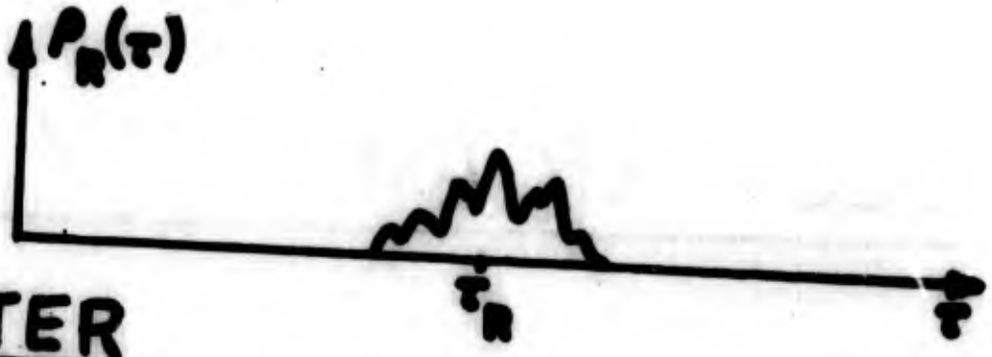

CLUTTER AMBIGUITY FUNCTION

$$\chi_{\rho_R}(\tau, f) = \int_{-\infty}^{\infty} \rho_R^*(t)\rho_R(t+\tau)e^{j2\pi ft}\,dt$$

= CROSS-CORRELATION OF (RADAR-SAMPLED) PATCH WITH ITSELF FREQUENCY* AND DELAY-SHIFTED.

*This is not the Doppler shift

FIGURE 2-15 - CLUTTER AMBIGUITY FUNCTION

CLUTTER AMBIGUITY FTN.

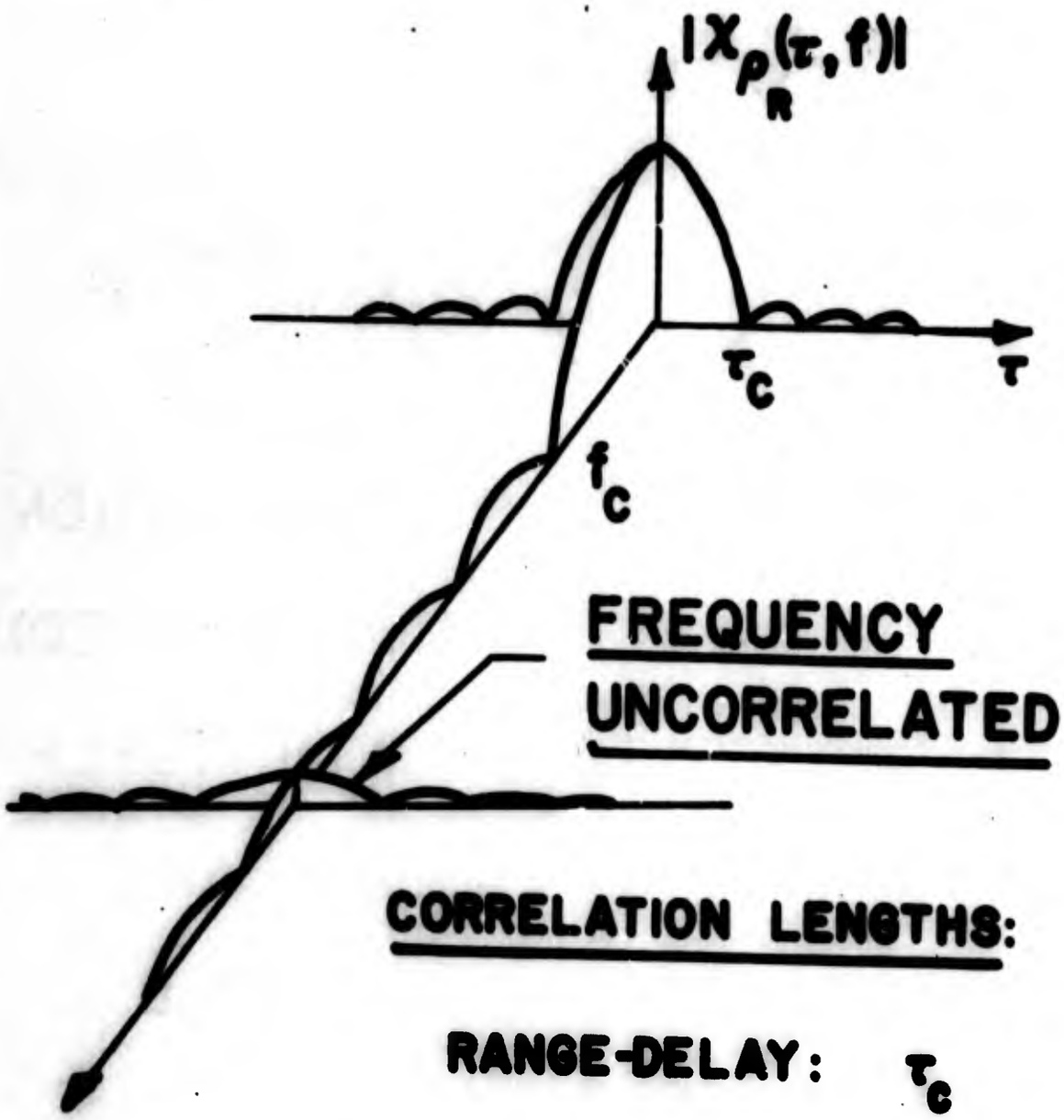

CORRELATION LENGTHS:

RANGE-DELAY: τ_c

FREQUENCY: f_c

FIGURE 2-16 - CLUTTER AMBIGUITY FUNCTION CORRELATION LENGTHS

At a range corresponding to a range-delay, τ_R, the instantaneous output is

$$v_R = e^{j\omega_o \tau_R} \int_{-\infty}^{\infty} \rho(\tau) \chi[-(\tau - \tau_R), 0] e^{-j\omega_o \tau} d\tau . \qquad (2-2)$$

The clutter patch sampled at τ_R is depicted in Figure 2-17 where the code-weighted reflection density is defined by

$$\rho_R(\tau) \triangleq \rho(\tau)\chi[-(\tau - \tau_R), 0]; \quad |\tau - \tau_R| \leq T. \qquad (2-3)$$

The range-spread of the sampled clutter patch is 2T where T is the time duration of the transmitted waveform code.

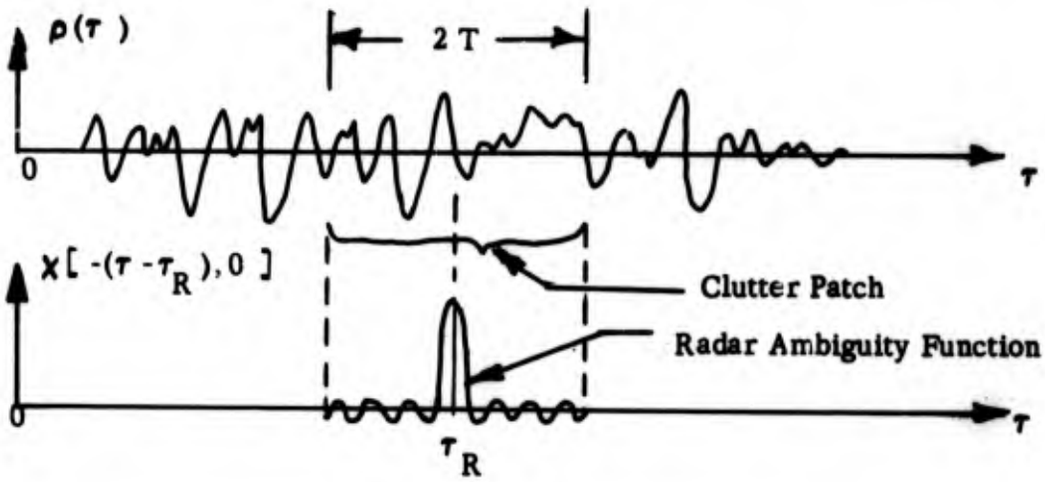

$$\rho_R(\tau) \triangleq \rho(\tau)\chi[-(\tau - \tau_R), 0]; \quad |\tau - \tau_R| \leq T$$

FIGURE 2-17 - WEIGHTED REFLECTION DENSITY

Thus, the instantaneous output

$$v_R = e^{j\omega_o \tau_R} \int_{-\infty}^{\infty} \rho_R(\tau) e^{-j\omega_o \tau} d\tau \qquad (2-4)$$

contains contributions from range-delays extending over the entire extent of the clutter patch centered at range-delay, τ_R.

The instantaneous clutter power output is *

$$|v_R|^2 = \int_{-\infty}^{\infty}\int \rho^*_R(t)\rho_R(t') e^{j\omega_o(t-t')} dtdt' \qquad (2-5)$$

*The asterisk denotes the complex conjugate.

which, letting $t' = t + \tau$ and re-arranging the double integral, may be expressed as

$$|v_R|^2 = \int_{-\infty}^{\infty} \chi_{\rho_R}(\tau, 0) e^{-j\omega_o \tau} \, d\tau \qquad (2\text{-}6)$$

where we have defined

$$\chi_{\rho_R}(\tau, 0) \triangleq \int_{-\infty}^{\infty} \rho^*_R(t) \rho_R(t + \tau) dt \qquad (2\text{-}7)$$

as the complex autocorrelation function of the weighted clutter patch reflection density. (This is a special case of the clutter patch complex ambiguity function described subsequently in this report).*

2.2.1 PARTIALLY COHERENT SCATTERING

The instantaneous clutter power output (2- 6) is neither pure noise scattering nor coherent scattering. It is the total instantaneous clutter response, including both amplitude and phase characteristics of the radar waveform and the clutter reflection density.

The spatial correlation of the clutter patch defined by (2- 7) has a range correlation length defined by

$$\tau_c \triangleq \frac{\int_{-\infty}^{\infty} |\chi_{\rho_R}(\tau, 0)|^2 \, d\tau}{|\chi_{\rho_R}(0, 0)|^2} \qquad (2\text{-}8)$$

expressed in terms of the magnitude of the patch correlation function. However, the patch correlation function is complex

$$\chi_{\rho_R}(\tau, 0) = |\chi_{\rho_R}(\tau, 0)| e^{j\eta(\tau)} \qquad (2\text{-}9)$$

---

* Section 2.3, Equation (2-29)

and is specified, in addition, by the phase characteristic, $\eta(\tau)$. Using (2- 9) in (2- 6), the instantaneous clutter power output may be also written as

$$|v_R|^2 = \int_{-\infty}^{\infty} |\chi_{\rho_R}(\tau,0)| e^{j[\eta(\tau) - \omega_o \tau]} d\tau \qquad (2\text{-}10)$$

which is seen to give appreciable response when the oscillatory factor, $\eta(\tau) - \omega_o\tau$, fluctuates at a rate comparable to the magnitude variations of the patch correlation function. Specifically, when $\tau_c > 1/f_o$ the clutter power output is due mainly to those portions of the integral (2- 10) which have stationary phase. This occurs when the slope of the phase characteristic of the patch correlation function equals the radar radian frequency,

$$\eta'(\tau) = \omega_o. \qquad (2\text{-}11)$$

From the property of complex correlation functions

$$\chi_{\rho_R}(\tau,0) = \chi^*_{\rho_R}(-\tau,0), \qquad (2\text{-}12)$$

it is determined that

$$|\chi_{\rho_R}(\tau,0)| = |\chi_{\rho_R}(-\tau,0)| \qquad (2\text{-}13)$$

$$\eta(\tau) = -\eta(-\tau), \qquad (2\text{-}14)$$

the magnitude of the patch correlation function is even whereas its phase has odd symmetry. In addition, the value of the phase at $\tau = 0$ is zero (or $k\,2\pi$ for $k = 0, \pm 1, \pm 2, --$).

The amplitude and phase characteristics of the patch correlation function are depicted in Figure 2-18 The phase characteristic is approximated as a linear ramp defined over a region equal to the spatial patch correlation length, τ_c. The behavior of the phase characteristic outside this region is unknown at this writing and is not made accountable herein. However, we assume a model in

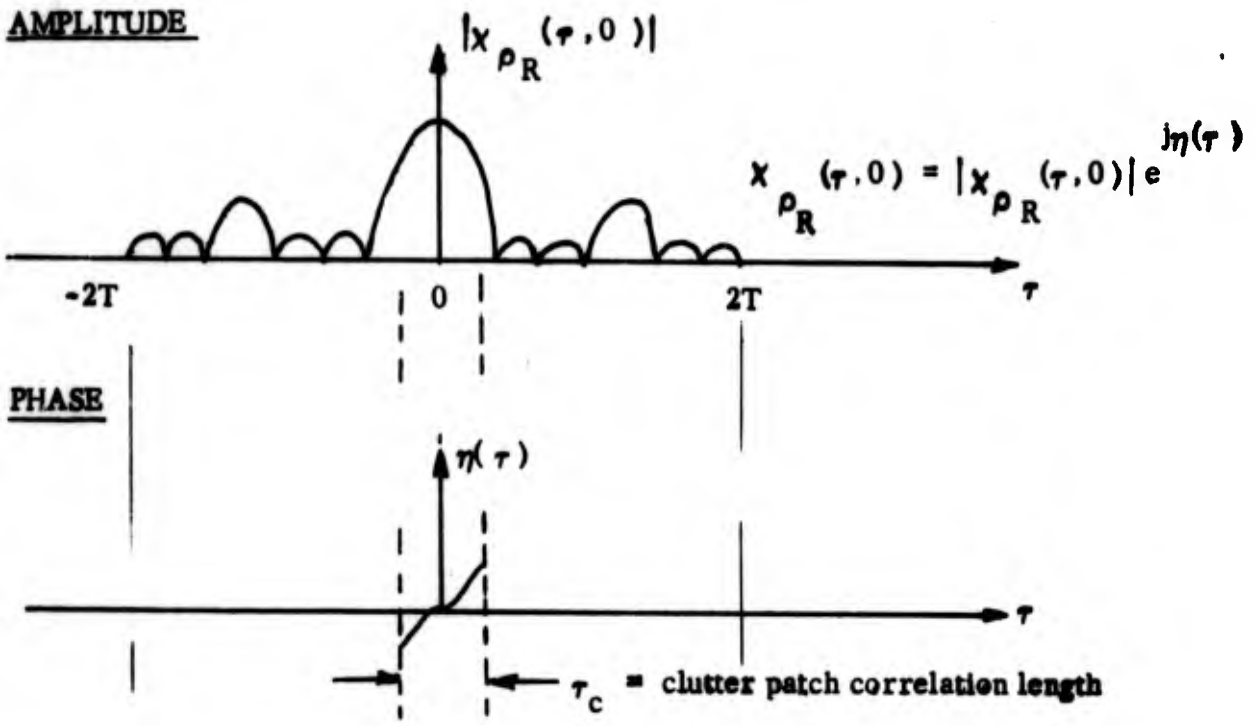

PHASE CHARACTERISTIC ASSUMED FOR COMPARISON OF SIGNAL PROCESSING TECHNIQUE

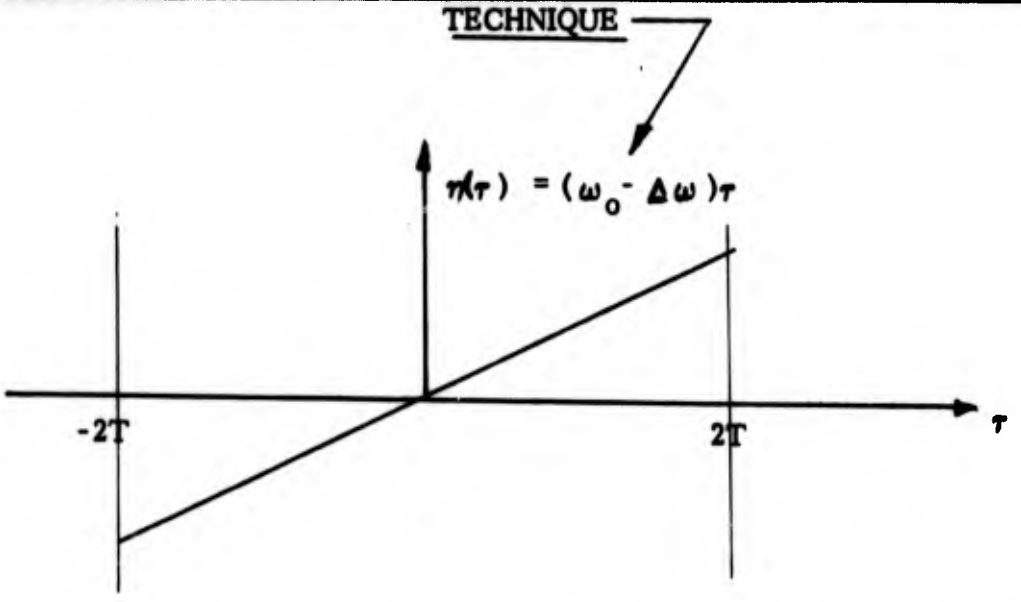

FIGURE 2-18- CLUTTER PATCH COMPLEX AUTOCORRELATION FUNCTION

which a phase ramp of arbitrary slope extends over the entire phase plane over which the correlation function exists, cf. Figure 2-18 This model is by no means rigorous. It is intended to provide a means for comparison of various signal processing techniques in a reasonably tractable manner, and it serves to demonstrate the primary importance of phase.

The phase ramp is given by

$$\eta(\tau) = (\omega_o - \Delta\omega)\tau \qquad (2\text{-}15)$$

where $\Delta\omega$ is an incremental slope, or frequency shift relative to the transmitted frequency. From (2-10), the instantaneous clutter power output becomes

$$|v_R|^2 = \int_{-\infty}^{\infty} |\chi_{\rho_R}(\tau,0)| e^{-j\Delta\omega\tau} d\tau . \qquad (2\text{-}16)$$

Maximum output, or phase-coherent scattering, occurs when (2-11) applies, i.e., when $\Delta f = 0$. Uncorrelated scattering is said to occur when the scatterers are phase-coherent at a frequency shift $|\Delta f| > 1/\tau_c$.

2.2.2 EXAMPLE

Uniform clutter patch: $|\rho(\tau)| = |\rho| \quad ; \quad |\tau - \tau_R| \leq T$

Phase-coherent at frequency: $f_o - \Delta f$

Carrier frequency: f_o

Radar Code: Simple pulse = rect t/T

then

$$\rho_R(\tau) = |\rho|\,|\chi[-(\tau - \tau_R), 0]| e^{j[(\omega_o - \Delta\omega)\tau + b]} \qquad (2\text{-}17)$$

$$\chi(t,0) = \chi(0,0)(1 - |t|/T) \qquad (2\text{-}18)$$

$$\chi_{\rho_R}(\tau,0) = e^{j(\omega_o - \Delta\omega)\tau} |\chi_{\rho_R}(\tau,0)|$$

$$= e^{j(\omega_o - \Delta\omega)\tau} |\rho|^2 \int_{-\infty}^{\infty} |\chi(t,0)||\chi(t+\tau,0)|\, dt. \qquad (2\text{-}19)$$

Hence, from (2-16)

$$|v_R|^2 = |\chi(0,0)|^2 |\rho|^2 T^2 \operatorname{sinc}^4 \Delta f T. \qquad (2\text{-}20)$$

From (2-8):

$$\tau_c \approx T.$$

But, peak signal power at range-delay, τ_R, is $|\chi(0,0)|^2$. Therefore, peak signal-to-instantaneous clutter power output is

$$S/C \triangleq |\chi(0,0)|^2 / |v_R|^2$$

$$= \frac{1}{|\rho|^2 T^2 \operatorname{sinc}^4 \Delta f T} \qquad (2\text{-}21)$$

The C/S ratio is plotted in Figure 2-19.

In this example, the scattering is incoherent, or uncorrelated, when the scatterers are phase-coherent at a frequency shift $\Delta f \geq 1/T$ from the carrier frequency. Since a uniform clutter patch was assumed, the spatial correlation length τ_c approximates the pulse length T transmitted by the radar. The worst S/C is $1/|\rho|^2 T^2$ which occurs for coherent scattering when $\Delta f = 0$. For coherent scattering, the S/C increases with the square of the transmitted bandwidth, i.e.,

$$C/S = \frac{|\rho|^2 T^2 \operatorname{sinc}^4 \Delta f T}{}$$

Code: Simple Pulse

Pulse Length: T

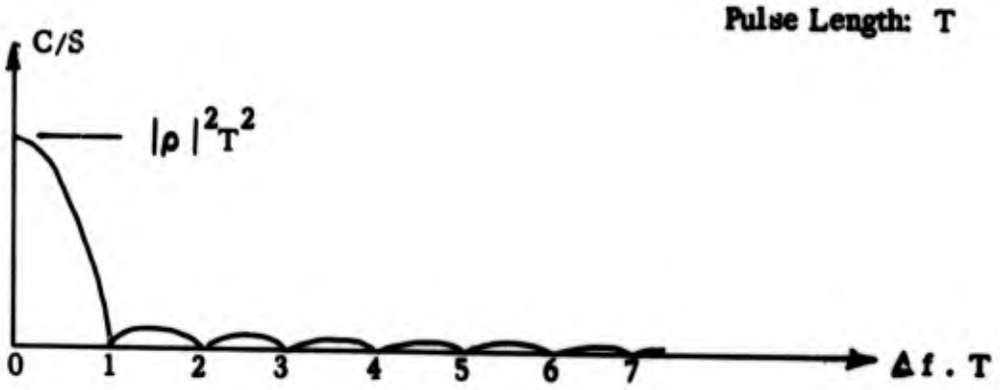

FIGURE 2-19- SIGNAL-TO-CLUTTER FOR A UNIFORM PATCH

proportional to $1/T^2$. For incoherent scattering where $\Delta f T >> 1$, the S/C is proportional to $1/(\Delta f)^4 T^2$.

2.2.3 INSTANTANEOUS INCOHERENT SCATTERING

The example of Section 2.2.2 describes the extreme case of instantaneous phase-coherent scattering from a clutter patch having a uniform amplitude reflection density over the patch extent. This produced the maximum clutter power output.

In this section, we go to the other extreme by assuming the patch correlation function is described by an impulse,

$$\chi_{\rho_R}(\tau, 0) = \chi_{\rho_R}(0,0)\delta(\tau) \qquad (2\text{-}22)$$

i.e., it is uncorrelated. Although this is impossible in nature on an instantaneous basis, the assumption together with those of Sections 2.2.1 and 2.2.2 place bounds upon the clutter responses which are attainable.

From (2-6), the instantaneous clutter power output becomes

$$|v_R|^2 = \chi_{\rho_R}(0,0) \tag{2-23}$$

$$= \int_{-\infty}^{\infty} |\rho_R(t)|^2 dt \tag{2-24}$$

$$= \int_{-\infty}^{\infty} |\rho(t)|^2 |\chi(t-\tau_R, 0)|^2 dt \tag{2-25}$$

which is observed to be the convolution of the squared magnitude clutter reflection density with the squared magnitude of the radar ambiguity function at range-delay τ_R.

For a uniform clutter patch described by

$$|\rho(\tau)| = |\rho| \; ; \; |\tau - \tau_R| \leq T, \tag{2-26}$$

the clutter power output becomes

$$|v_R|^2 = |\rho|^2 \int_{-\infty}^{\infty} |\chi(\tau, 0)|^2 d\tau$$

$$= |\rho|^2 Q(0) \tag{2-27}$$

where $|\rho|^2$ is dimensioned in reciprocal time.

The peak signal-to-clutter output is

$$S/C = \frac{|\chi(0,0)|^2}{|v_R|^2}$$

$$= \frac{|\chi(0,0)|^2}{|\rho|^2 Q(0)}$$

$$= \frac{W}{|\rho|^2} \qquad (2\text{-}28)$$

where the bandwidth is W = 1/T for a simple rectangular pulse. The signal-to-clutter ratio is observed to be proportional to the bandwidth in agreement with the incoherent independent point scatterers model, found in the literature.

2.3 CLUTTER PATCH COMPLEX AMBIGUITY FUNCTION

Recent work has shown that clutter may be de-correlated based upon frequency. Figure 2-11 describes the frequency de-correlation of rain clutter obtained from calculating the frequency correlation coefficient using ensemble averages of measured data. Similar results are obtained (Fig. 2-12) from measured on the frequency de-correlation of sea return based upon a time-average frequency correlation coefficient.

Figure 2-20 is a reproduction of work performed by Kennedy*. The figure depicts a portion of the actual measured radar cross-section of the upper section of the Vela Hotel satellite for various separate frequencies and the cross-sections by averaging over eight frequencies. The first curve shows the effects of averaging over several of the separate curves in the rear of the photograph as would occur in a frequency diversity radar.

It is evident from the photograph that the satellite (which is a spread target) is partially correlated in that there are regularities at a single frequency with varying aspect angle and there are also regularities at a single aspect angle with varying frequency. Thus, we may define the range-delay correlation of the satellite and the correlation at a single frequency as a function of aspect angle.

---

* Ref. 7

FIGURE 2-20: RADAR CROSS-SECTION

vs.

ASPECT ANGLE & FREQUENCY

We may also define the frequency correlation coefficient at a single aspect angle as a function of frequency*.

In Section 4 of this report a technique termed SPECOR is analyzed and then simulated relative to a simple pulse radar. This technique bases its clutter reduction capability upon the frequency de-correlation properties of clutter. It is a radar processing technique which actually performs the frequency correlation coefficient on each transmitted pulse.

A correlation involves a product. Referring to Fig. 2-20, if we take the product of the cross-sections resulting from two frequencies at a particular aspect angle, the result will be a suppressed output, on the average. If we take many non-overlapping products all at the same frequency deplacement, sum the product, and normalize, we have defined and obtained a frequency correlation coefficient, cf. Figures 2-11 and 2-12.

The Woodward ambiguity function** of Figure 2-13 is strictly applicable to an ideal point target. Radar resolution is defined in terms of this ambiguity function for two ideal point targets. What definition is used when there are more than two targets present? How does one define and/or characterize a spread target, cf. Figure 2-20, or clutter which is a continuum of scatterers? By what method are the correlation properties of spread targets and clutter described? Is there an appropiate formulation which describes the interaction and effect of the particular radar processing mode employed? How do we account for the frequency correlation properties of spread targets and clutter?

We define a function, cf. Figure 2-15 and 2-16, and Figure 2-21

$$\chi_{\rho_R}(\tau, f) = \int_{-\infty}^{\infty} \rho^*_R(t)\rho_R(t+\tau)e^{j2\pi ft}\,dt \qquad (2\text{-}29)$$

termed the clutter patch complex ambiguity function which describes the spatial and frequency correlation properties of the sampled clutter patch, $\rho_R(t)$, cf. (2-3), in much the same manner that the radar ambiguity function describes the range-Doppler correlation properties of a radar waveform code. It is important to note, however, that the frequency, f, is not the Doppler frequency but rather the frequency parameter accounting for the frequency correlation characteristics of spread targets, or clutter.

The following properties of the sampled clutter patch are of interest:

PROPERTY 1

$$\int_{-\infty}^{\infty}\int |\chi_{\rho_R}(\tau, f)|^2 d\tau\, df = |\chi_{\rho_R}(0,0)|^2 = \left|\int_{-\infty}^{\infty} |\rho_R(\tau)|^2 d\tau\right|^2$$

$$= \left|\int |\rho(t)|^2 \, |\chi(t-\tau_R, 0)|^2 \, dt\right|^2 \qquad (2\text{-}30)$$

* See Figures 2-11 and 2-12. Also, see Refs. 2, 4, 5, 6

** Refs. 8, 9, 10

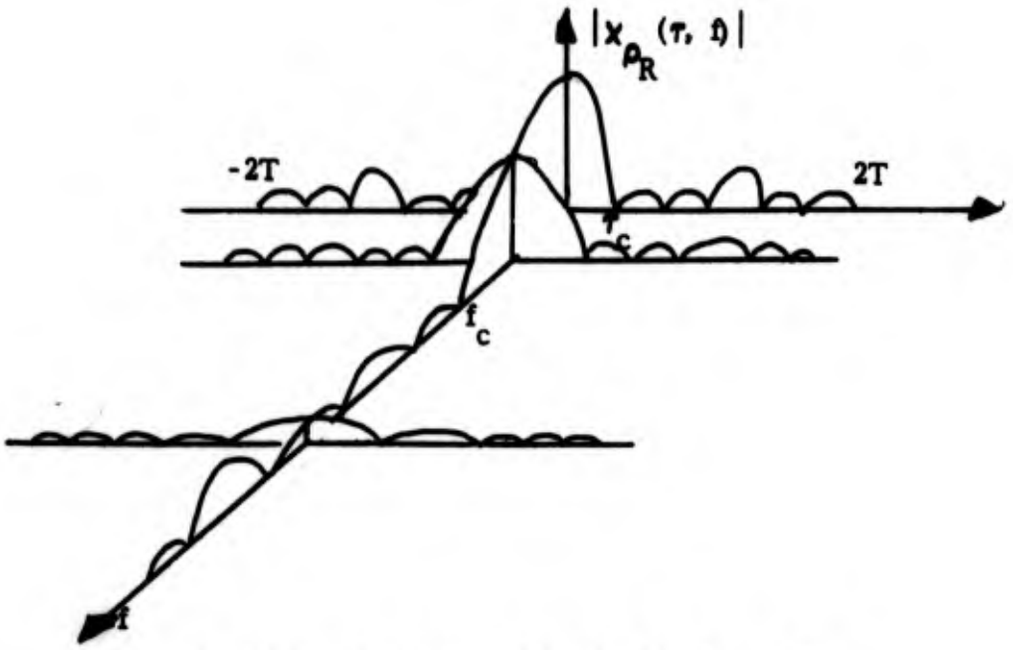

- Complex clutter reflection density: $\rho(t)$
- Complex clutter patch reflection density (patch at τ_R range-delay)

$$\rho_R(t) = \rho(t)\,\chi\,[-(t-\tau_R),\ 0]$$

- Complex clutter patch ambiguity function

$$\chi_{\rho_R}(\tau, f) = \int_{-\infty}^{\infty} \rho^*_R(t+\tau) e^{j2\pi ft}\, dt$$

- Clutter patch spatial correlation length

$$\tau_c = \int_{-\infty}^{\infty} |\chi_{\rho R}(\tau, 0)|^2 d_\tau / |\chi\rho_R(0,0)|^2$$

- Clutter patch frequency correlation length

$$f_c = \int_{-\infty}^{\infty} |\chi_{\rho_R}(0, f)|^2 df / \chi_{\rho_R}(0,0)|^2$$

FIGURE 2-21 - CLUTTER PATCH AMBIGUITY FUNCTION

The patch ambiguity volume is a constant proportional to square of the "sampled intrinsic radar cross-section", $\chi_{\rho_R}(0,0)$, of the clutter patch at range-delay, τ_R.

PROPERTY 2

The spatial (range-delay) correlation length of the clutter patch is defined by

$$\tau_c \triangleq \frac{\int_{-\infty}^{\infty} |\chi_{\rho_R}(\tau,0)|^2 d\tau}{|\chi_{\rho_R}(0,0)|^2} \qquad (2\text{-}31)$$

PROPERTY 3

The frequency correlation length of the clutter patch is defined by

$$f_c \triangleq \frac{\int_{-\infty}^{\infty} |\chi_{\rho_R}(0,f)|^2 df}{|\chi_{\rho_R}(0,0)|^2} . \qquad (2\text{-}32)$$

A patch ambiguity function is shown in Figure 2-21 .

2.4 A STATISTICAL MODEL

The matched filter output due to clutter prior to any (nonlinear) detection process is given by

$$v(t) = e^{j\omega_o t} \int_{-\infty}^{\infty} \rho(\tau)\chi(t-\tau,0)e^{-j\omega_o \tau} d\tau . \qquad (2\text{-}1)$$

This represents the entire range-spread of the clutter and is a time function which has a spectrum

$$V(f) = \hat{\rho}(f)\,\hat{\chi}(f-f_o,0) \qquad (2\text{-}33)$$

where the spectrum of the clutter reflection density is

$$\hat{\rho}(f) = \int_{-\infty}^{\infty} \rho(\tau) e^{-j2\pi f \tau} \, d\tau \qquad (2\text{-}34)$$

and the spectrum of the ambiguity function is

$$\hat{\chi}(f,0) = \int_{-\infty}^{\infty} \chi(\tau,0) e^{-j2\pi f \tau} \, d\tau. \qquad (2\text{-}35)$$

Considering the reflection density as a random function, we may obtain the ensemble mean power output, (the output of a square-law detector). Our

$$\overline{\Gamma(t)} \triangleq \overline{|v(t)|^2} \qquad (2\text{-}36)$$

interest is in the spectrum of (2-36)

$$\overline{\gamma}(f) = \int_{-\infty}^{\infty} V^*(\beta) V(\beta + f) \, d\beta$$

$$= \int_{-\infty}^{\infty} \overline{\hat{\rho}^*(\beta) \hat{\rho}(\beta + f) \chi^*(\beta - f_o, 0) \chi(\beta - f_o + f, 0)} \, d\beta. \qquad (2\text{-}37)$$

By definition of the reflection density as an aggregate of complex point scatterers,

$$\rho(\tau) \triangleq \sum_{n=0}^{N-1} \rho_n \delta(\tau - \tau_n) \qquad (2\text{-}38)$$

where

$$\rho_n = |\rho_n| e^{j\beta_n}, \qquad (2\text{-}39)$$

a representation useful for computer simulation purposes is obtained.

The spectrum of (2-38)

$$\hat{\rho}(f) = \sum_{n=0}^{N-1} \rho_n e^{-j2\pi f \tau_n} \qquad (2\text{-}40)$$

has an autocorrelation

$$\overline{\hat{\rho}^*(\beta)\hat{\rho}(\beta+f)} = \sum_{m,n=0}^{N-1}\sum \rho^*_m \rho_n \overline{e^{j2\pi\beta\tau_m} e^{-j2\pi(\beta+f)\tau_n}}. \qquad (2\text{-}41)$$

If the range-delay at which the scatterers appear is independent of the value of the scatterer reflection, the autocorrelation may be written as

$$\overline{\hat{\rho}^*(\beta)\hat{\rho}(\beta+f)} = \sum_{m,n=0}^{N-1}\sum \overline{\rho^*_m \rho_n}\ \overline{e^{j2\pi\beta\tau_m} e^{-j2\pi(\beta+f)\tau_n}}. \qquad (2\text{-}42)$$

But the joint characteristic function of the exponential in (2-42) is

$$C(\beta, \beta+f) \triangleq \overline{e^{j2\pi\beta\tau_m} e^{-j2\pi(\beta+f)\tau_n}}$$

$$= \int\int p(\tau_m, \tau_n) e^{j2\pi\beta\tau_m} e^{-j2\pi(\beta+f)\tau_n} d\tau_m d\tau_n \qquad (2\text{-}43)$$

The characteristic function is defined by

$$C(f) \triangleq \overline{e^{-j2\pi f\tau}} = \int_{-\infty}^{\infty} p(\tau) e^{-j2\pi f\tau} d\tau. \qquad (2\text{-}44)$$

In (2-43), $p(\tau_m, \tau_n)$ is the joint probability density for the range-delay of two scatterers; in (2-44) $p(\tau)$ is the probability density for the range-delay of a scatterer. Thus, we write the spectrum of the ensemble-mean power output as, cf. (2-37):

$$\overline{\gamma(f)} = \sum_{m\neq n=0}^{N-1}\sum \overline{\rho^*_m \rho_n} \int_{-\infty}^{\infty} C(\beta, \beta+f)\hat{\chi}^*(\beta - f_o, 0)\hat{\chi}(\beta - f_o, 0) d\beta$$

$$+ \sum_{n=0}^{N-1} \overline{|\rho_n|^2} \cdot C(f) \int_{-\infty}^{\infty} \hat{\chi}^*(\beta, 0)\hat{\chi}(\beta+f, 0) d\beta. \qquad (2\text{-}45)$$

The first term represents the cross-correlation among the scatterers. If the scatterer positions are independent, or alternately if the reflection coefficients are independent, the first term goes to zero. However, even if the reflection coefficients are correlated but the scatterer range-delays are independent, then

$$C(\beta, \beta + f) = C^*(\beta)C(\beta + f) \qquad (2\text{-}46)$$

and the first term of (2-45) will nonetheless tend to zero resulting in

$$\overline{\gamma(f)} = \sum_{n=0}^{N-1} \overline{|\rho_n|^2}\, C(f) \int_{-\infty}^{\infty} \hat{\chi}^*(\beta, 0)\hat{\chi}(\beta + f, 0)\, d\beta. \qquad (2\text{-}47)$$

Noting that

$$Q(f) \triangleq \int_{-\infty}^{\infty} \hat{\chi}^*(\beta, 0)\hat{\chi}(\beta + f, 0)\, d\beta = \int_{-\infty}^{\infty} |\chi(\tau, 0)|^2 e^{-j2\pi f\tau}\, d\tau \qquad (2\text{-}48)$$

and

$$\sum_{n=0}^{N-1} \overline{|\rho_n|^2} = N\overline{|\rho|^2} \qquad (2\text{-}49)$$

where $\overline{|\rho|^2}$ is proportional to the ensemble-mean clutter cross-section density, the ensemble-mean power output of the matched filter radar and its spectrum may be written, respectively, as

$$\overline{\Gamma(t)} = \overline{|v(t)|^2} = N\overline{|\rho|^2} \int_{-\infty}^{\infty} p(\tau)\, |\chi(t - \tau, 0)|^2\, d\tau \qquad (2\text{-}50)$$

and

$$\overline{\gamma(f)} = N\overline{|\rho|^2}\, C(f)Q(f). \qquad (2\text{-}51)$$

These results express a noise-like model for clutter scattering in which the mean power output is proportional to the convolution of the range-delay probability law with the magnitude-square of the ambiguity function. The expressions provide the basis of the clutter simulation for scattering without specular in Section 4.

2.5 SPATIALLY DISTRIBUTED RANDOM CLUTTER WITH SPECULARS

Clutter theory treated on a statistical basis usually results in a noise-model for clutter in which all genuine specular are averaged out. A probability description of the clutter scatterers is obtained where large responses can occur only due to the tails of the probability law, cf. Section 2.4.

The radar return from a collection of scatterers is a mixture of noise-like and specular contributions. The noise-like contribution is the sum of all the elemental

intensities, i.e., the total noise radar cross-section in the radar spatial resolution cell. The phase of the scatterers due to their reflection properties and their location relative to the radar is absent, on the average. In addition, the radar return from these noise scatterers is insensitive to the radar operating frequency.

The pure speculars are due to aggregates of scatterers in which there is phase addition, cf. Figs. 2-7 and 2-8, of the vectors. Speculars result from the linear sum of the amplitudes of the element scatterers. This produces a large response causing false alarms above the radar output threshold. Coherent (specular) scattering occurs when the clutter scattering surface is such that distances to various portions of the surface provide in-phase addition at the frequency of operation. Coherent scattering is sensitive to aspect changes if it is due to a large surface.

In the real world, pure incoherent (noise) scattering and pure coherent (specular) scattering do not exist. Rather, a situation of partially coherent scattering bounded by pure incoherent and pure coherent scattering is the case.

2.6 SIMPLIFIED MODELS FOR PARTIALLY COHERENT CLUTTER

The pre-detection response of a (matched filter) radar operating at carrier frequency, f_o, is given by (2-1). The instantaneous response at range-delay, τ_R, is given by (2-2) which is depicted in Figures 2-2 through 2-8. The instantaneous video output for range-delay, τ_R, becomes

$$|v_R|^2 = \left| \int \rho_R(\tau) e^{-j\omega_o \tau} \, d\tau \right|^2 \qquad (2\text{-}52)$$

where we have defined

$$\rho_R(\tau) \triangleq \rho(\tau) \chi(\tau_R - \tau, 0). \qquad (2\text{-}3)$$

In our model, we represent the clutter by a distribution of point scatterers along a line in the time-delay dimension, in which case, (2-3) becomes

$$\rho_R(\tau) = \sum_n^N |\rho_n| e^{j\beta(\tau_n)} \chi(\tau_R - \tau_n, 0) \delta(\tau - \tau_n) \qquad (2\text{-}53)$$

which is a series of ambiguity functions weighted by the amplitude $|\rho_n|$ and phase $\beta(\tau_n)$. Substituting (2-53) in (2-52), the instantaneous clutter output is

$$|v_R|^2 = \left|\sum_n^N |\rho_n| e^{j[\beta(\tau_n)-\omega_o\tau_n]} \chi(\tau_R-\tau_n, 0)\right|^2, \qquad (2\text{-}54)$$

which may be further simplified to

$$|v_R|^2 = \left|\Sigma |\rho_n| e^{-j\omega_o\tau_n} \chi(\tau_R-\tau_n, 0)\right|^2 \qquad (2\text{-}55)$$

by recognizing that the oscillatory term in the exponential controls the aggregate phase characteristics.

INCOHERENT SCATTERING

For pure incoherent noise scattering, the probability law for the distribution of the N scatterers has been found to be more, or less, uniform as depicted in Figure 2-22, cf. Fig. 3.3 of Section 3.

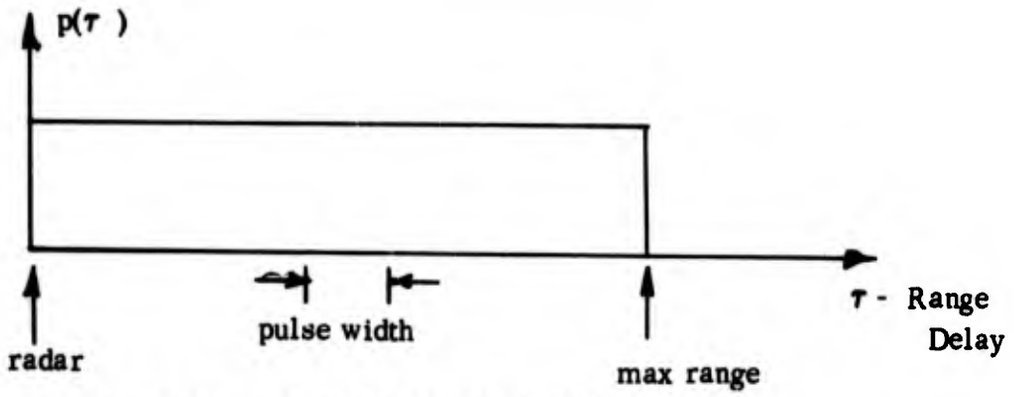

FIGURE 2-22 - INCOHERENT SCATTERING LAW

This form of law was obtained from NRL-measurement data producing the results of Section 4.

PARTIALLY COHERENT SCATTERING

For this case, the probability law should include provisions for

1) Noise scattering
2) Specular scattering
3) Speculars with varying sizes, intensities, and rate of occurrence

Methods for obtaining partially coherent scattering in a relatively simple model are shown in Figures 2-23 through 2-25. In Figure 2-23 a series of impulses placed on top of the uniform distribution provides a mixture of specular and noise scattering when the impulses are separated by an integer multiple, the reciprocal of the radar operating frequency. The impulses so spaced provide linear summation of their amplitudes, cf. Equation (2-55) and Figures 2-7 and 2-8.

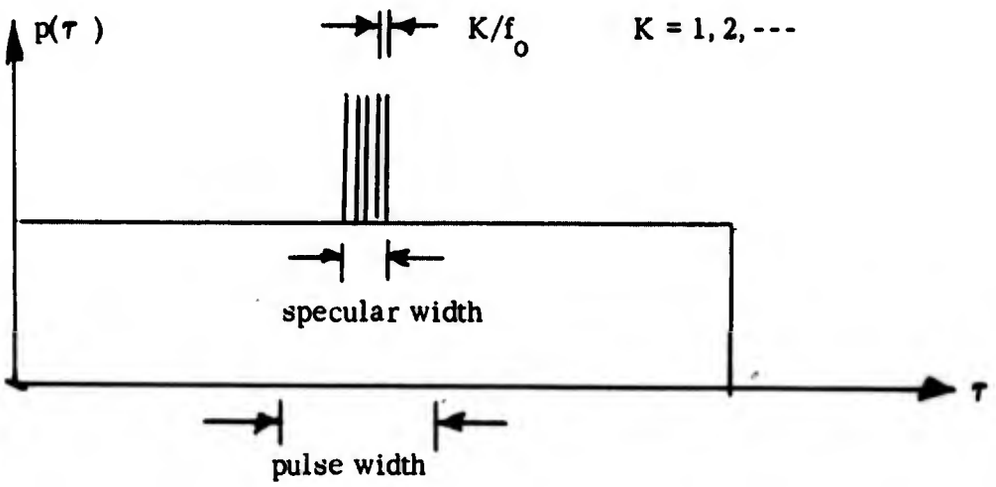

FIGURE 2-23 - PARTIALLY COHERENT SCATTERING; ONE SPECULAR IN RANGE CELL

The shape and size of the specular relative to the background noise scattering may take on various forms in the mixed probability laws of Figure 2-24.

a) Strong Specular

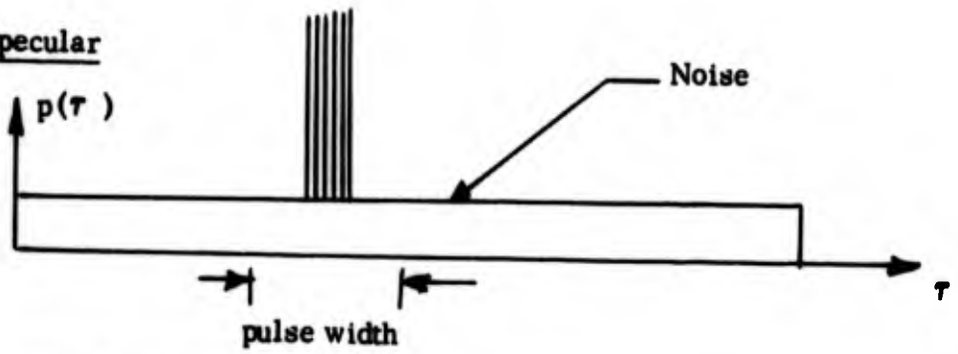

b) Tapered Strong Specular

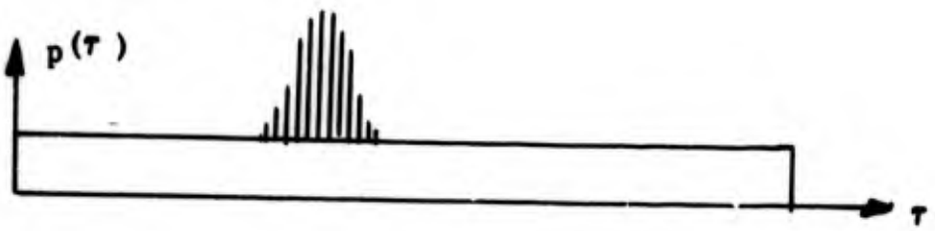

c) Narrow Weak Specular

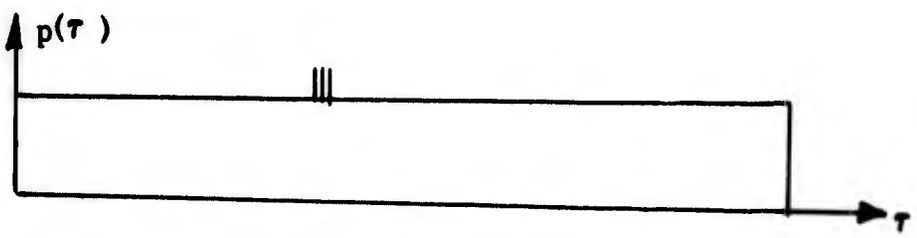

d) Strong Narrow Specular (such as round water tower)

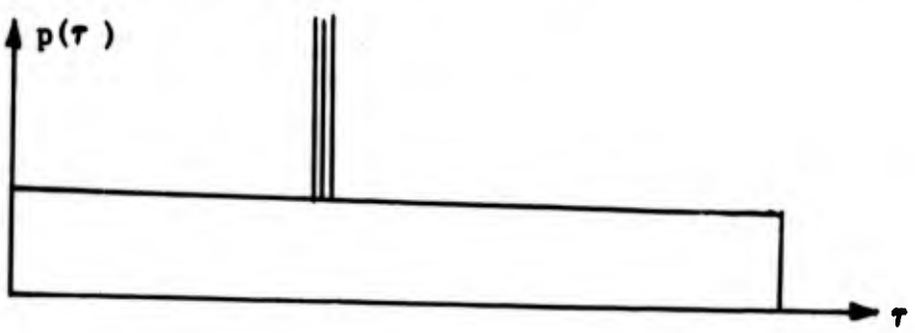

FIGURE 2 - 24 - PARTIALLY COHERENT SCATTERING:
ONE SPECULAR

Multiple speculars appearing in the resolution cell are also made accountable, as shown in Fig. 2-25. This is the case in which not only does each specular contribute to the radar output, but the interference between the speculars

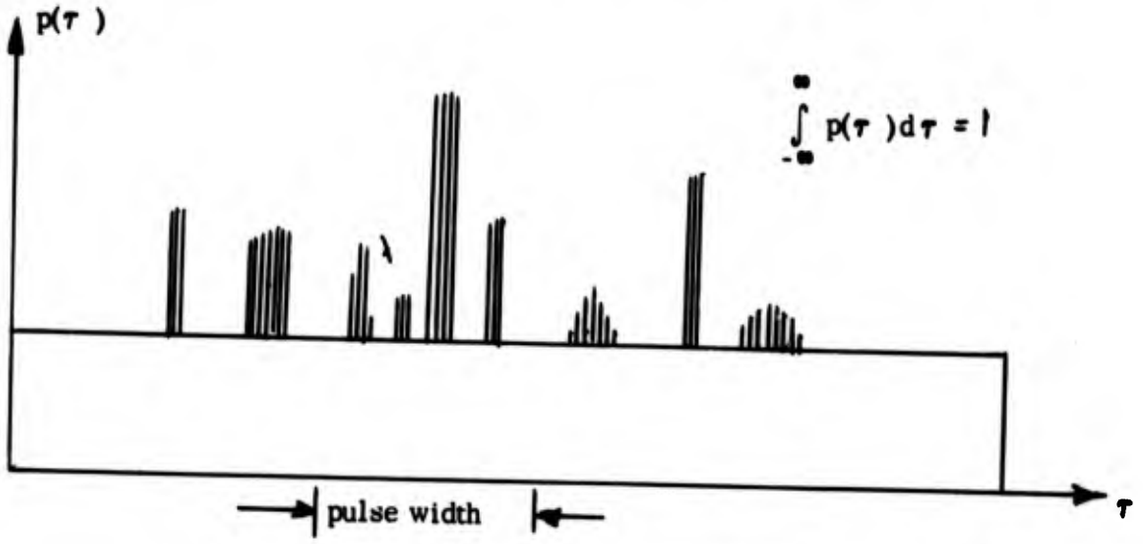

FIGURE 2-25 - PARTIALLY COHERENT SCATTERING; MULTIPLE SPECULARS

also can be a major contributor. This so-called cross-correlation of speculars is exceedingly aspect sensitive giving rise to scintillation effects when observed from a moving radar platform.

Speculars may be frequency sensitive - the specular may exist over a band of frequencies. In order to account for this effect, this type of specular is represented as aggregates of equally-spaced impulses, cf. Figure 2-26. The spacing of each impulsive series corresponds to a particular frequency. The effect is similar to a variable slot diffraction grating.

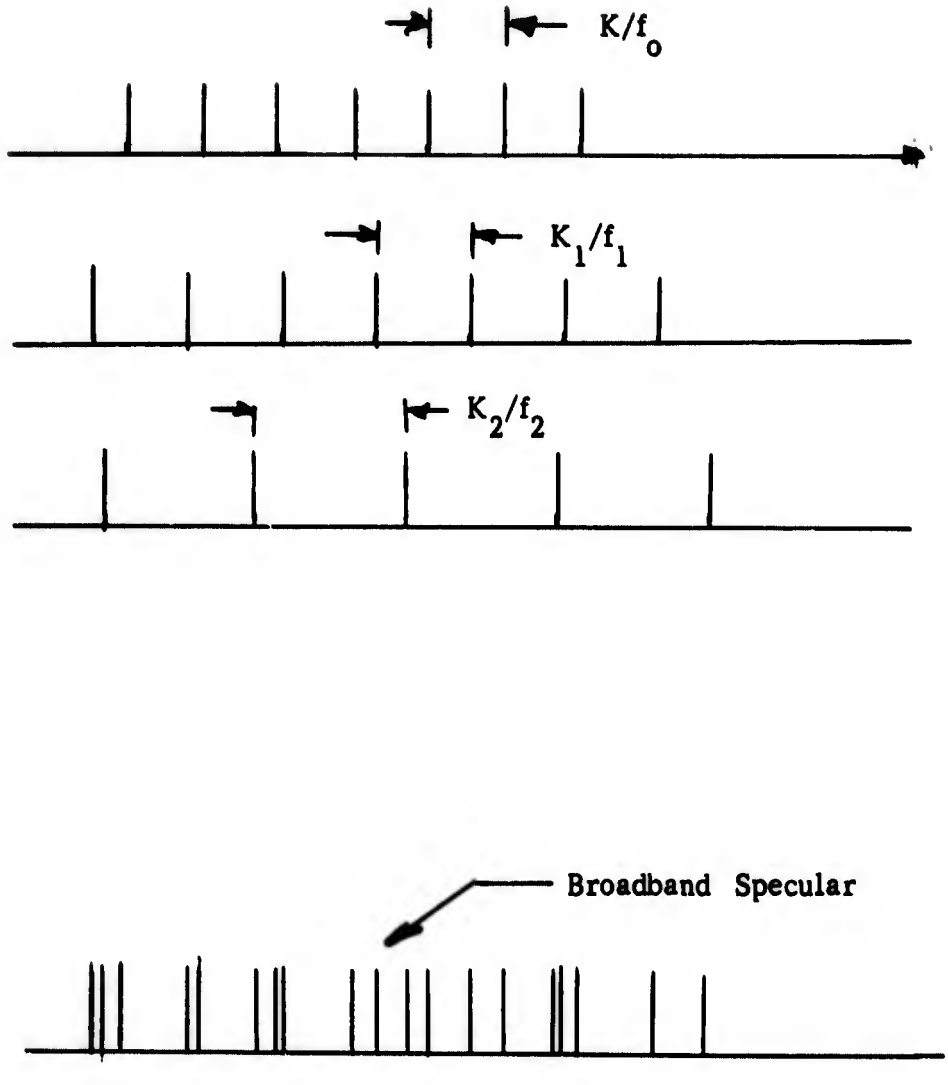

FIGURE 2-26 - BROADBAND SPECULAR REPRESENTATION

3.0 COMPUTER SIMULATION

3.1 INTRODUCTION

The stated objective of the SPECTRONICS work is to provide a simulation method for the evaluation of radar performance in a clutter environment, thereby providing a tool for the synthesis and comparison of radar processing techniques operating in a clutter environment. The method involves the use of clutter models. Work with clutter models, however, must be in relation to real data.

The Wave Propagation Branch of the Naval Research Laboratory monitored the Spectronics investigation and provided technical data which included a clutter data tape and information required for using this data in the computer simulation. The major portion of the radar instrumentation carried by the NRL aircraft used in clutter studies is the four-frequency (4F) radar system.* For each pulse transmission, the horizontal and vertical components of the backscatter are separately sensed by the antenna system, converted coherently to i-f, and fed to lin-log and linear i-f amplifier pairs which are designed to preserve amplitude and phase of the envelope of the return respectively. In the logarithmic strip, the dynamic range is compressed for easy digitalization, incoherently detected (square-law), and used as output to the range-gating and digitalization circuitry. The NRL 4F Radar System is capable of making synthetic aperture maps from which specular densities may be determined.

3.2 CLUTTER DATA

The data which was employed in the following and in Section 4 is a result of the radar amplitude (square law detected) return data recorded on film over Richmond, Va. on 21 November 1967, cf. Table I.

The square law detected returns modulate the intensity of an oscilloscope which is being photographed on a trace by trace basis. The amplitude of the radar return is converted to light intensity which in turn is converted to density on a film. The distance from the edge of the film, along the width of the film, is proportional to range and the film density to amplitude. Because the film advancement between traces is comparable to the width of the light beams on the film, data smoothing occurs resulting in a loss of specular data so that the clutter information obtained tends to be incoherent or noise-like. The aircraft took data as shown on Fig. 3-1. The triangle represents the horizontal beam pattern coverage over the terrain from which data was obtained. A typical range trace of the data is shown in Fig. 3-2.

*Ref. 11

TABLE I - FLIGHT TEST PARAMETERS

Location	Richmond, Va.
Date	11/21/67
Frequency	8910 Mc
PRF	788 pps
Pulsewidth	.1 μsec
Aircraft velocity	92.6 meters/sec.
Range	2.74 Km
Recording interval (range)	24 μ sec
Recording interval (along track)	39 sec.
Sampling window (range)	.061 μsec
Sampling window (along track)	.012 sec.
Initial Range	2.74 Km
Range increment per scan	.061 μsec
Along track sampling rate	$\sim$ 155 samples/sec.

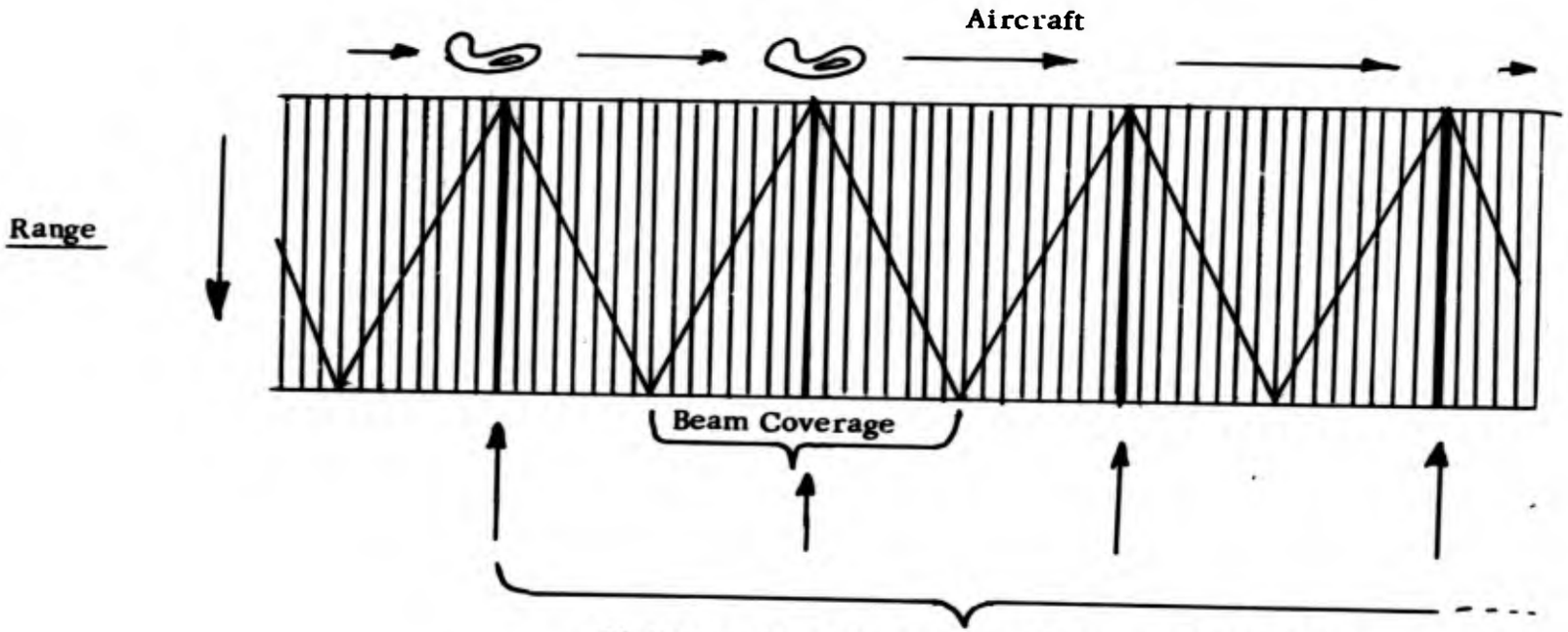

FIGURE 3-1 - TAPE DATA

3.3 DIGITAL CONVERSION

The clutter data on film is digitized by means of a microdensitomer which is scanned at constant range for the total section of recorded data. After every scan the range is incremented and the process continued until the whole film is digitized.

The format resulting from this process is an 18 bit word for each sampled window; for the Richmond data this window is .061 μ sec along range and .012 μ sec along track. Of the 18 bit word, 11 bits are used to code the density count and one more bit is used to signal the end of a scan. Double end of file marks are used to signal the end of the total film data.

3.4 THE UNPACK PROGRAM

To facilitate the use of the NRL clutter tapes with computer programs written in FORTRAN IV a special program called UNPACK was written in FAP for the IBM 7090/94 computer system. This system is rather useful for processing the clutter tapes since its word length, 36 bits, is a multiple of the NRL clutter tape word length 18 bit.

UNPACK performs the following functions:

a) Converts the 11 bit count to a 36 bit word, stripping the end of scan bit.
b) Assembles the complete scan into a FORTRAN logical record.
c) Writes a FORTRAN compatible tape. The first logical record contains the number of sample counts in the following scan and an indicator to establish whether the scan about to be read is the last in the picture or not and whether all pictures have been read.

The following logical record contains the scan itself. This process is repeated until all scans are read. With this reformatted clutter data, the programmer has at his disposal total flexibility to read under a FORTRAN IV program any desired portion or the whole of the clutter data.

3.5 THE ENSEMBLE PROGRAM

This computer program written in FORTRAN IV performs the following functions:

Using the reformatted clutter tape the program reads each scan, which was digitized at constant range and assembled in a logical record by the UNPACK program. From this data the program takes a priori selected

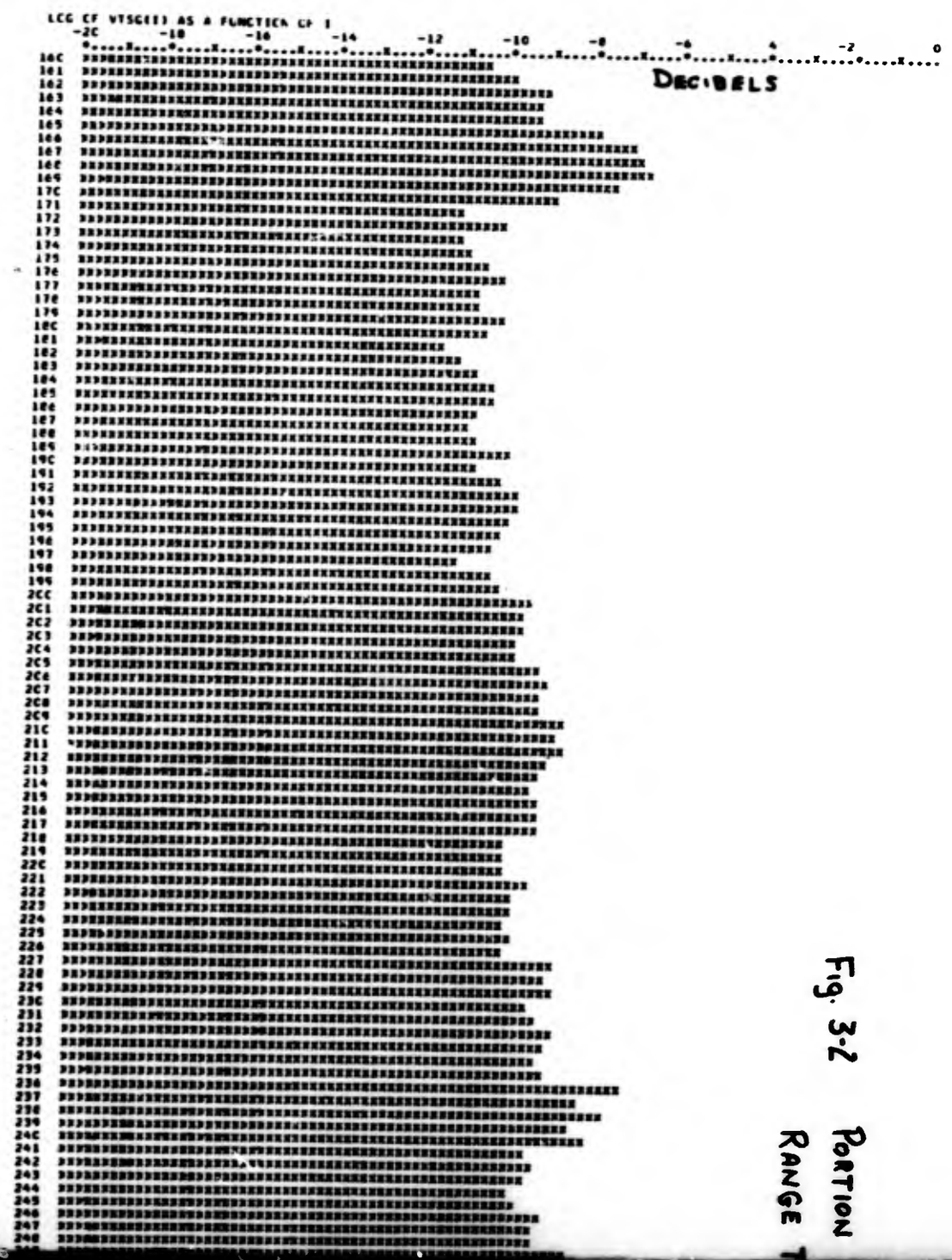

Fig. 3-2 Portion of Range

F REPRESENTATIVE
ACE FROM NRL DATA-TAPE

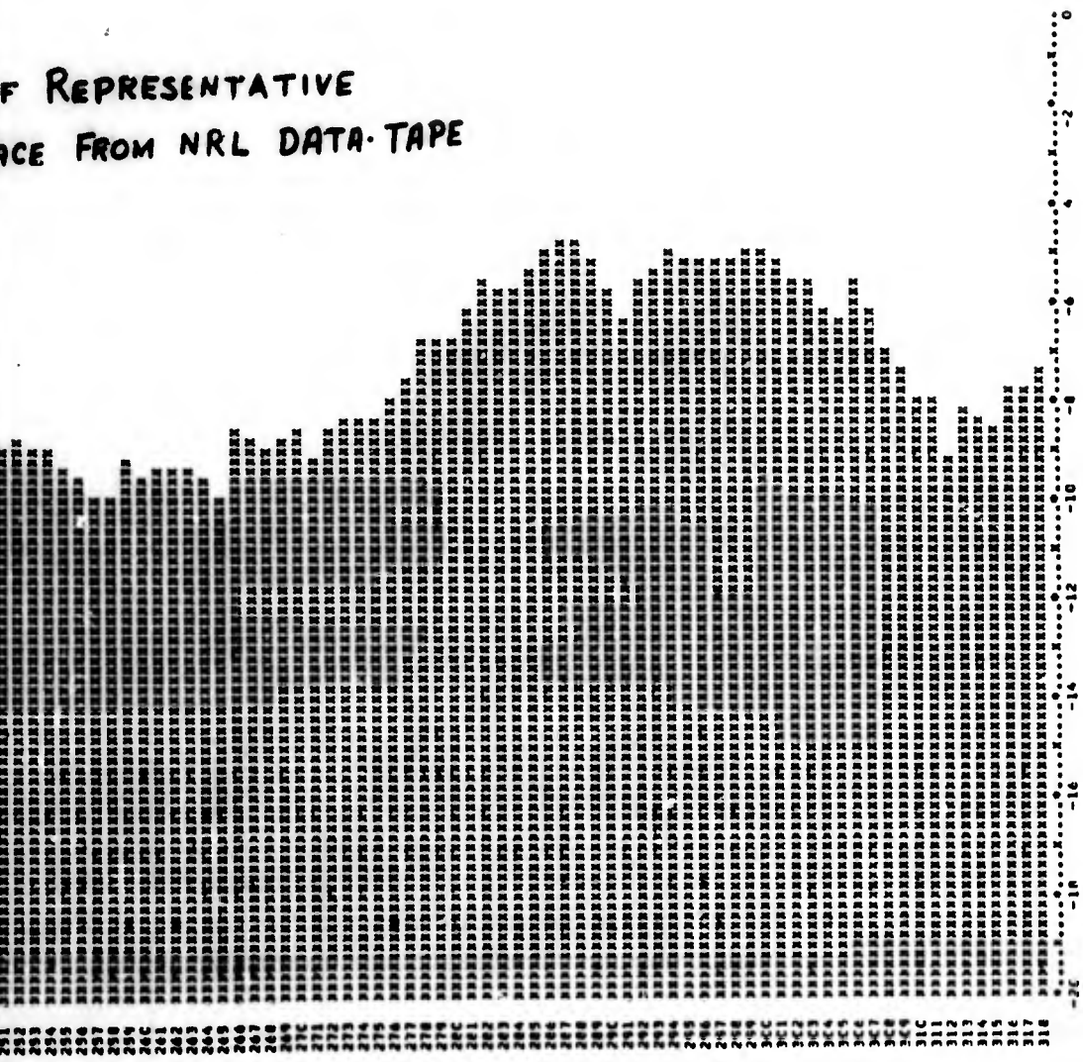

← 0.05 msec.

independent range cells. By independent we mean those range traces where the antenna illuminated terrain is completely different, as shown in Fig. 3-1. As the clutter data is recorded in density counts, it has to be converted to amplitude square. A calibration curve has been provided by the NRL Wave Propagation Branch which corresponds to the Richmond, Va. data. The ONR-CLUTTER program uses any externally supplied calibration curve to interpolate and convert from counts to amplitude square. A sample trace plotted in db is shown in Fig. 3-2.

Once the data is calibrated the program proceeds to compute the ensemble trace. With the ensemble trace its Fourier transform is computed by means of the Cooley-Tukey routine. Because we know the transmitted pulse for this particular date, its Q (f) function is also known, as given in (2-48). We then compute C (f) by solving Eqn. (2-51). Numerically this is nothing more than dividing each of the frequencies of the ensemble trace by the appropriate Q (f) value.. The Fourier transform of the resulting ratio is now performed, thus obtaining p (τ), the probability of unit scatterer at a delay τ. This p (τ) is printed by the program.

The computed scatterer position probability law obtained by this method from NRL is shown in Figure 3.3. Except for a spike near zero range which persistently showed in the data and has been ascribed to a transmitter-receiver leakage transient, the probability law assumes the roller-coaster shape of Figure 3.3. Repeated computation using additional independent NRL data reproduces the 3 db valley in the curve which is attributed to the weighting of the 4F radar antenna pattern. Removal of the antenna pattern and initial transient spike produces a uniform probability law for the range-distributed scatterers. The uniform probability law is consistent with physical interpretation and henceforth was employed in the simulation procedure which produced the results summarized in Section 4.

3.6 - THE SAMPLING PROGRAM

This program employes a uniform distribution of scatterers, but provides the option of employing any supplied p (τ) from which, by means of sampling, a number of scatterers are located. Since all scatterers are of equal strength a delay line model is constructed. In addition, the program admits the introduction of non-overlapping line groups cf. Fig. 2-25, to simulate coherent clutter, and of a target. The relative intensity of the lines can be specified, as well as that of the target and of the incoherent scatterers. The delays are put in increasing order. The program offers the option of employing the technique called SPECOR, cf. Section 4, or of using common radar techniques

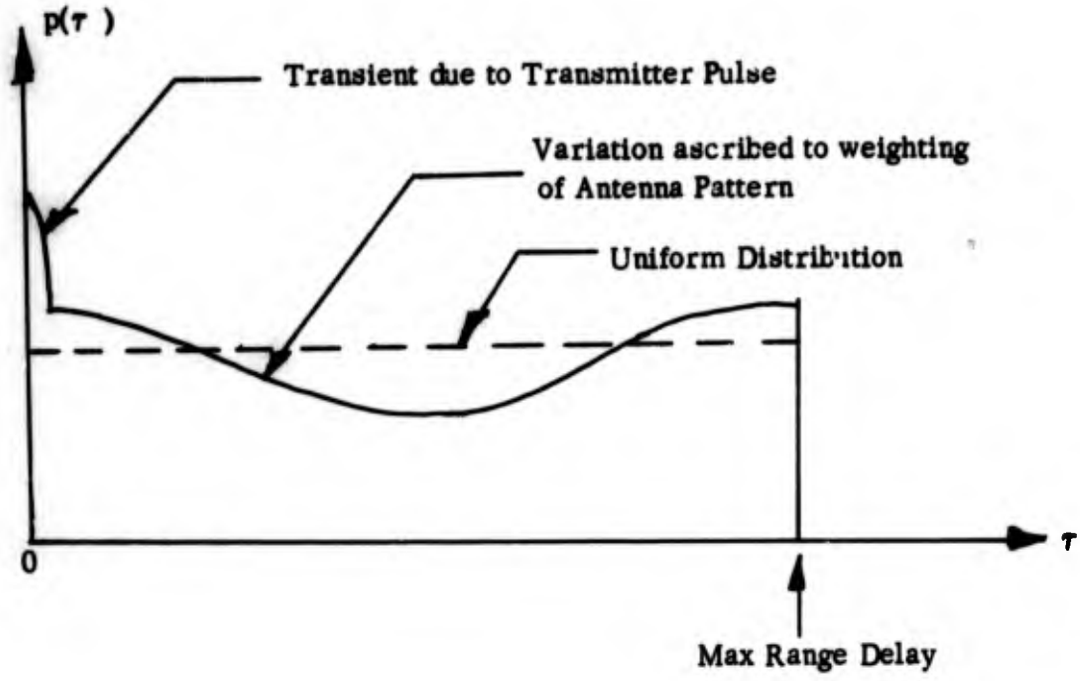

FIGURE 3.3 - SCATTERER POSITION PROBABILITY DENSITY LAW COMPUTED FROM NRL DATA

or both. The programming steps are basically similar in both cases.

The computation of the return is performed by subroutine NSUM. This subroutine receives the input data and processes it to obtain an A-scope trace. To accomplish this, the delay line is segmented into a supplied number of equal cells and the complex response corresponding to each cell is computed from the arrays containing the incoherent clutter points and the coherent lines. Since we are interested in obtaining the signal-to-clutter ratio, two computations are performed for the cells affected by the target. First a computation is performed without the target and a second computation with the target present. NSUM returns to the main program two arrays, one containing the complex returns produced by clutter alone, and another one that contains the complete returns for those cells affected by the target presence, including the effects of both target and clutter.

A subroutine called NTRCE is used to find the norm of the complex returns, and to compute the signal-to-clutter and the peak-to-clutter ratios (which should usually coincide).

Subroutine PLOT is used to plot the results as would be seen on a scope.

4.0 RADAR PERFORMANCE: Results of the Target-in-Clutter Simulation.

4.1 INTRODUCTION

This section of the report presents the results of simulating a target-in-clutter for three types of radars operating at X-band: a 5 μsec simple pulse radar, a 0.5 μsec simple pulse radar, and a spectral correlation radar with the acronym, SPECOR, * which bases its clutter suppression upon the frequency correlation properties of the clutter, cf. Figs. 2-11, 2-12, references 1, 2, 3, 5, section 2.3, and figures 2-15, 2-16. The SPECOR technique ** is specifically included in the simulation to show the power of the simulation approach for evaluation of a new radar technique. The 5 μsec pulse radars are conventional and serve as a control in the simulation experiment.

Section 4.2 describes the results of radar performance of a target in clutter for the three radar types operating against the identical target and clutter. The clutter is essentially noisy clutter devoid of speculars.

Section 4.3 describes the results of radar performance of a target-in-clutter when both noisy and specular clutter are present with the target.

4.2 INCOHERENT (NOISY) CLUTTER

Figures 4.1, 4.2 and 4.3 show the signal-to-clutter (S/C) performance of three types of radars operating against the same clutter obtained via mathematical modeling of NRL clutter measurement data, cf. Section 3. The data is shown for a single target in a portion of a range sweep (as it would appear on an A-scope). The range sweep is calibrated in decibels. The granularity of the computer output is 0.05 microseconds. Rectangular "radar windows" or pulse ambiguity functions are used to save computer time. Figures 4.1, 4.2 and 4.3 are repeat runs of the three radar types with increasing target level. The target is a point target entirely confined within 0.05 μsec.

Each figure shows

Part A: A 5 μsec pulse radar
Part B: A 0.5 μ sec pulse radar
Part C: SPECOR*

*U. S. Patent #3, 374, 478. Also see Appendix A.
**See Appendix A for a mathematical analysis of SPECOR.

Operating frequency is at X-band. The runs show the effect of the radar processing methods when operated in the identical target-clutter environment.

The 5 μsec pulse radar (Fig. 4.1-A) has the target buried in the clutter. (Note: False alarms labeled on the figures are due to computer noise and the rectangular radar window employed for simulation). Decreasing the pulse length by a factor of ten to 0.5 μsec produces a S/C of 11.07 db as shown in Figure 4.1-B. SPECOR improves the S/C to 14.62 db as shown in Figure 4.1-C. It is noted that the pulse processed in SPECOR is 5 μsec, i. e., a narrow processing bandwidth.

Figure 4.2 depicts a similar situation with a somewhat stronger target. The target from the 5 μ sec radar is more visible although target breakup is evident due to the low S/C ratio where interaction with the clutter background is present. Using the same target and clutter, the 0.5 μsec radar output is clearly visible in Figure 4.2-B due to the increased S/C = 18.98 db. The SPECOR technique (Figure 4.2-C) again displays the 5 μsec narrow processing bandwidth with a still higher S/C = 29.21 db which is approximately 10 db higher than the 0.5 μ sec radar.

Finally, Figure 4.3 shows the effect for the three radars all operating against the same clutter with a very strong target. The 5 μsec radar (Figure 4.3-A) has a S/C = 19.23 db; the 0.5 μsec radar (Figure 4.3-B) is again approximately 10 db better; the SPECOR technique (Figure 4.3-C) has a S/C = 48.4 db which is 20 db better than the 0.5 μ sec radar. The results are tabulated in Table II.

Table II

Signal-to-Clutter Comparison

Figure / Target	A 5 μsec radar	B 0.5 μsec radar	C SPECOR
4.1 Weak	4.28 db	11.07 db	14.62 db
4.2 Med.	8.32 db	18.98 db	29.21 db
4.3 Strong	19.28 db	28.55 db	48.40 db

FIG. 4.1-A

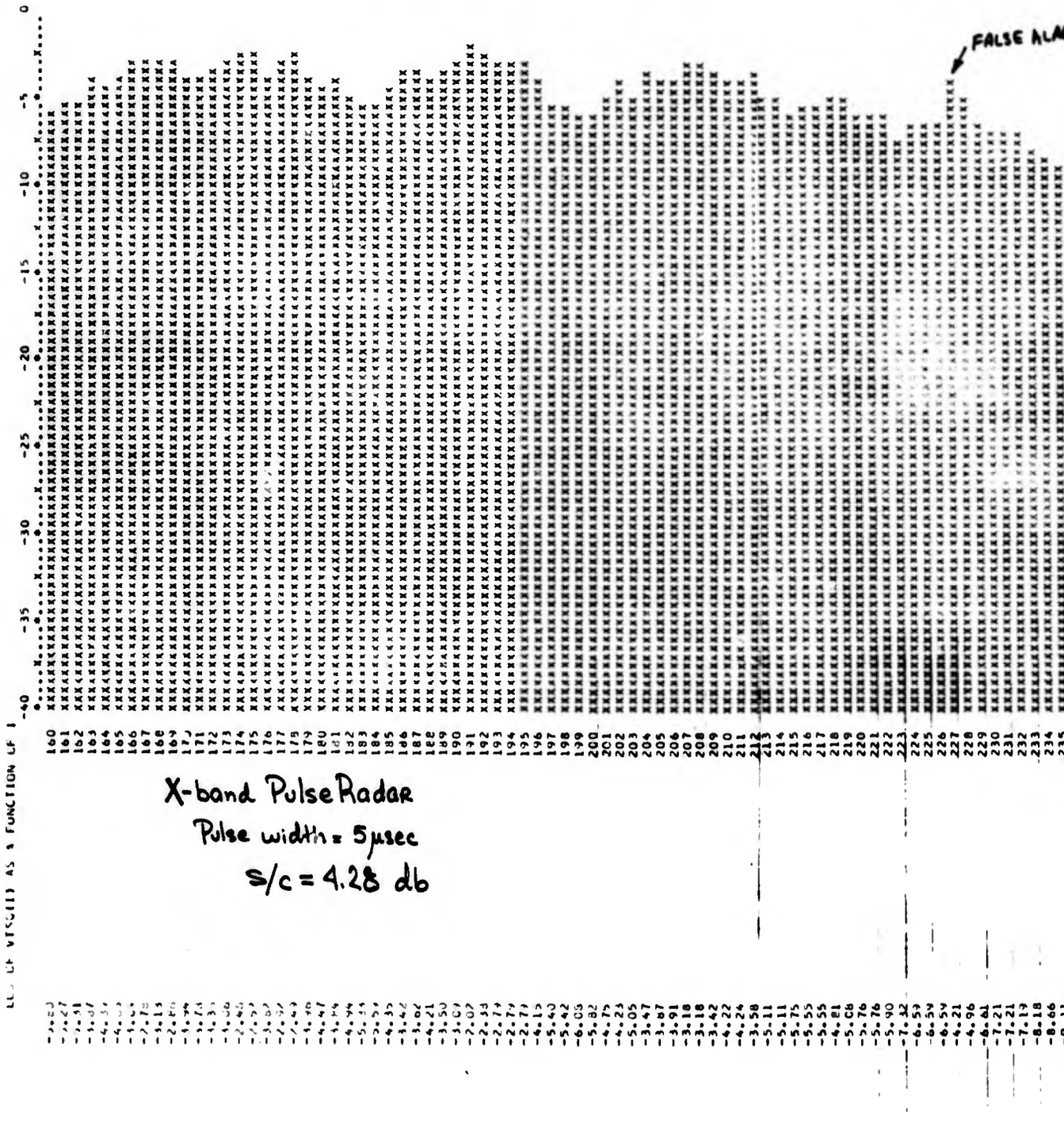

A

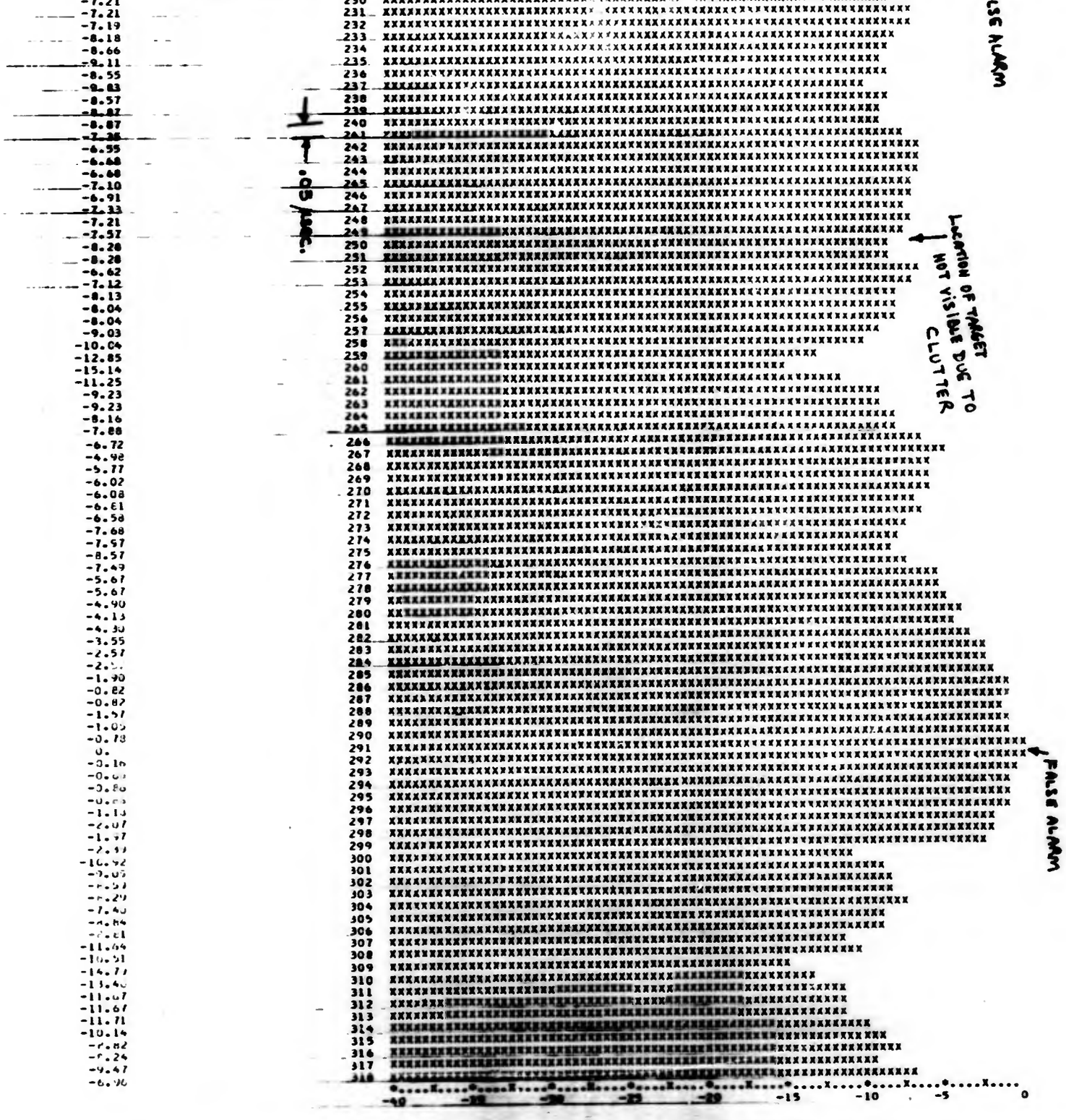
FALSE ALARM
LOCATION OF TARGET NOT VISIBLE DUE TO CLUTTER
FALSE ALARM
-40
-35
-30
-25
-20
-15
-10
-5
0

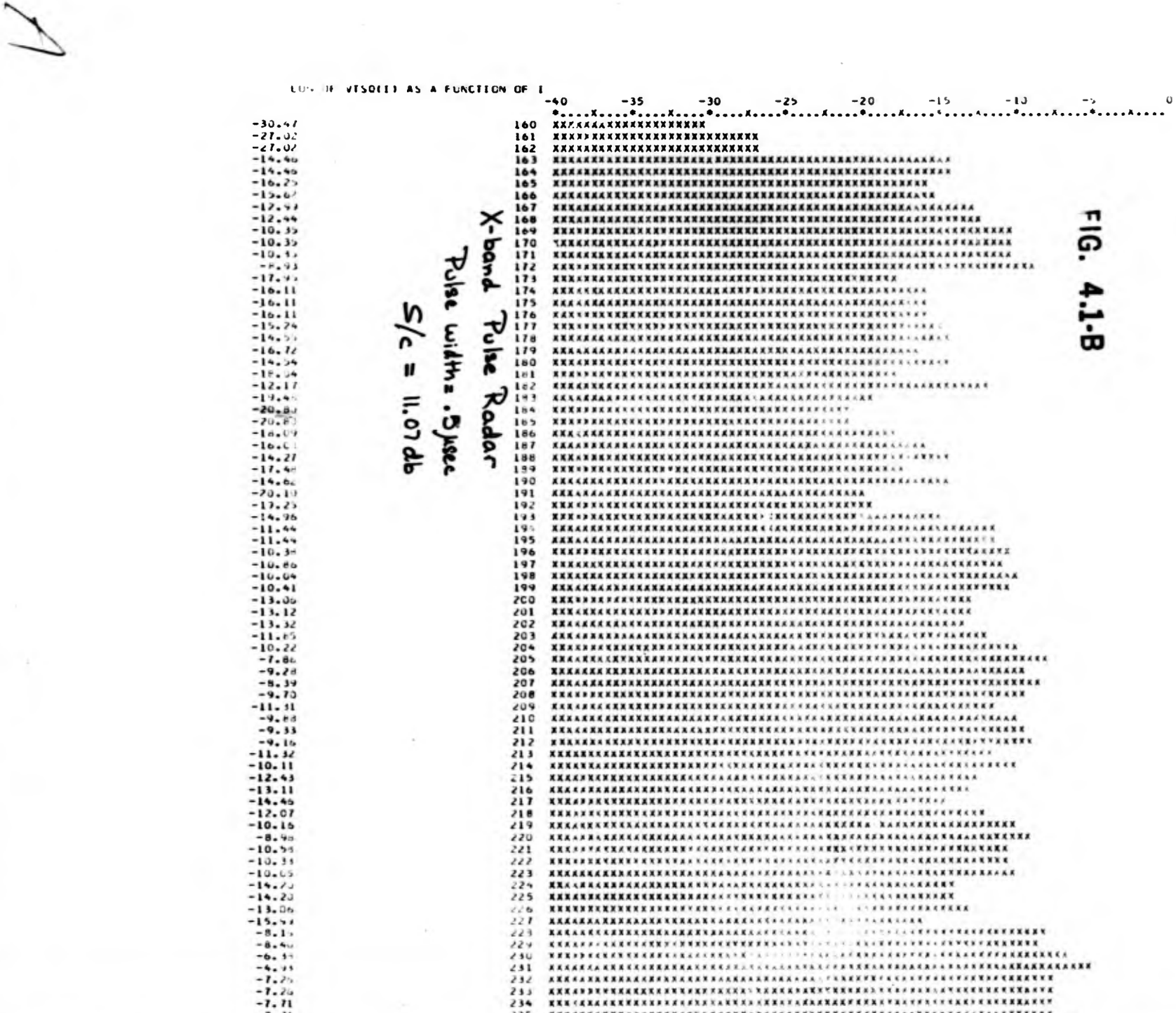
X-band Pulse Radar
Pulse width = .5 μsec
S/c = 11.07 db
-40
-35
-30
-25
-20
-15
-10
-5
0

FIG. 4.1-B

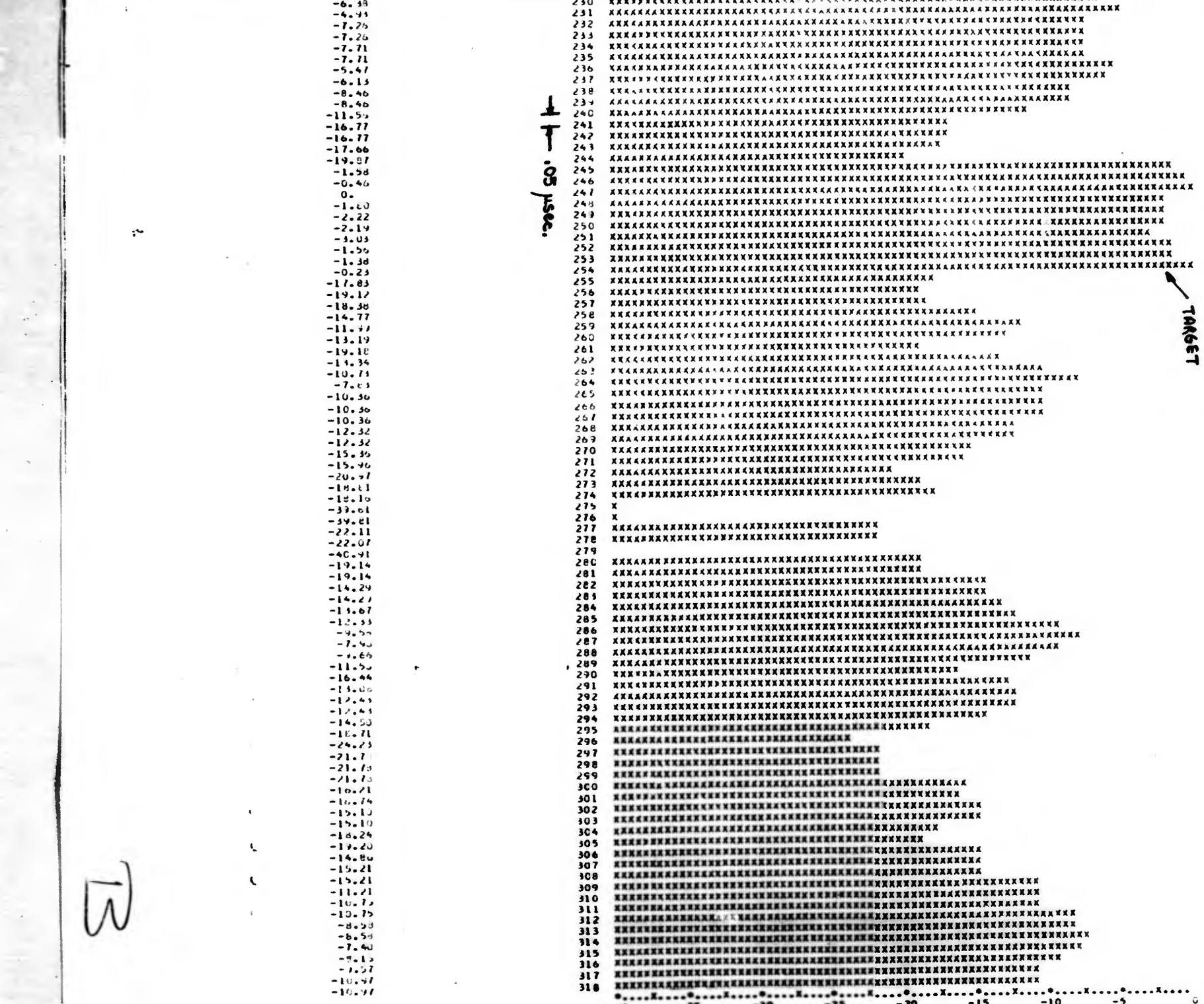
T + .05 μsec.
TARGET
-40
-35
-30
-25
-20
-15
-10
-5
0

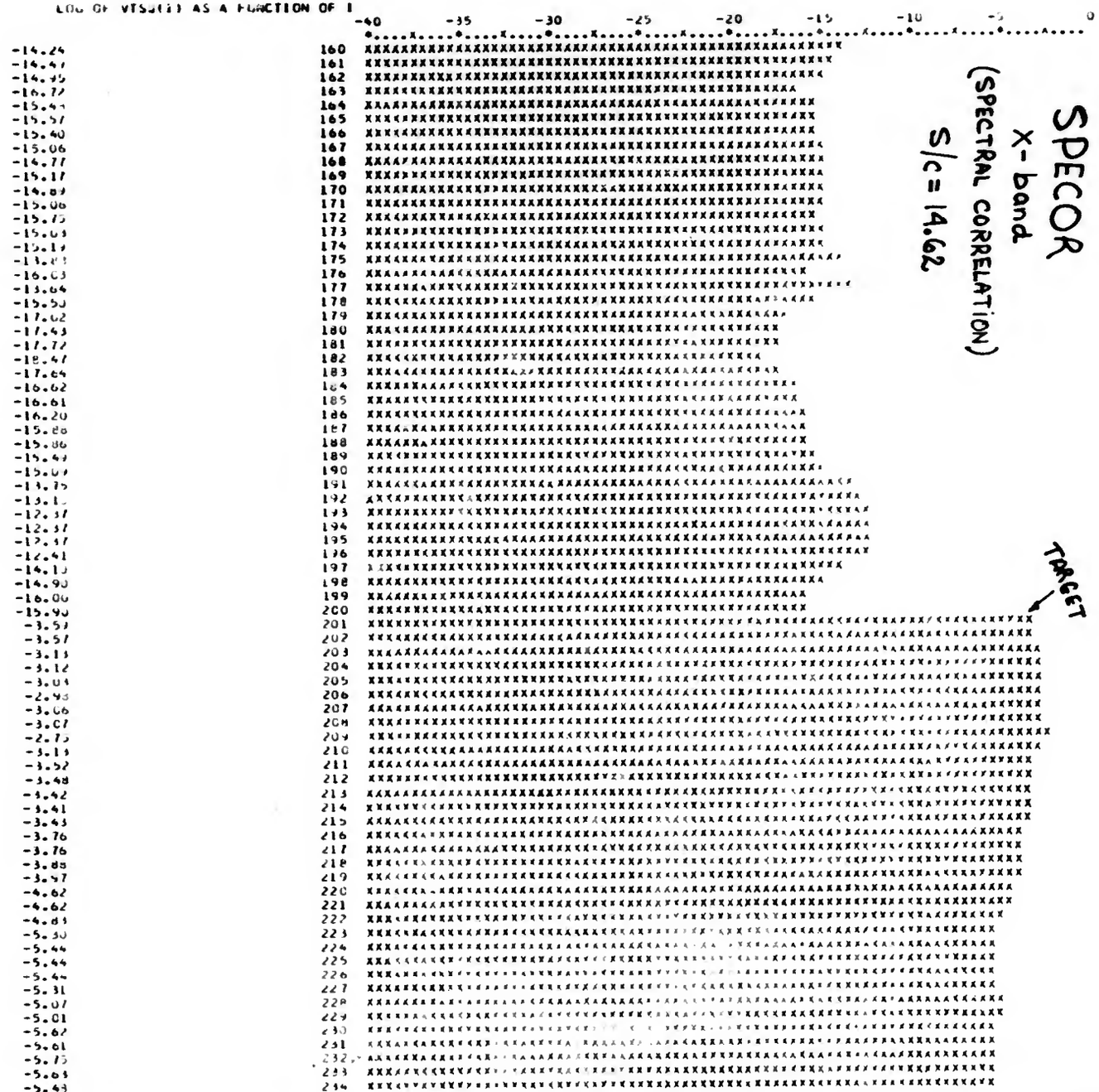

FIG. 4.1-C

SPECOR

X-band

(SPECTRAL CORRELATION)

S/C = 14.62

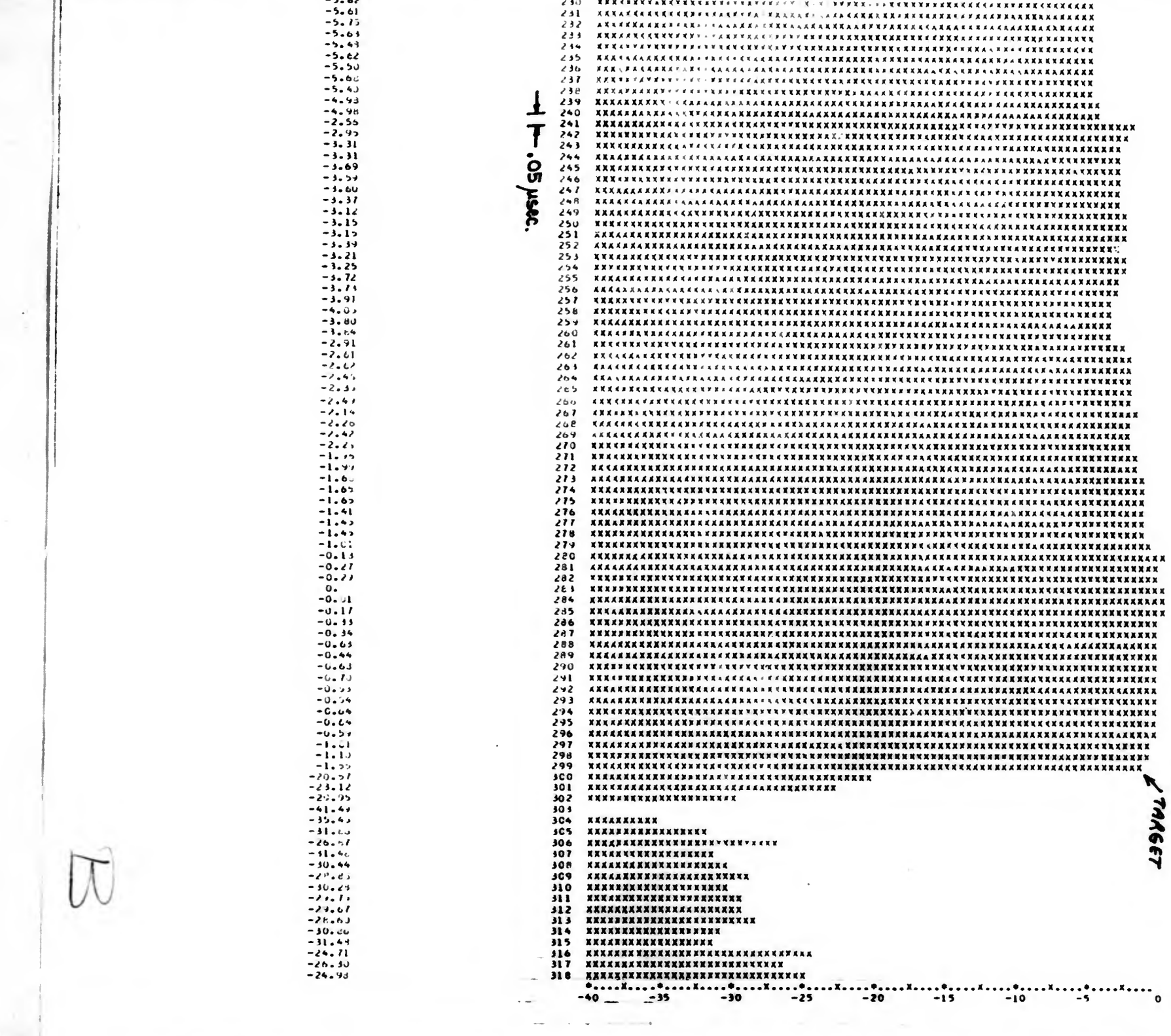
T = .05 sec.
TARGET
-40
-35
-30
-25
-20
-15
-10
-5
0

A

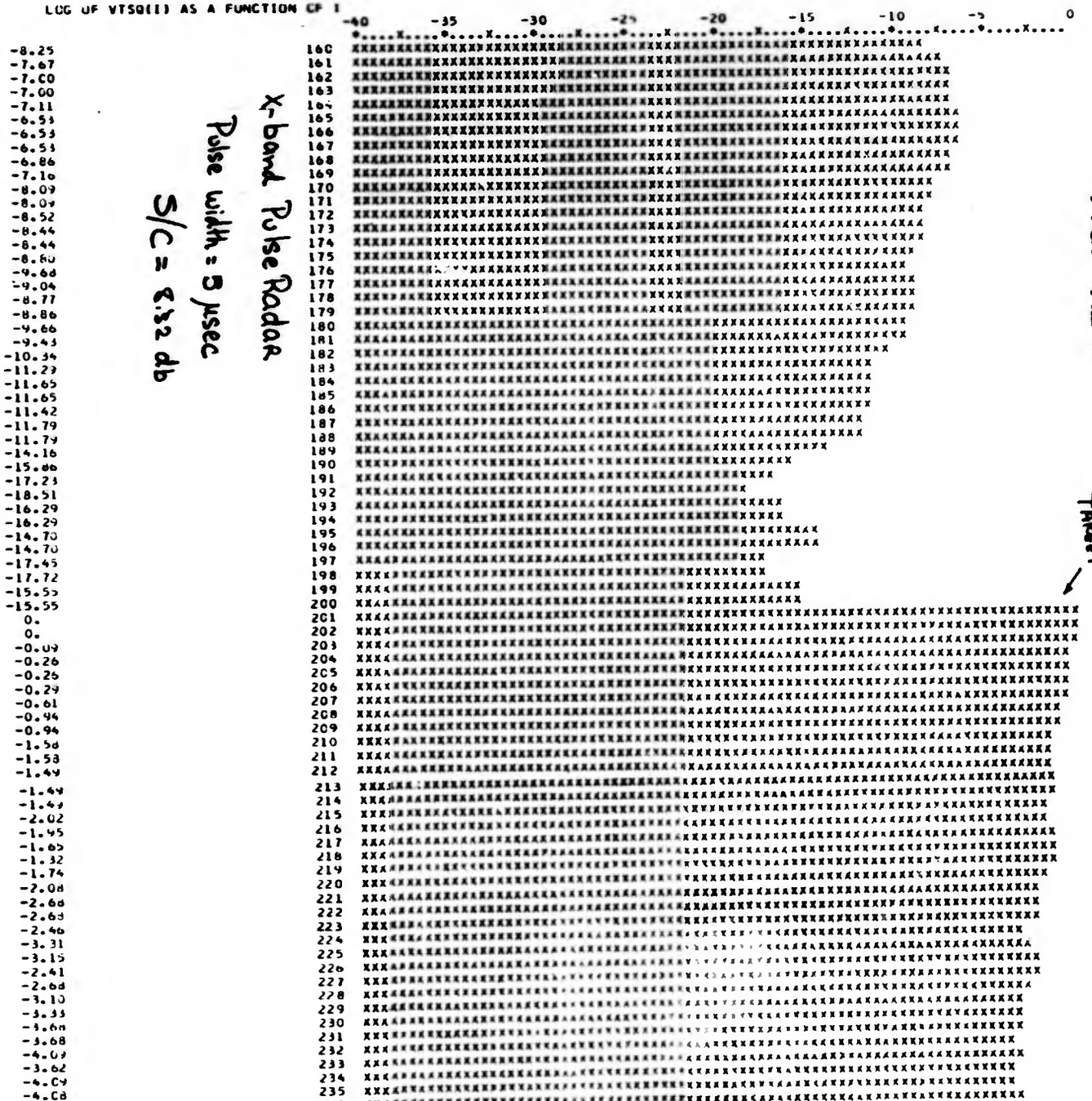
LOG OF VTSQ(I) AS A FUNCTION OF I
-40 -35 -30 -25 -20 -15 -10 -5 0
-8.25
-7.67
-7.60
-7.00
-7.11
-6.53
-6.53
-6.53
-6.86
-7.16
-8.09
-8.09
-8.52
-8.44
-8.44
-8.80
-9.66
-9.04
-8.77
-8.86
-9.66
-9.43
-10.34
-11.29
-11.65
-11.65
-11.42
-11.79
-11.79
-14.16
-15.86
-17.23
-18.51
-16.29
-16.29
-14.70
-14.70
-17.45
-17.72
-15.55
-15.55
0.
0.
-0.09
-0.26
-0.26
-0.29
-0.61
-0.94
-0.94
-1.56
-1.58
-1.49
-1.49
-1.49
-2.02
-1.95
-1.65
-1.32
-1.74
-2.08
-2.66
-2.63
-2.46
-3.31
-3.15
-2.41
-2.68
-3.10
-3.33
-3.68
-3.68
-4.09
-3.62
-4.09
-4.08
160
161
162
163
164
165
166
167
168
169
170
171
172
173
174
175
176
177
178
179
180
181
182
183
184
185
186
187
188
189
190
191
192
193
194
195
196
197
198
199
200
201
202
203
204
205
206
207
208
209
210
211
212
213
214
215
216
217
218
219
220
221
222
223
224
225
226
227
228
229
230
231
232
233
234
235
X-band Pulse Radar
Pulse width = 5 μsec
S/C = 8.32 db
TARGET

FIG. 4.2-A

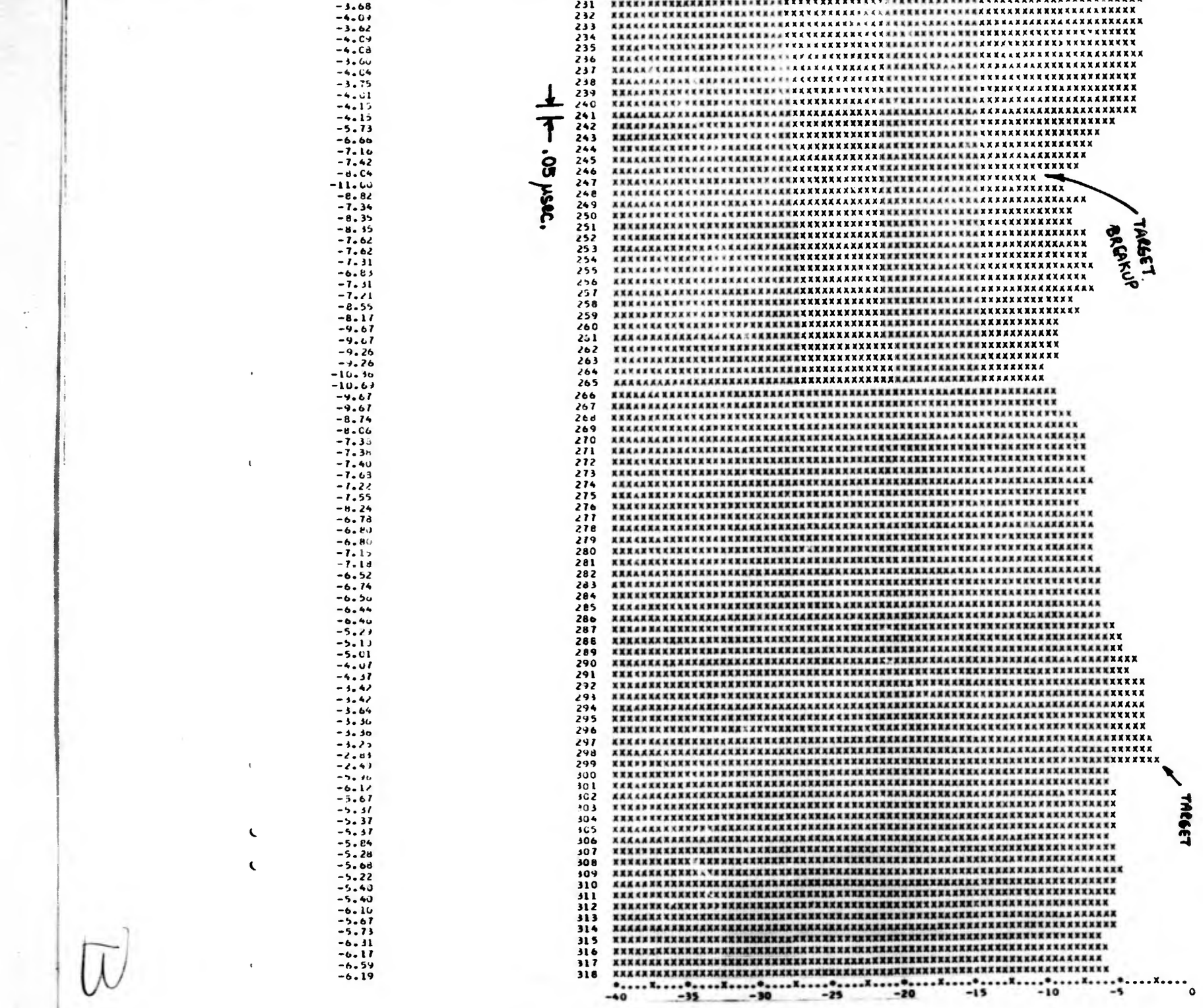
.05 μsec.
TARGET BREAKUP
TARGET
-40
-35
-30
-25
-20
-15
-10
-5
0

-40 -35 -30 -25 -20 -15 -10 -5 0
X-band Pulse Radar
Pulse width = .5 μsec.
S/C = 18.98 db

FIG. 4.2-B

A

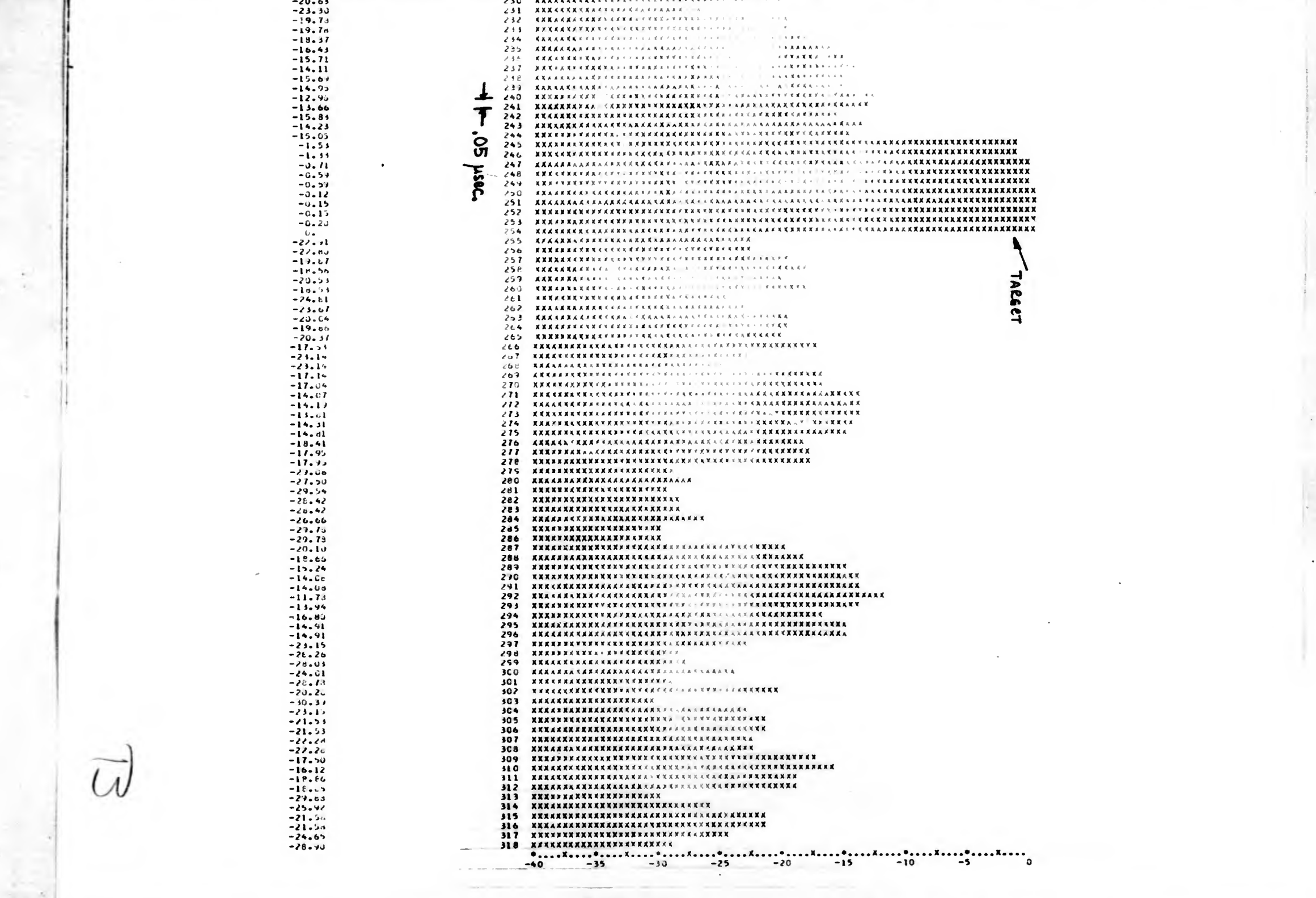
+ T - .05 μsec.
TARGET
-40
-35
-30
-25
-20
-15
-10
-5
0

FIG. 4.2-C

SPECOR

X-band

(SPECTRAL CORRELATION)

S/C = 29.21 db

A

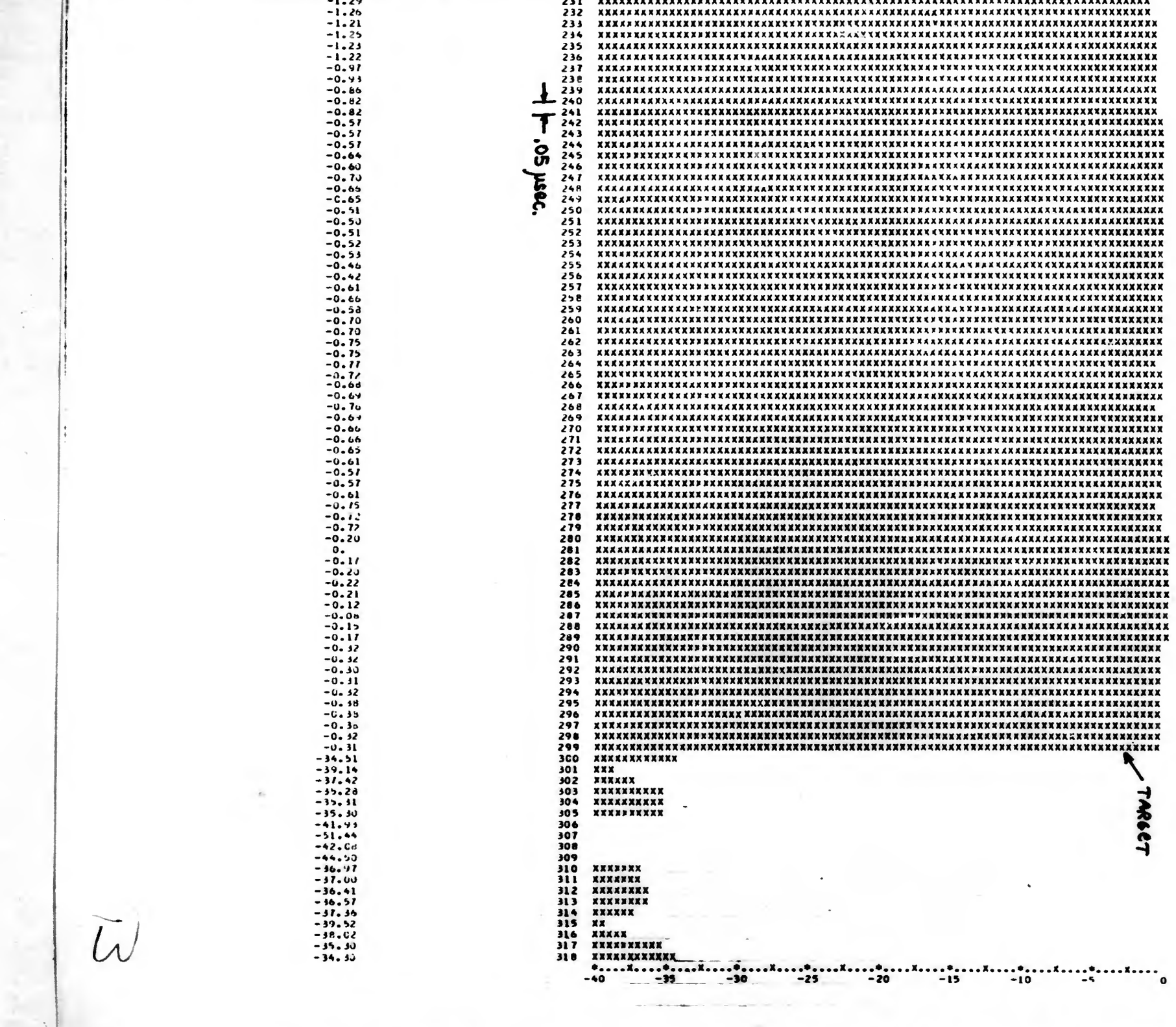
-1.29
-1.26
-1.21
-1.25
-1.23
-1.22
-0.97
-0.93
-0.86
-0.82
-0.82
-0.57
-0.57
-0.57
-0.64
-0.60
-0.70
-0.66
-0.65
-0.51
-0.50
-0.51
-0.52
-0.53
-0.46
-0.42
-0.61
-0.66
-0.58
-0.70
-0.70
-0.75
-0.75
-0.77
-0.72
-0.68
-0.69
-0.76
-0.64
-0.66
-0.66
-0.65
-0.61
-0.57
-0.57
-0.61
-0.75
-0.72
-0.72
-0.20
0.
-0.17
-0.20
-0.22
-0.21
-0.12
-0.08
-0.15
-0.17
-0.32
-0.32
-0.30
-0.31
-0.32
-0.38
-0.35
-0.36
-0.32
-0.31
-34.51
-39.14
-37.42
-35.28
-35.31
-35.30
-41.93
-51.44
-42.08
-44.50
-36.97
-37.00
-36.41
-36.57
-37.36
-39.52
-38.02
-35.30
-34.50
1 T .05 μsec.
231
232
233
234
235
236
237
238
239
240
241
242
243
244
245
246
247
248
249
250
251
252
253
254
255
256
257
258
259
260
261
262
263
264
265
266
267
268
269
270
271
272
273
274
275
276
277
278
279
280
281
282
283
284
285
286
287
288
289
290
291
292
293
294
295
296
297
298
299
300
301
302
303
304
305
306
307
308
309
310
311
312
313
314
315
316
317
318
TARGET
-40
-35
-30
-25
-20
-15
-10
-5
0

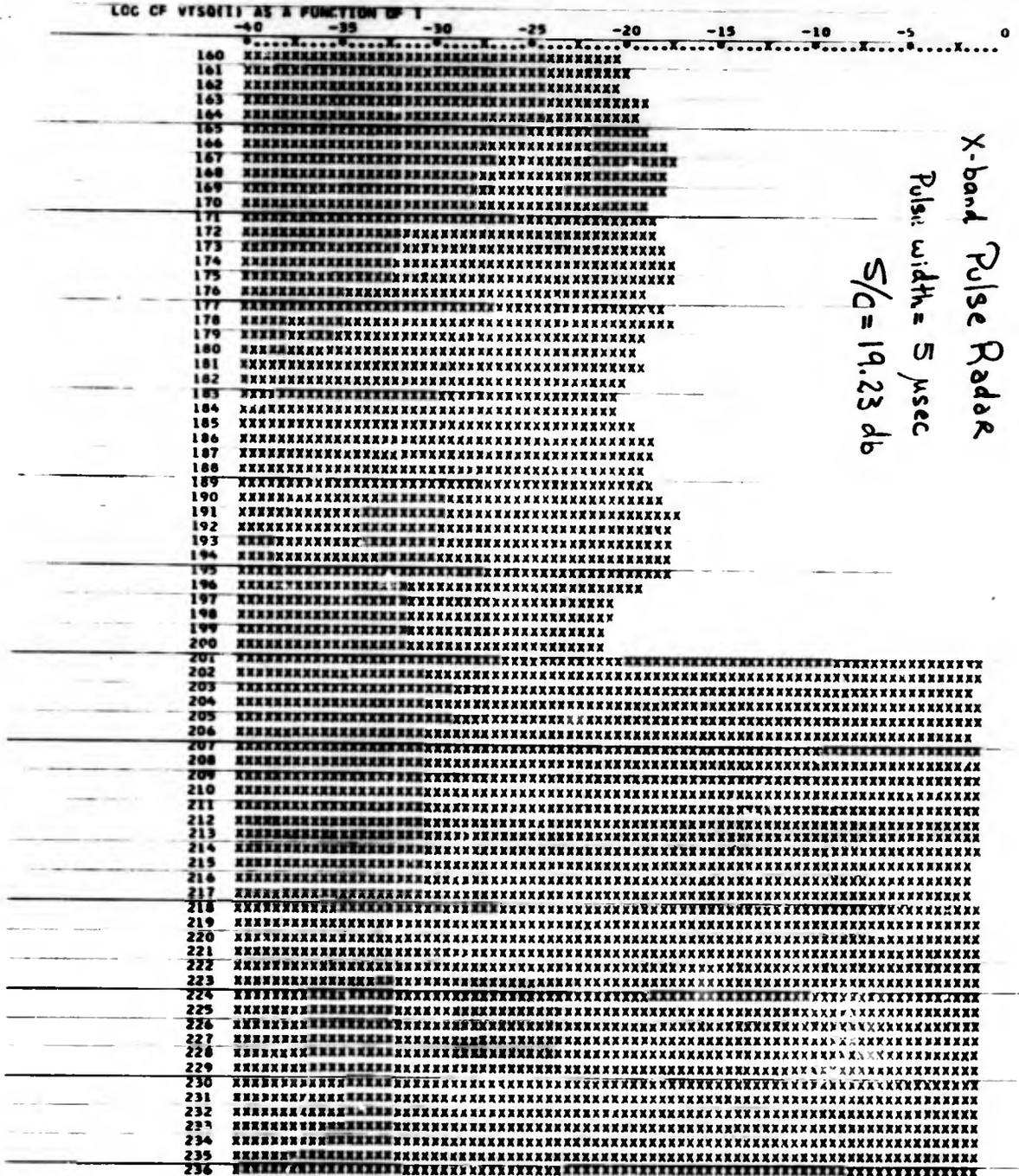

X-band Pulse Radar

Pulse width = 5 μsec

S/C = 19.23 db

FIG. 4.3-A

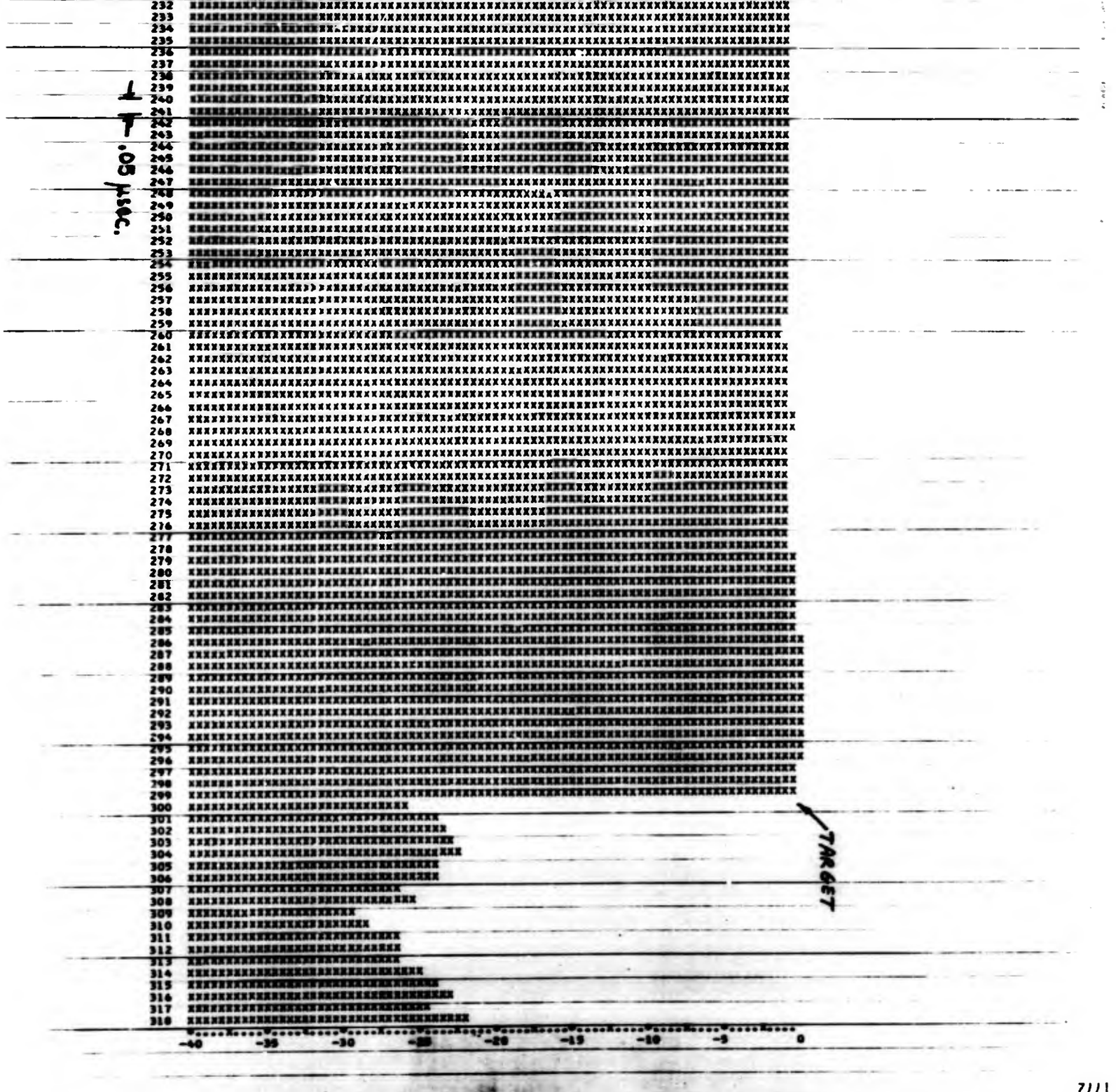
1 T .05 μsec.
TARGET
-40
-35
-30
-25
-20
-15
-10
-5
0

FIG. 4.3-B

X-band Pulse Radar

Pulse Width = .5 μsec

S/C = 28.55 db

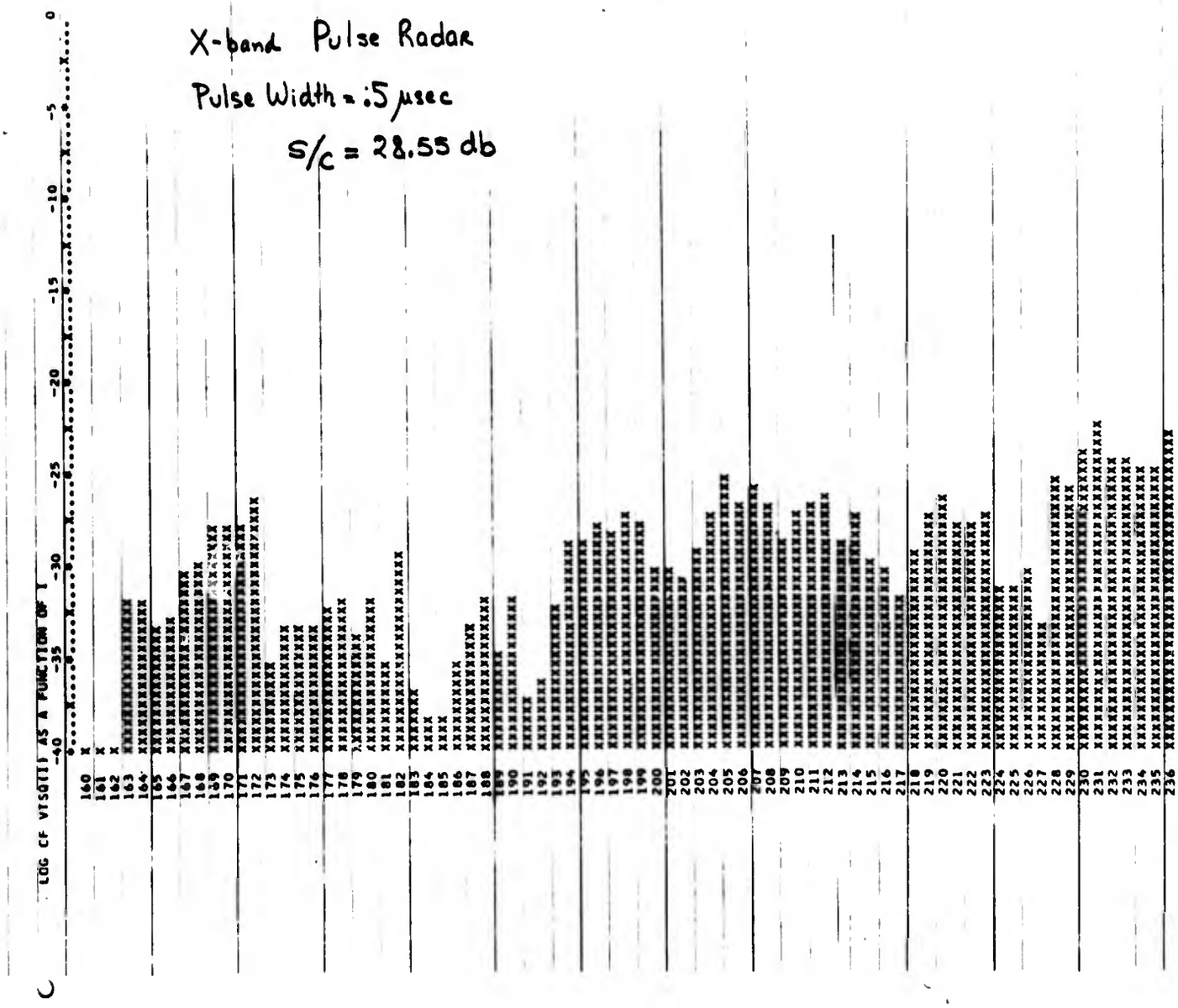

A

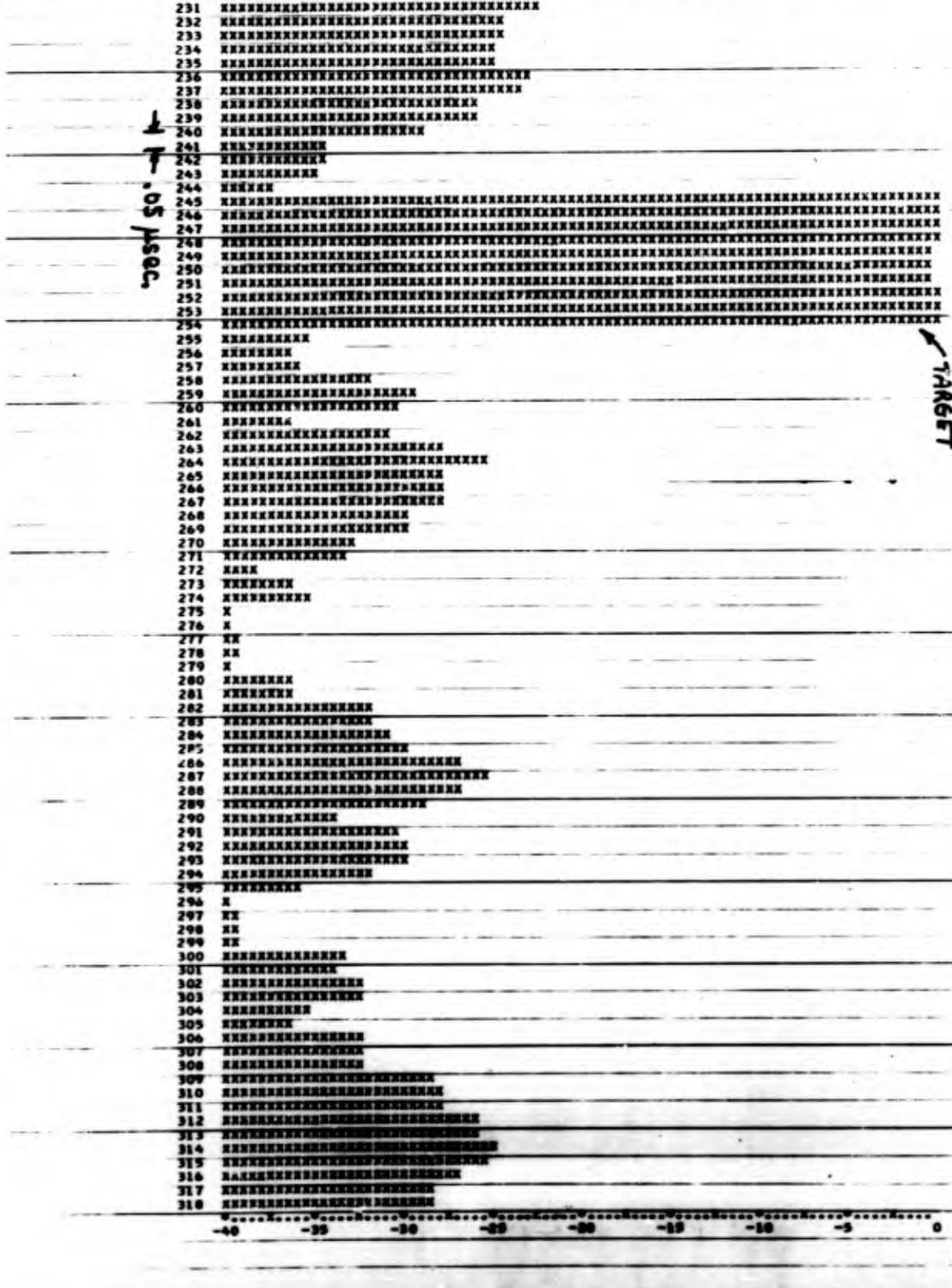
231
232
233
234
235
236
237
238
239
240
241
242
243
244
245
246
247
248
249
250
251
252
253
254
255
256
257
258
259
260
261
262
263
264
265
266
267
268
269
270
271
272
273
274
275
276
277
278
279
280
281
282
283
284
285
286
287
288
289
290
291
292
293
294
295
296
297
298
299
300
301
302
303
304
305
306
307
308
309
310
311
312
313
314
315
316
317
318
-40
-35
-30
-25
-20
-15
-10
-5
0
TARGET
T = .05 MSEC

FIG. 4.3-C

SPECOR
(SPECTRAL CORRELATION)
X-band
S/C = 48.4 db

A

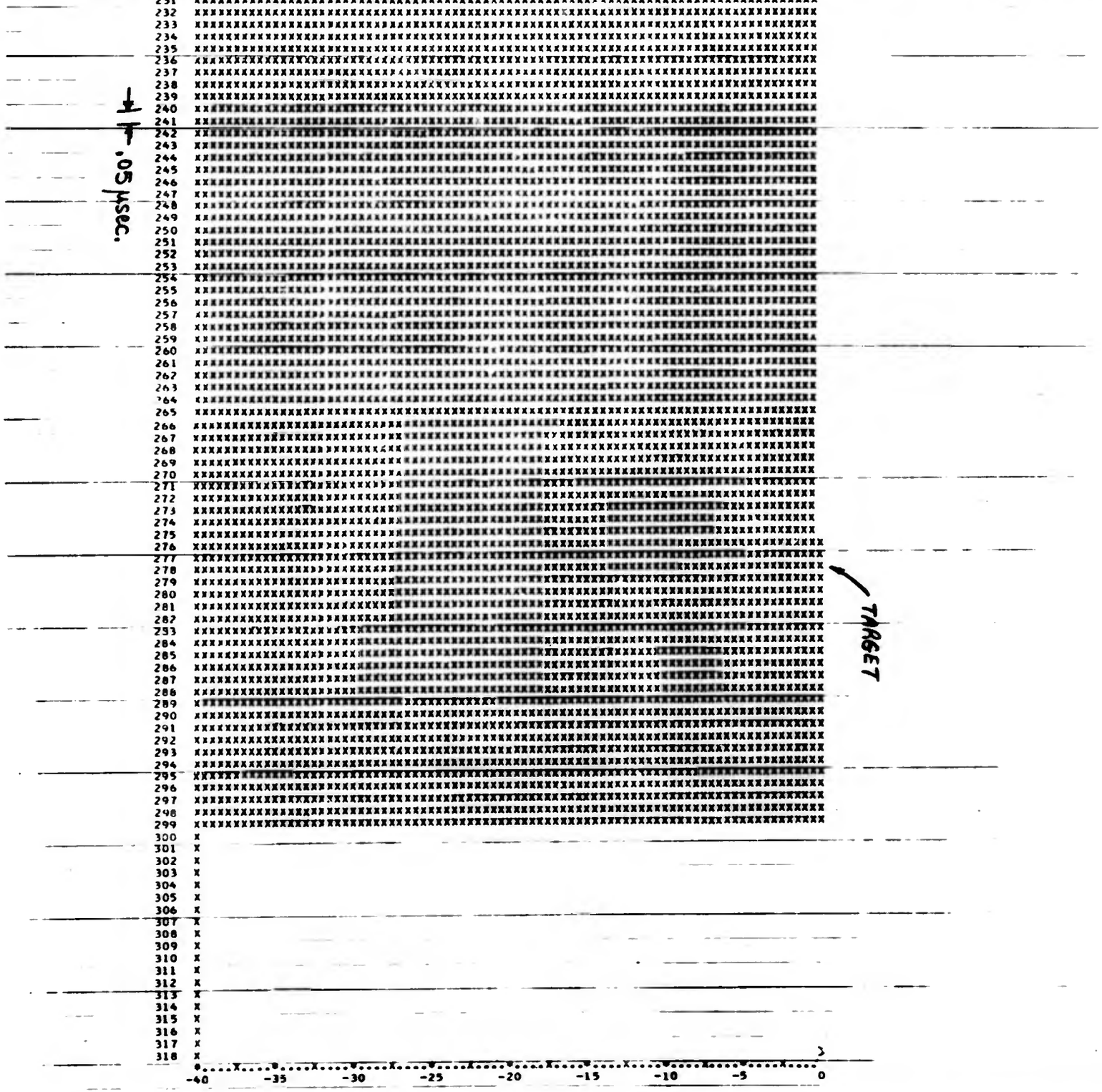
± .05 μsec.
TARGET
-40
-35
-30
-25
-20
-15
-10
-5
0

BLANK PAGE

Since the clutter is "noisy", the 5 μsec and 0.5 μsec runs provide a control in the experiment of evaluating a new processing technique, SPECOR, based up frequency de-correlation for enhancement of S/C. Approximately, a 10 db increase in S/C was obtained in going from the 5 μsec to the 0.5 μsec radar as predicted by theory.

Increasing the target level provided larger S/C improvements in SPECOR than in the pulse radar. This effect is predicted due to the double-detection nonlinear processing employed in SPECOR, cf. Appendix A.

4.3 PARTIALLY COHERENT SCATTERING

Using the partially coherent clutter models of Section 2.6, an experiment was performed for a comparison of the 5 μsec and 0.5 μsec pulse radars with each other and with SPECOR. The target was an ideal point target. Two speculars were placed near the target. One of the speculars preceded the target by 1.5 μsec; the other was placed 1.5 μsec behind the target. The specular widths were 0.1 μ second, i. e., spread speculars of approximately 50 foot dimension. The spacing between the speculars was 3 μsec or approximately 1500 feet. The two speculars and the target were then set in a background of random clutter, cf. Figure 2-25. The responses of the 5 μsec, 0.5 μsec pulse radars and SPECOR are shown in Figures 4.4, 4.5 and 4.6, respectively. A triangular radar pulse window (ambiguity function) was employed.

Except for the spread of the speculars and their amplitude, the target and the speculars are coherent returns at 9 Gc. The 0.5 μsec pulse radar resolves the target and speculars as shown in Figure 4.5 with a signal-to-clutter (S/C) ratio of 22 db. Using the same target and clutter speculars, the 5 μsec pulse radar does <u>not</u> provide resolution, as shown in Figure 4.4. Indeed, for this experiment the presence of the speculars with the target exhances the peak appearing 22 db above the surrounding clutter noise level. However, the experiment is incomplete since if other speculars were present, they could be mistaken for targets. If the amplitude of the target far exceeded that of the speculars, the target could then be distinguished on this basis solely. If on the other hand, many speculars appeared within the resolution cell with a target, the presence of the target could be lost entirely even though the target was larger than any single specular. This could occur when many of the speculars are phase-coherent, i. e., the amplitudes of the speculars add linearly far exceeding that of the target.

Increasing the transmitted bandwidth or reduction of the pulse length as in Figure 4.5 with the 0.5 μsec radar resolves the speculars and the target so that only the self-coherence (correlation) of each specular and/or target contributes to the output. In this fashion, the cross correlation of the speculars goes to zero providing resolution and enhanced S/C performance.

Using the same clutter, noisy and specular, and the same target, the SPECOR spectral correlation technique is exercised in Figure 4.6. The dramatic increase in S/C to 44 db is evident. An explanation for this superlative performance is given in the following with reference to APPENDIX A.

For these experiments, SPECOR transmitted two bands of 10 frequencies where each band was 100 MHz. Responses on all paired frequencies separated by Δf = 400 MHz were multiplied and then integrated thereby performing an (unnormalized) frequency correlation coefficient form of processing (see the pictorial and mathematical description of Appendix A). This form of processing is directed toward the detection of small size targets in clutter.

The first consequence of this form of processing is the destruction of phase coherence, i. e., the speculars are suppressed since they are speculars at one frequency. Even broadband speculars would be suppressed if their specularity extended over a band of less than 400 MHz. An additional consequence is the finite spread, the range-delay correlation τ_c = 0.1 μsec, of the speculars. From Appendix A, we note that $\Delta f \cdot \tau_c = 4$ which results in both a spatial and frequency decorrelation of the speculars and the destruction of the cross-correlation between the two speculars spaced 3 μsec apart. The small size target, on the other hand, is not suppressed due to its small dimensions and hence small spatial correlation length e. g., $\Delta f \tau_c \ll 1$ for the target.

The result as shown in Figure 4.6 for SPECOR is the retention of the target, enhanced in S/C, with suppression of both specular and noise clutter.

FIG. 4-4 X-BAND PULSE RADAR

PULSE WIDTH = 5μsec.

(PARTIALLY COHERENT CLUTTER)

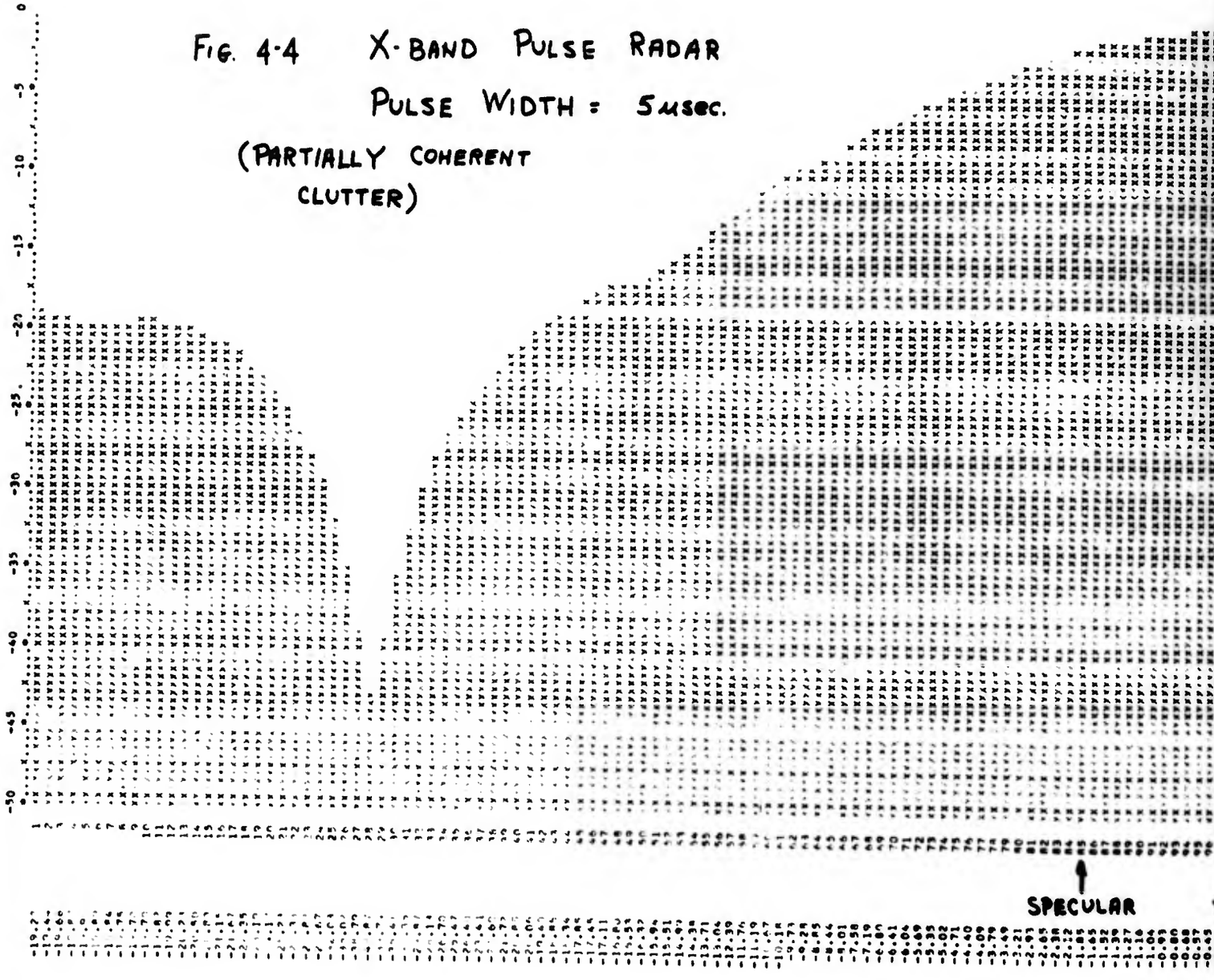

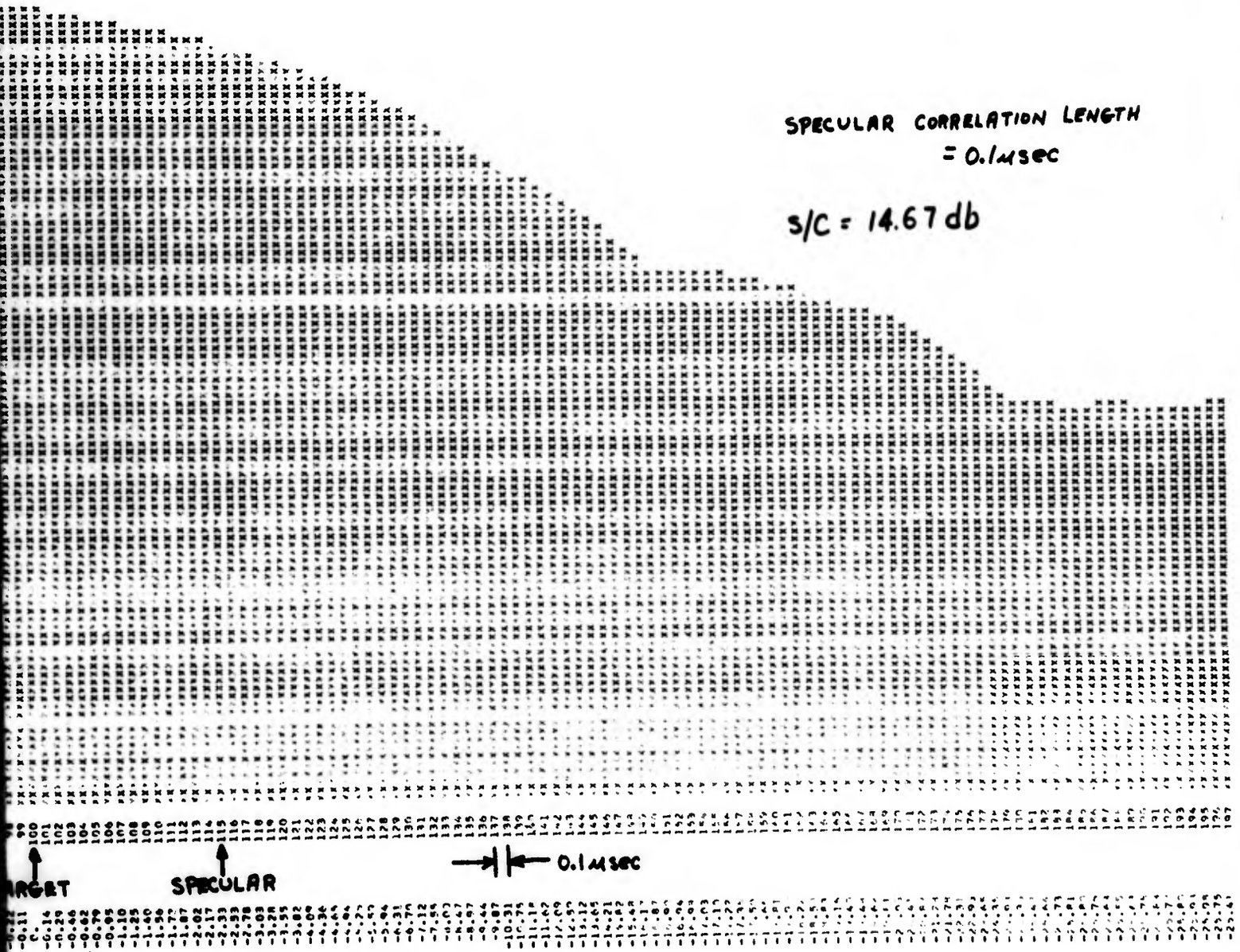
SPECULAR CORRELATION LENGTH
= 0.1 msec
S/C = 14.67 db
SPECULAR
0.1 msec

B

FIG. 4-5 X-BAND PULSE RADAR

PULSE WIDTH = 0.5 μsec

(PARTIALLY COHERENT CLUTTER)

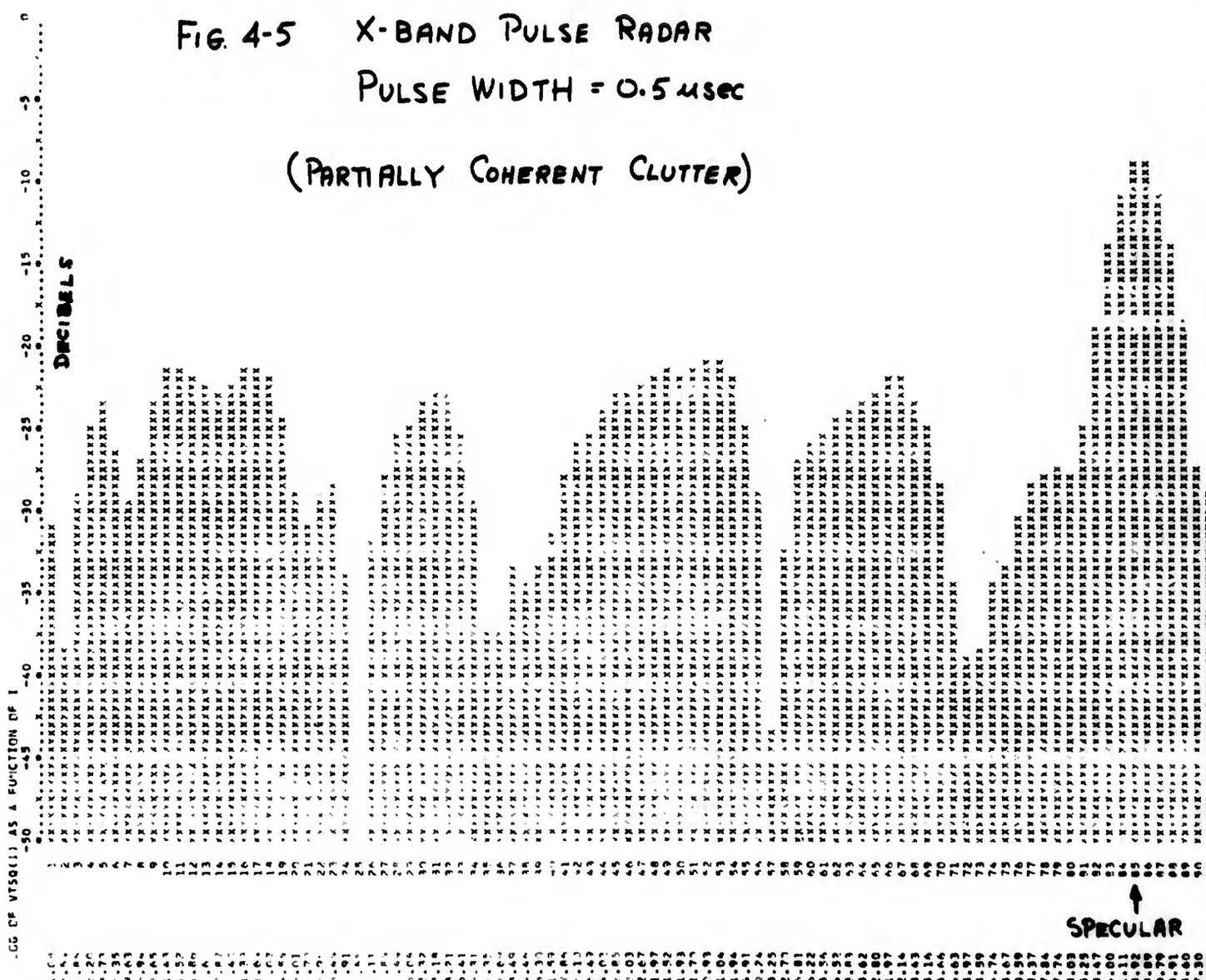

A

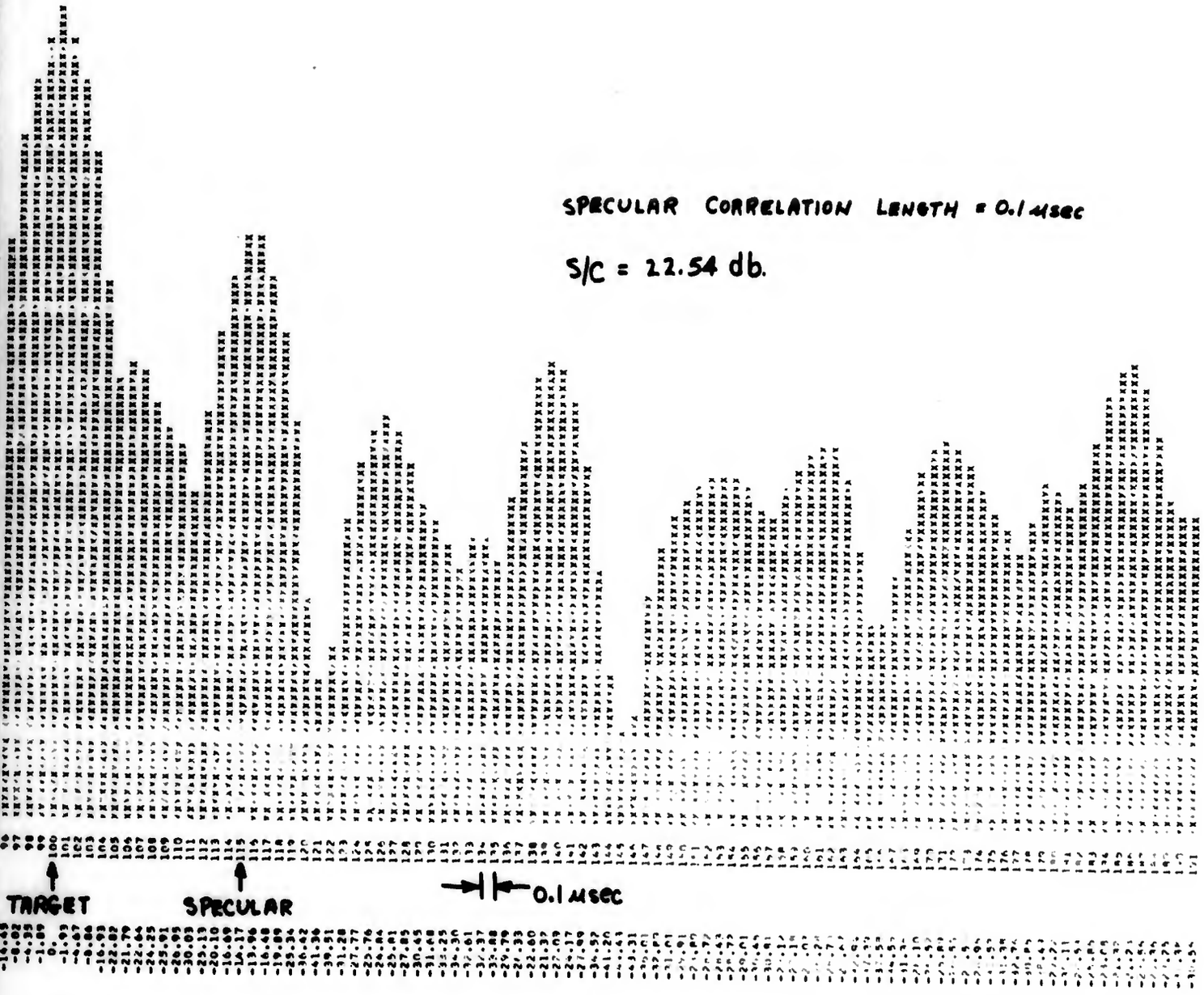
SPECULAR CORRELATION LENGTH = 0.1 msec
S/C = 22.54 db.
TARGET
SPECULAR
0.1 msec

FIG. 4-6 SPECOR
(SPECTRAL CORRELATION RADAR)
X-BAND; PULSE WIDTH = 5 μsec
(PARTIALLY COHERENT CLUTTER)

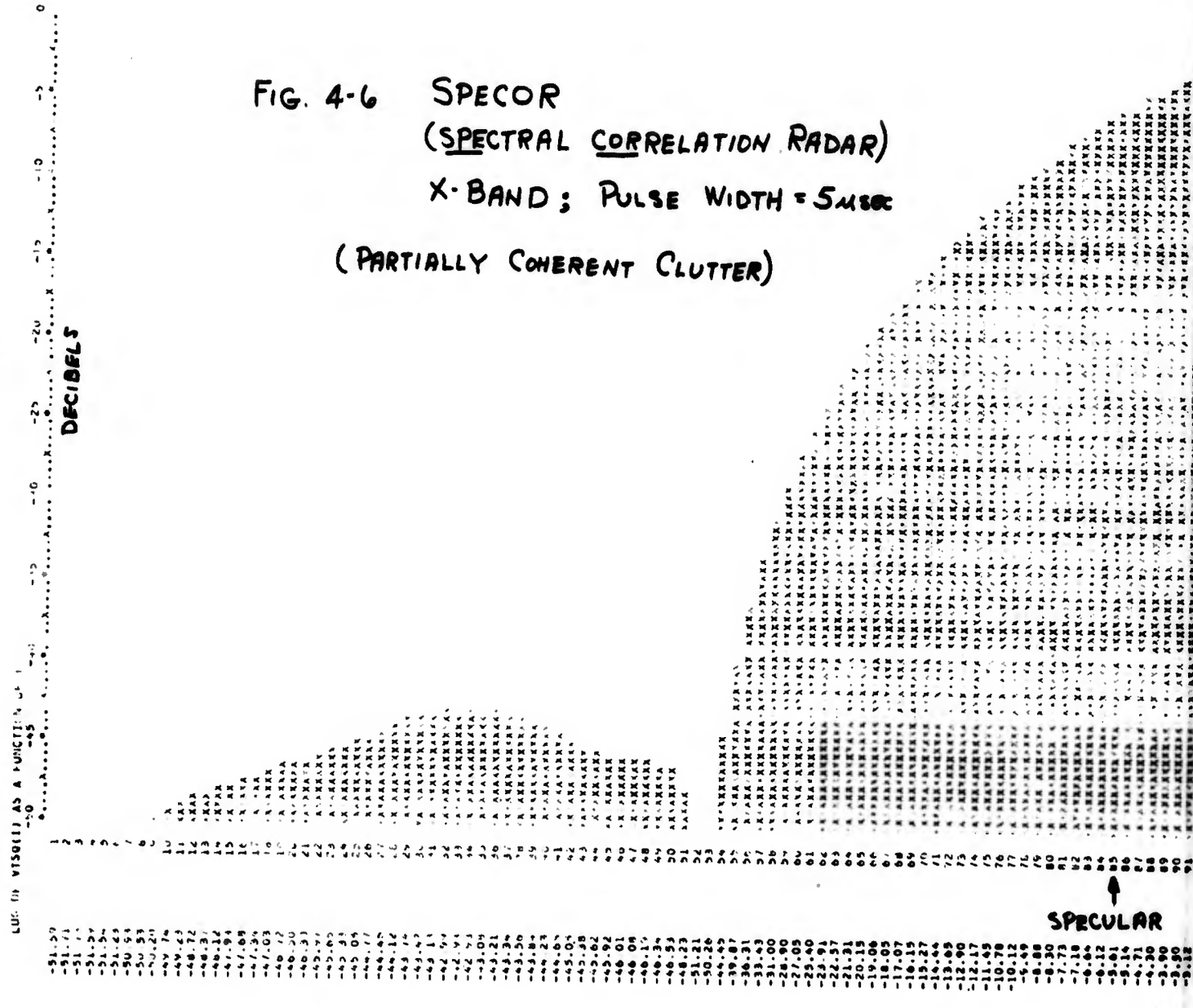

A

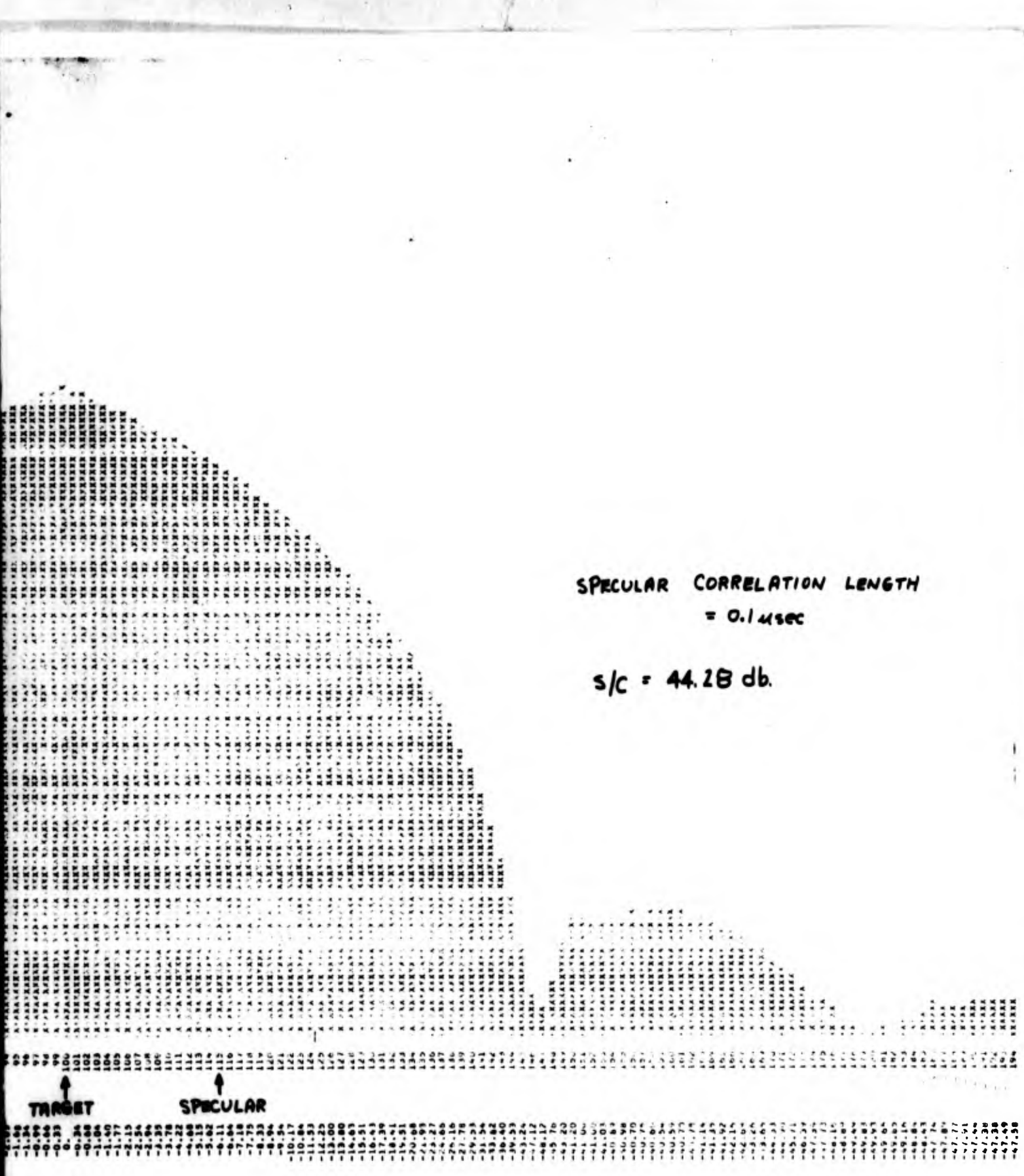

SPECULAR CORRELATION LENGTH
= 0.1 μsec

S/C = 44.28 db.

5.0 CONCLUSIONS AND RECOMMENDATIONS

The method of this investigation has shown the feasibility of the simulation approach for the evaluation of radar performance in a clutter environment. The approach is consistent with a theory of clutter (Section 2) which permits incoherent, partially coherent, and coherent (specular) scattering.

The demonstration of Section 4 provides an indication of the usefulness of simulation methods to obtain a common basis of comparison among various radar processing techniques and their ability to "see into clutter". The corroboration of the frequency correlation properties as manifested in the SPECOR technique is an example.

During the course of the investigation, a method was devised in which specular and/or near-specular reflections could be categorized by the NRL-4F measurement radar. Thus data may be obtained on specular amplitude, specular correlation length, and specular rate of occurence. This information, when available, permits probability modeling of various types of clutter scattering.

Based upon measurement data and the probability models obtained (which include partially coherent and specular scattering), an analytic and computer investigation can be performed to obtain P_D (probability of detection), P_{fa} (probability of false alarm) versus threshold setting, transmitted bandwidth, and radar-clutter viewing aspect. The end objective of this recommendation is to obtain a set of performance curves which can be employed by a radar designer for the particular class of clutter in much the same manner as the performance curves for a signal in receiver thermal noise.

REFERENCES

1. W. Blau, "Radar Partial Coherence Theory: An Introduction", IEEE Trans. Aerospace & Electronic Systems, Vol. AES-2, No. 5, Sept. 1966; pp. 536-543.

2. W. Blau, "Anti-Clutter Techniques Feasibility Study". Contract AF33(615)-5341 Tech. Rpt. AFAL-TR-67-230, May 1968; Spectronics, Inc. (formerly Spectra Associates).

3. D. Middleton, "Statistical Models of Reverberation and Clutter," Tech. Rpt. TR65-2-BF, Litton Systems, Inc., Waltham, Mass., 15 April 1965 (Performed under ONR Contr. Nonr 3320(00).

4. F.E. Nathanson, J. P. Reilly, "Radar Precipitation Echoes - Experiments on Temporal, Spatial, and Frequency Correlation". Applies Physics Laboratory, Rept. TG-899, April 1967 (AD652818).

5. F. E. Nathanson, J. P. Reilly, "Clutter Statistics which Affect Radar Performance Analysis, "IEEE Trans. Aerospace and Electronic Systems, Vol. AES-3, No. 6, November 1967.

6. V. W. Pidgeon, "Time, Frequency and Spatial Correlation of Radar Sea Return", American Astronautical Society. Use of Space Systems for Planetary Geology and Geophysics, May 1967.

7. R. W. Kennedy, "The Spatial and Spectial Characteristics of the Radar Cross Section of Satellite-type Targets", Tech. Rpt. AFAL-TR-66-17, Air Force Avionics Lab., WPAFB, Ohio, March 1966.

8. P. M. Woodward, Probability and Information Theory with Applications to Radar, London: Permagon. New York: McGray-Hill 1953.

9. W. M. Siebert, "Studies of Woodward's Uncertainty Function", M.I.T. Lab. of Electronics, Cambridge, Mass., Quart. Prog. Report; April 15, 1958.

10. G. L. Turin, "An Introduction to Matched Filters", IRE Trans. on information Theory, Vol IT-6, pp. 311-329, June 1960.

11. N. W. Guinard et al., "NRL Terrain Clutter Study, Phase I" NRL Rpt. 6487, Naval Res. Lab. Wash., D.C., May 10, 1967.

12. J. W. Cooley, J. W. Tukey, "An Algorithan for the Machine Calculation of Complex Fourier Series "Math. of Computations, Vol. 19 (April 1965).

APPENDIX A

S P E C O R

SPECOR

IS

A

DOUBLE - DETECTION FREQUENCY

DIVERSITY TECHNIQUE

WITH

COHERENT INTEGRATION

IN THE

FREQUENCY DOMAIN

S P E C O R

- N DISSIMILAR DIFF. FREQ. AMPLITUDE-PHASE PATTERNS ARE SUMMED (COHERENT INTEGRATION)

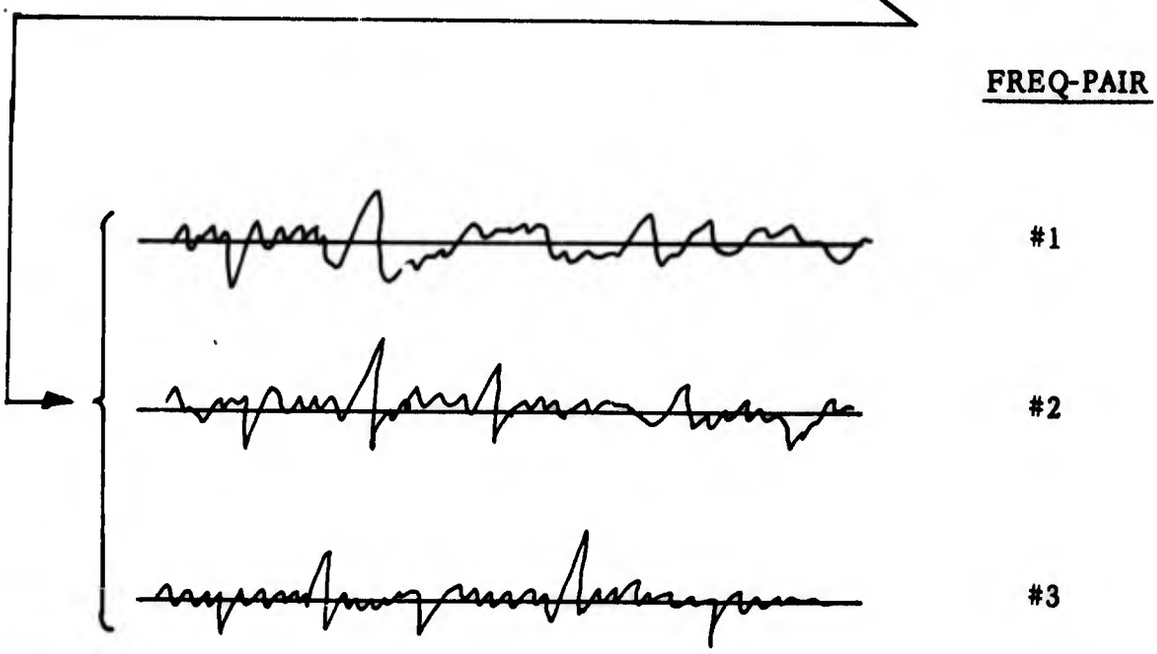

- AFTER SUMMING - DETECT TO VIDEO - DISPLAY

- TARGET PATTERN INSENSITIVE TO PAIRED FREQ'S OVER THE BAND

S P E C O R

- PATCH SCATTERERS PRODUCE "ANTENNA" PATTERN ON FREQ.'S SPACED Δf APART.
- Δf SPACED AMPLITUDE - PHASE PATTERNS ARE MULTIPLIED

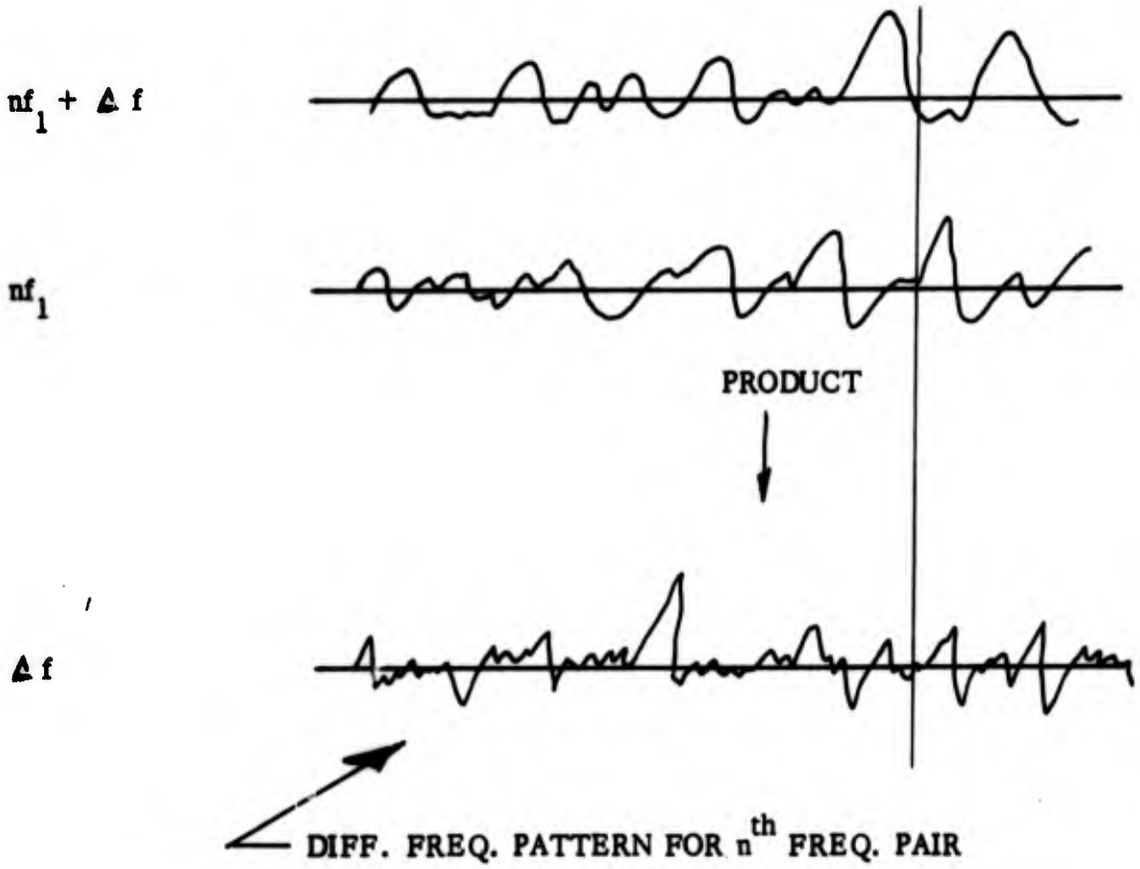

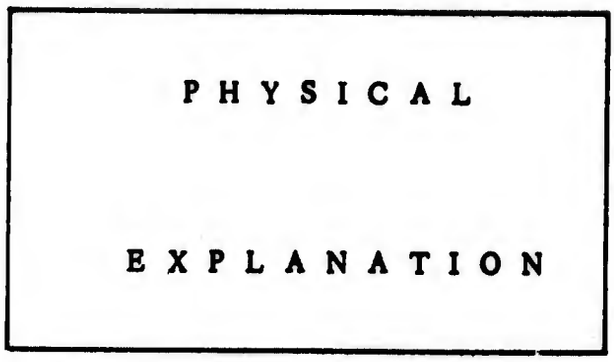

(See next page)

S P E C O R

- RECEIVE IN UPPER & LOWER BAND FILTERS
- DETECT & FILTER DIFF. FREQ. Δ f
  (THIS IS COHERENT FREQ. DOMAIN INTEGRATION)
- DETECT AGAIN - VIDEO TO DISPLAY

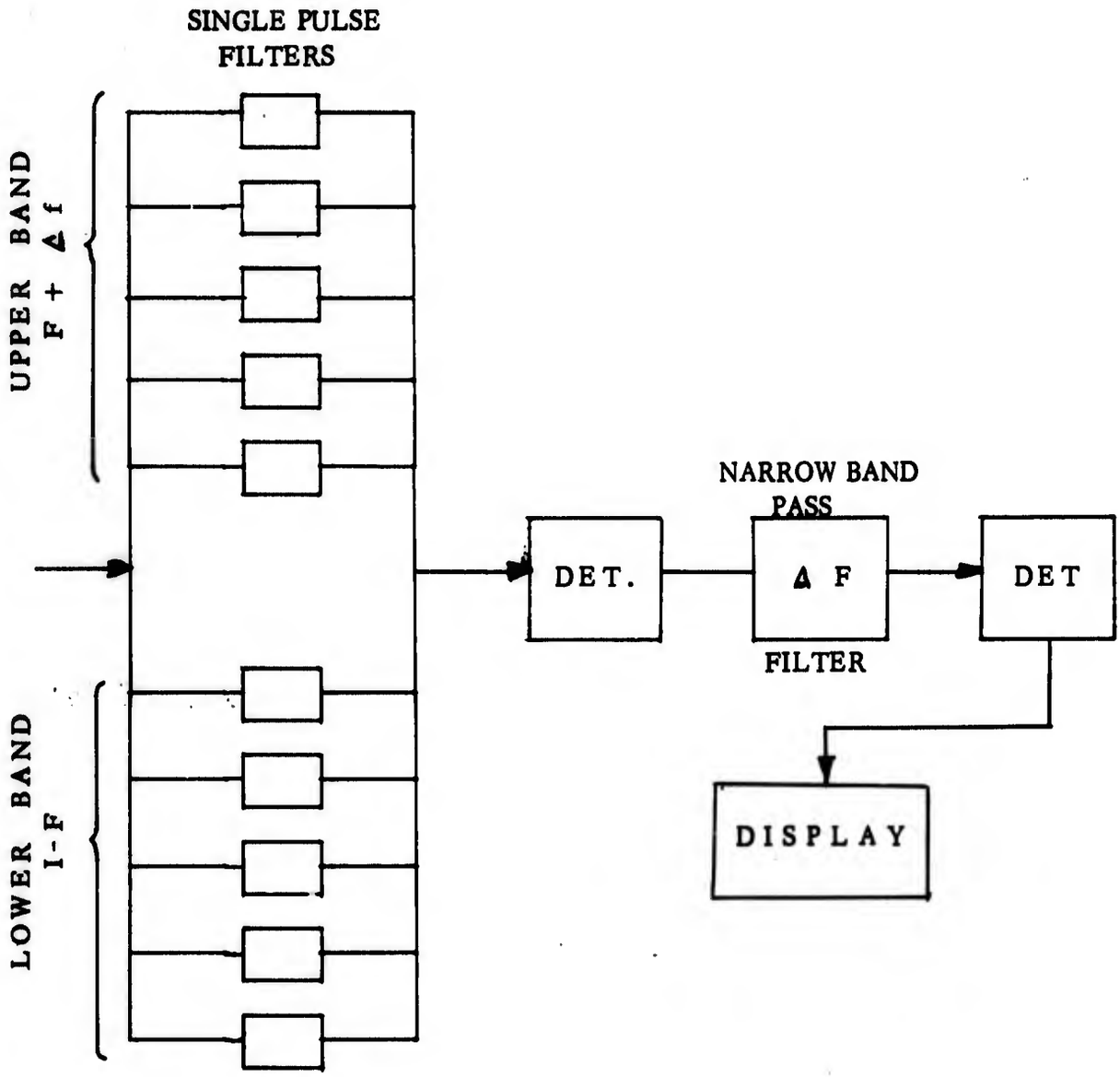

- SINUSOIDAL FM TRANSMISSION

SPECTRUM

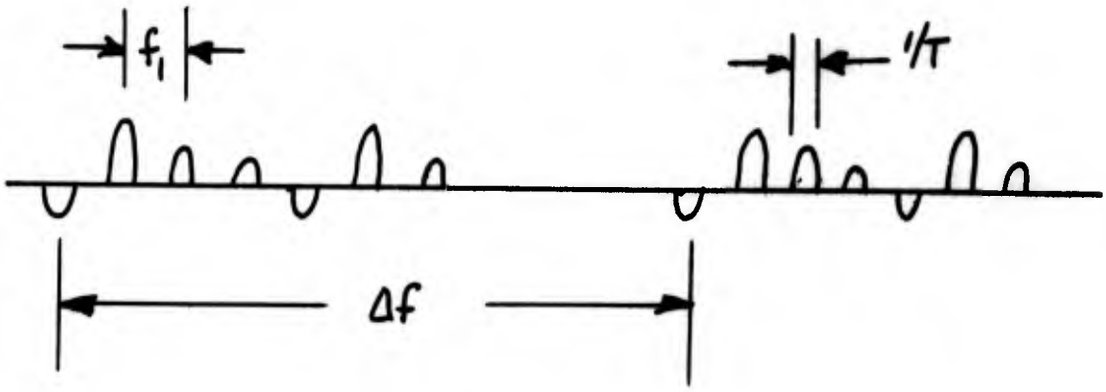

- SINUSOIDAL FM TRANSMISSION

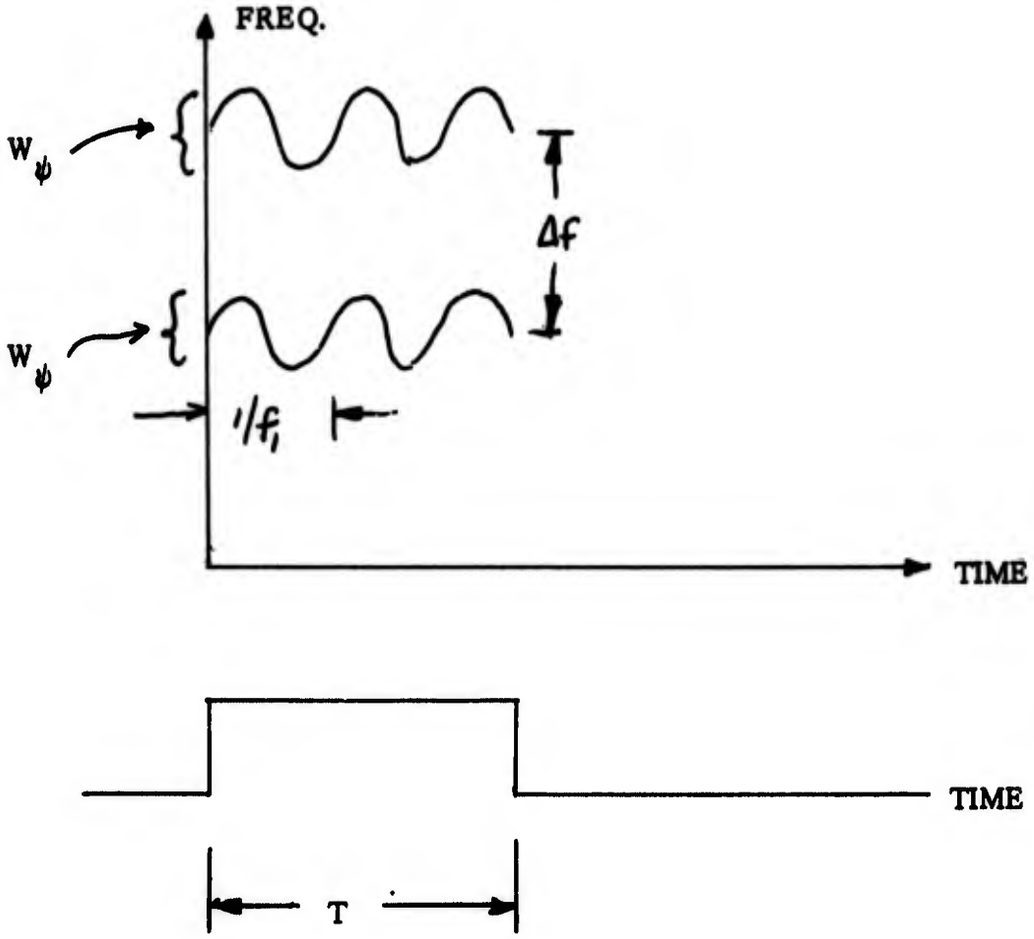

S P E C O R

- TRANSMIT A PULSE OF N FREQUENCIES IN TWO BANDS

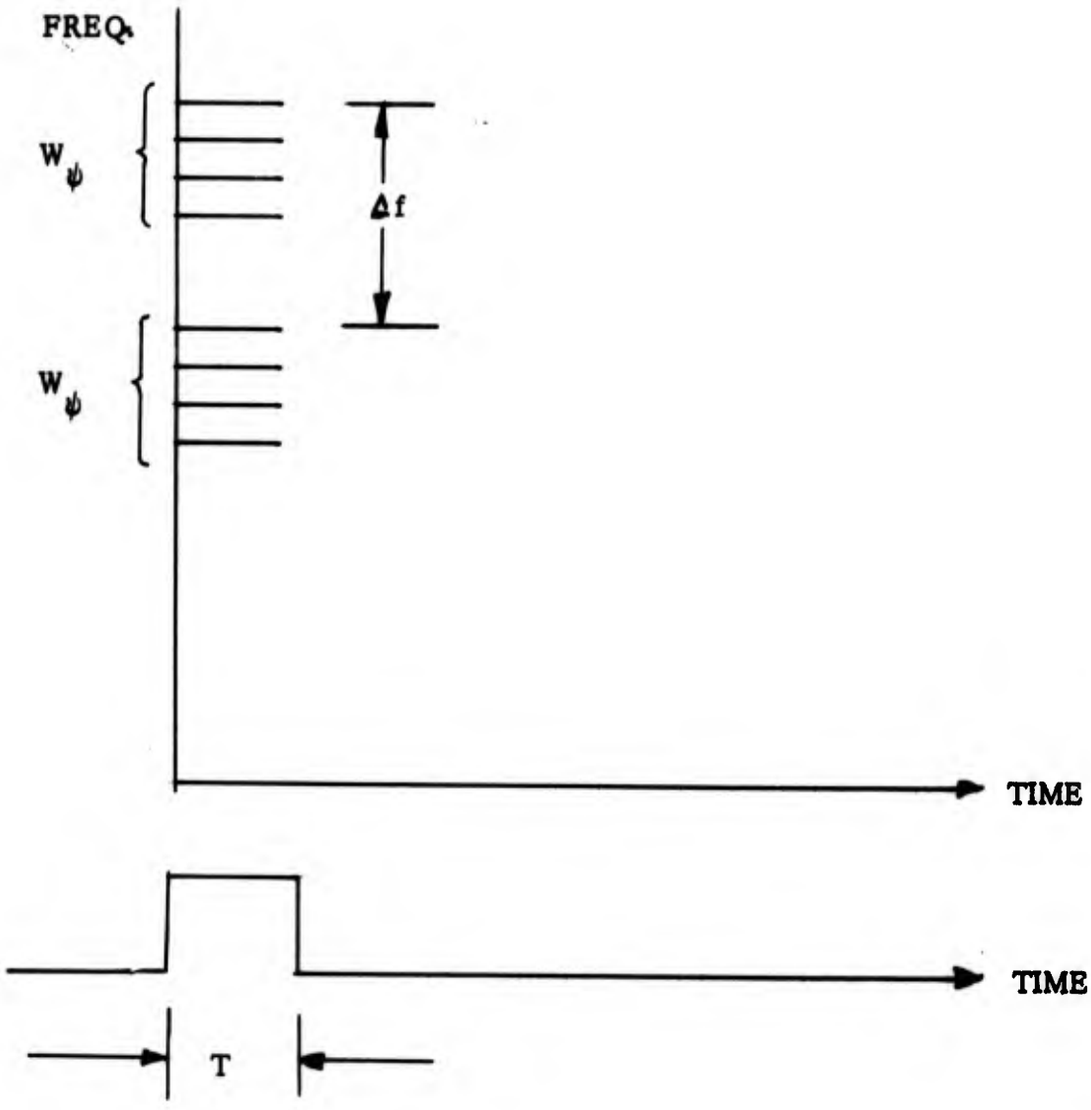

SPECOR

- 10 frequencies transmitted in two bands

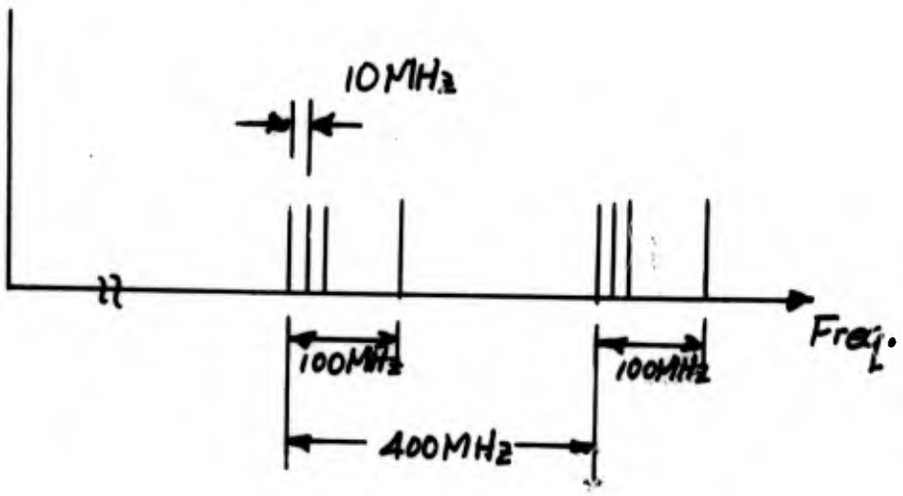

- Clutter discrimination based upon spectral decorrelation of clutter. Technique results in narrow processing bandwidth.

SPECOR transmits in two bands: the upper band and the lower band. The clutter return from the low band is given by

$$v(t) = \sum_{n=0}^{N-1} a_n \int \rho(\tau)\chi(t-\tau, 0)\, e^{j(\omega_o + n\omega_1)(t-\tau)}\, d\tau$$

$$= e^{j\omega_o t} \sum_{n=0}^{N-1} a_n e^{jn\omega_1 t} \int \rho(\tau)\chi(t-\tau, 0)\, e^{-j(\omega_o + n\omega_1)\tau}\, d\tau \quad (1)$$

where a_n is the amplitude of the n^{th} transmitted frequency, $\omega_o + n\omega_1$, the clutter reflection density is $\rho(\tau)$, and $\chi(t, 0)$ is the zero Doppler cut of the pulse ambiguity function.

The transmitted high band is identical to the transmitted low band except for its frequency up-translation of Δf. The clutter return viewed prior to the nonlinear element (the first detector) is

$$v_1(t) = e^{j(\omega_o + \Delta\omega)t} \sum_{n=0}^{N-1} a_n e^{jn\omega_1 t} \int \rho(\tau)\chi(t-\tau, 0)\, e^{-j(\omega_o + n\omega_1 + \Delta\omega)\tau}\, d\tau \quad (2)$$

The upper and lower returns are summed and appear at the input of the first detector. The output of the detector produces all sums and difference frequency components due to the nonlinear action. However, only those components in a region, Δf, are passed. In this region, the output of the nonlinear element may be written as,

$$\Gamma(t) = v^*(t)v_1(t)$$

$$= e^{j\Delta\omega t} \sum_{m \neq n=0}^{N-1} \sum a_m a_n e^{j(n-m)\omega_1 t} \int\int \rho^*(\tau)\rho(\tau').$$

$$\chi^*(t-\tau, 0)\chi(t-\tau', 0)\, e^{j\omega_o(\tau-\tau')}\, e^{j\omega_1(m\tau - n\tau')}\, e^{-j\Delta\omega\tau'}\, d\tau d\tau'$$

$$+ e^{j\Delta\omega t} \sum_{n=0}^{N-1} a_n^2 \int\int \rho^*(\tau)\rho(\tau')\, e^{j\omega_o(\tau-\tau')}\, e^{jn\omega(\tau-\tau')}\, e^{-j\Delta\omega\tau'}.$$

$$\chi^*(t-\tau,0)\chi(t-\tau',0)\,d\tau\,d\tau'. \qquad (3)$$

But the $m \neq n$ terms of (3) are displaced from the upper-lower band difference frequency, $\Delta\omega$, and are rejected by the bandpass filter at $\Delta\omega$. The passed narrowband frequency components are

$$\eta(t) = e^{j\Delta\omega t} \sum_{n=0}^{N-1} a_n^2 \int\int \rho^*(\tau)\rho(\tau')e^{j\omega_o(\tau-\tau')} e^{jn\omega_1(\tau-\tau')} e^{-j\Delta\omega\tau'}.$$

$$\chi^*(t-\tau,0)\chi(t-\tau',0)\,d\tau\,d\tau'. \qquad (4)$$

At range-delay, τ_R, the instantaneous clutter response is given by

$$\eta_R \triangleq \eta(\tau_R) = e^{j\angle\omega\tau_R} \sum_{n=0}^{N-1} a_n^2 \int\int \rho^*_R(t)\rho_R(t')e^{j\omega_o(t-t')} e^{jn\omega_1(t-t')} e^{-j\Delta\omega t'} dt\,dt' \qquad (5)$$

where we have defined the code-weighted complex reflection density by

$$\rho_R(t) \triangleq \rho(t)\chi(\tau_R - t, 0) \qquad (6)$$

By suitable change of variable, and definition of the clutter patch complex ambiguity function

$$\chi_{\rho_R}(\tau, f) \triangleq \int_{-\infty}^{\infty} \rho^*_R(t)\rho_R(t+\tau)e^{j2\pi ft}\,dt, \qquad (7)$$

equation (5) is expressed as

$$\eta_R = e^{j\Delta\omega\tau_R} \int_{-\infty}^{\infty} \chi_{\rho_R}(\tau, -\angle f)\psi(\tau)e^{-j(\omega_o+\Delta\omega)\tau}\,d\tau \qquad (8)$$

where

$$\psi(\tau) \triangleq \sum_{n=0}^{N-1} a_n^2 e^{-jn\omega_1\tau}. \qquad (9)$$

Equation (8) is the pre-second-detector SPECOR output which is noted to depend upon the Δf-cut of the clutter ambiguity function and the bandwidth factor, $\psi(\tau)$.

The second detector output of SPECOR is given by

$$|\eta_R|^2 = \left| \int \chi_{\rho_R}(\tau, -\Delta f)\psi(\tau) e^{-j(\omega_o + \Delta\omega)\tau} d\tau \right|^2 \qquad (10)$$

which by the Swartz inequality is

$$|\eta_R|^2 \leq \int_{-\infty}^{\infty} |\chi_{\rho_R}(\tau, -\Delta f)|^2 d\tau \int_{-\infty}^{\infty} |\psi(\tau)|^2 d\tau \qquad (11)$$

which has a maximum value when

$$\chi^*_{\rho_R}(\tau, -\Delta f) = \psi(\tau) e^{-j(\omega_o + \Delta\omega)\tau} \qquad (12)$$

in which case the maximum clutter power output is

$$|\eta_R|^2_{max} = \left| \int_{-\infty}^{\infty} |\chi_{\rho_R}(\tau, -\Delta f)| d\tau \right|^2 . \qquad (13)$$

But it can be shown that

$$Q_{\rho_R}(\Delta f) \triangleq \int_{-\infty}^{\infty} |\chi_{\rho_R}(\tau, \Delta f)|^2 d\tau \qquad (14)$$

$$= \int_{-\infty}^{\infty} |\chi_{\rho_R}(\tau, 0)|^2 e^{j2\pi\Delta f\tau} d\tau , \qquad (15)$$

i.e., the zero-frequency cut of the clutter ambiguity function is related to the Δf-cut. Thus, when the range-delay correlation* length of the clutter is τ_c, the clutter is frequency de-correlated when

---

* Reference 5

$$\Delta f \tau_c > 1 \qquad (16)$$

Using (14) and (15) in (13), the clutter power output of SPECOR is

$$|\eta_R|^2 \leq |Q_{\rho_R}(\Delta f)|^2 . \qquad (17)$$

Security Classification

DOCUMENT CONTROL DATA - R&D

(Security classification of title, body of abstract and indexing annotation must be entered when the overall report is classified)

1. ORIGINATING ACTIVITY (Corporate author) Spectronics, Inc. 122 Green Avenue Woodbury, New Jersey 08096	2a. REPORT SECURITY CLASSIFICATION Unclassified 2b. GROUP

3. REPORT TITLE

Radar Clutter Modeling

4. DESCRIPTIVE NOTES (Type of report and inclusive dates)

Final Report - November 1968

5. AUTHOR(S) (Last name, first name, initial)

Blau, W., Farber, J.

6. REPORT DATE	7a. TOTAL NO. OF PAGES	7b. NO. OF REFS
November 1968	100	12

8a. CONTRACT OR GRANT NO. N00014-68-C-0120 b. PROJECT NO. c. d.	9a. ORIGINATOR'S REPORT NUMBER(S) TR 68/053 9b. OTHER REPORT NO(S) (Any other numbers that may be assigned this report)

10. AVAILABILITY/LIMITATION NOTICES Distribution - This document is subject to special export controls and each transmittal to foreign governments or foreign nationals may be made only with the prior approval of the Office of Naval Research, Code 461, Navy Department, Washington, D. C. 20360

11. SUPPLEMENTARY NOTES	12. SPONSORING MILITARY ACTIVITY
	Office of Naval Research, Code 461 Washington, D. C. 20360

13. ABSTRACT

A simulation method for the evaluation of radar performance in a clutter environment is explored. Three radar processors are tested on a common basis using measurement data in a theoretical model which displays both the spatial and frequency correlation properties of clutter. The effects of coherent, partially coherent, and specular scattering interacting with the radar processing are made evident.

DD FORM 1 JAN 64 1473

Security Classification

14. KEY WORDS	LINK A		LINK B		LINK C	
	ROLE	WT	ROLE	WT	ROLE	WT
Clutter						
Radar Clutter						
Scattering						
Clutter Simulation						

INSTRUCTIONS

1. ORIGINATING ACTIVITY: Enter the name and address of the contractor, subcontractor, grantee, Department of Defense activity or other organization *(corporate author)* issuing the report.

2a. REPORT SECURITY CLASSIFICATION: Enter the overall security classification of the report. Indicate whether "Restricted Data" is included. Marking is to be in accordance with appropriate security regulations.

2b. GROUP: Automatic downgrading is specified in DoD Directive 5200.10 and Armed Forces Industrial Manual. Enter the group number. Also, when applicable, show that optional markings have been used for Group 3 and Group 4 as authorized.

3. REPORT TITLE: Enter the complete report title in all capital letters. Titles in all cases should be unclassified. If a meaningful title cannot be selected without classification, show title classification in all capitals in parenthesis immediately following the title.

4. DESCRIPTIVE NOTES: If appropriate, enter the type of report, e.g., interim, progress, summary, annual, or final. Give the inclusive dates when a specific reporting period is covered.

5. AUTHOR(S): Enter the name(s) of author(s) as shown on or in the report. Enter last name, first name, middle initial. If military, show rank and branch of service. The name of the principal author is an absolute minimum requirement.

6. REPORT DATE: Enter the date of the report as day, month, year; or month, year. If more than one date appears on the report, use date of publication.

7a. TOTAL NUMBER OF PAGES: The total page count should follow normal pagination procedures, i.e., enter the number of pages containing information.

7b. NUMBER OF REFERENCES: Enter the total number of references cited in the report.

8a. CONTRACT OR GRANT NUMBER: If appropriate, enter the applicable number of the contract or grant under which the report was written.

8b, 8c, & 8d. PROJECT NUMBER: Enter the appropriate military department identification, such as project number, subproject number, system numbers, task number, etc.

9a. ORIGINATOR'S REPORT NUMBER(S): Enter the official report number by which the document will be identified and controlled by the originating activity. This number must be unique to this report.

9b. OTHER REPORT NUMBER(S): If the report has been assigned any other report numbers *(either by the originator or by the sponsor)*, also enter this number(s).

10. AVAILABILITY/LIMITATION NOTICES: Enter any limitations on further dissemination of the report, other than those imposed by security classification, using standard statements such as:

(1) "Qualified requesters may obtain copies of this report from DDC."

(2) "Foreign announcement and dissemination of this report by DDC is not authorized."

(3) "U. S. Government agencies may obtain copies of this report directly from DDC. Other qualified DDC users shall request through _____."

(4) "U. S. military agencies may obtain copies of this report directly from DDC. Other qualified users shall request through _____."

(5) "All distribution of this report is controlled. Qualified DDC users shall request through _____."

If the report has been furnished to the Office of Technical Services, Department of Commerce, for sale to the public, indicate this fact and enter the price, if known.

11. SUPPLEMENTARY NOTES: Use for additional explanatory notes.

12. SPONSORING MILITARY ACTIVITY: Enter the name of the departmental project office or laboratory sponsoring *(paying for)* the research and development. Include address.

13. ABSTRACT: Enter an abstract giving a brief and factual summary of the document indicative of the report, even though it may also appear elsewhere in the body of the technical report. If additional space is required, a continuation sheet shall be attached.

It is highly desirable that the abstract of classified reports be unclassified. Each paragraph of the abstract shall end with an indication of the military security classification of the information in the paragraph, represented as *(TS), (S), (C), or (U)*.

There is no limitation on the length of the abstract. However, the suggested length is from 150 to 225 words.

14. KEY WORDS: Key words are technically meaningful terms or short phrases that characterize a report and may be used as index entries for cataloging the report. Key words must be selected so that no security classification is required. Identifiers, such as equipment model designation, trade name, military project code name, geographic location, may be used as key words but will be followed by an indication of technical context. The assignment of links, rules, and weights is optional.